NASA Technical Memorandum 4359

A Static Investigation of the Thrust Vectoring System of the F/A-18 High-Alpha Research Vehicle

Mary L. Mason, Francis J. Capone,
and Scott C. Asbury

JUNE 1992

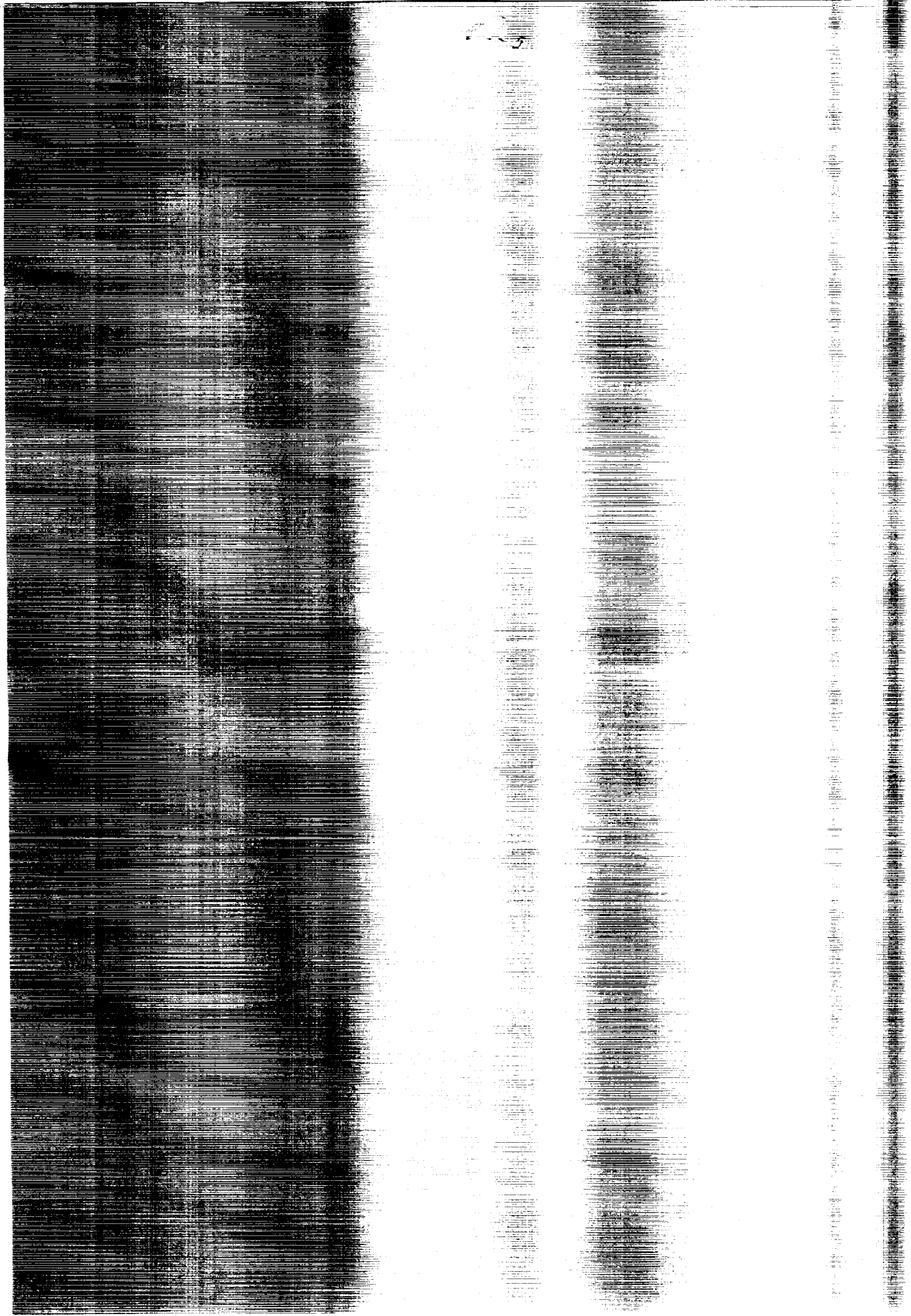

NASA Technical Memorandum 4359

A Static Investigation of the Thrust Vectoring System of the F/A-18 High-Alpha Research Vehicle

Mary L. Mason, Francis J. Capone,
and Scott C. Asbury
Langley Research Center
Hampton, Virginia

National Aeronautics and
Space Administration

Office of Management

Scientific and Technical
Information Program

1992

Abstract

A static (wind-off) test was conducted in the static test facility of the Langley 16-Foot Transonic Tunnel to evaluate the vectoring capability and isolated nozzle performance of the proposed thrust vectoring system of the F/A-18 high-alpha research vehicle (HARV). The thrust vectoring system consisted of three asymmetrically spaced vanes installed externally on a single test nozzle. Two nozzle configurations were tested: a maximum afterburner-power nozzle and a military-power nozzle. Vane size and vane actuation geometry were investigated, and an extensive matrix of vane deflection angles was tested. The nozzle pressure ratio ranged from 2 to 6. The results indicate that the three-vane system can successfully generate multiaxis (pitch and yaw) thrust vectoring. However, large resultant vector angles incurred large thrust losses. Resultant vector angles were always lower than the vane deflection angles. The maximum thrust vectoring angles achieved for the military-power nozzle were larger than the angles achieved for the maximum afterburner-power nozzle.

Introduction

The next generation of fighter/attack aircraft must surpass current configurations in high-speed and low-speed agility, maneuverability, and high-angle-of-attack (high-alpha) capability to ensure survivability and air superiority. Over the last decade, numerous studies have been conducted to determine how the best qualities of today's fighter aircraft can be enhanced and extended. One potential enhancement of aircraft control power is the addition of a multiaxis thrust vectoring system to the aircraft propulsion geometry and controls package (refs. 1–10). A multiaxis thrust vectoring system would deflect the exhaust jet or jets to provide longitudinal and directional control power in flight regimes where conventional aerodynamic controls may fail. Thrust vectoring can extend maneuvering capability to both low-speed and high-speed flight conditions and increase the angle-of-attack range to the extremes of post-stall maneuvering or "supermaneuverability."

The F/A-18 high-alpha research vehicle (HARV) is a prototype F/A-18 aircraft being modified specifically for flight research at high angles of attack up to 70° (refs. 10–13). The baseline F/A-18 aircraft is a highly maneuverable twin-engine fighter aircraft with some high-alpha capability. One of the HARV adaptations to the baseline aircraft is the modification of the conventional axisymmetric-nozzle propulsion system into a multiaxis thrust vectoring system. Studies of axisymmetric thrust-vectoring concepts indicate that these systems can indeed provide effective levels of multiaxis flow turning (refs. 14–19). Thrust vectoring concepts for axisymmetric nozzles that have been researched include gimballed nozzles (refs. 15 and 19), swiveling or hinged nozzles (refs. 15 and 18), and externally mounted deflecting vanes (refs. 16 and 17). The external-vane multiaxis vectoring concept was chosen for the F/A-18 HARV because the thrust vectoring vane system required no nozzle development and could be easily adapted to the F/A-18 afterbody with little interference on existing control surfaces. To add the vanes with minimal afterbody changes, the divergent section of the nozzle was removed. The vane system consisted of three asymmetrically spaced vanes installed on each nozzle. The vanes were designed to fully retract away from the exhaust flow during unvectored operation. It was assumed that only two vanes would deflect into the jet at any given time. An artist's concept of the F/A-18 HARV with the proposed multiaxis vectoring system installed is shown in figure 1.

To initially evaluate the vectoring capability and isolated nozzle performance of the F/A-18 HARV thrust vectoring system, a static (wind-off) test was conducted in the static test facility of the Langley 16-Foot Transonic Tunnel. High-pressure air was used to simulate the jet flow. Nozzle pressure ratio was varied from 2 to 6. The operational nozzle pressure ratio for the F/A-18 HARV is approximately 4 at a Mach number of 0.3. The test hardware simulated the nozzle vane geometry for one engine only, the left engine. The models were sized to 14.25 percent of full scale. Two nozzle configurations were tested: a maximum afterburner-power nozzle (with a large throat area) and a military-power nozzle (with a small throat area). Vane size and two different vane-actuation geometries were also investigated. The

number of vanes deployed and the vane angles were varied to produce a thrust vectoring envelope for each nozzle configuration. Results are presented as nozzle internal performance and resultant thrust vector angles. Selected results of this experiment were presented in an earlier report (ref. 20).

Symbols

All forces (except for resultant gross thrust) and angles are referred to the model centerline.

A_t	nozzle throat area (the minimum internal geometric area), in^2
D	maximum external nozzle diameter, in.
d_t	nozzle throat (minimum) diameter, in.
F	measured thrust along body axis, positive in forward direction, lbf
F_i	ideal isentropic gross thrust, lbf, $w_p \left\{ \frac{R_j T_{t,j}}{g^2} \frac{2\gamma}{\gamma - 1} \left[1 - \left(\frac{1}{\mathrm{NPR}} \right)^{(\gamma-1)/\gamma} \right] \right\}^{1/2}$
F_N	measured normal force, lbf
F_r	resultant gross thrust, lbf, $\sqrt{F^2 + F_N^2 + F_S^2}$
F_S	measured side force, lbf
g	acceleration due to gravity (where $1g \approx 32.174$ ft/sec^2)
H	height from nozzle centerline to bottom of vane mounting bracket, in.
L	total length of nozzle from attachment station to exit, in.
p_a	ambient pressure, psi
$p_{t,j}$	average jet total pressure, psi
R	height of shims used to position vane actuation hardware (see fig. 6), in.
R_j	gas constant, 1716 ft^2/sec^2-°R
r	vertical coordinate, measured from nozzle internal centerline, used to define vane center of rotation (see fig. 6), in.
$T_{t,j}$	jet total temperature, °R
w_i	ideal weight-flow rate, lbf/sec
w_p	measured weight-flow rate, lbf/sec
X	length measured from downstream face of nozzle attachment flange to start of vane actuation system (see fig. 6), in.
x	axial coordinate, measured from nozzle attachment station, used to define vane center of rotation (see fig. 6), in.
α	nozzle internal convergence angle, deg
γ	ratio of specific heats, 1.3997 for air
δ_A, δ_B, δ_C	geometric deflection angle of vanes at positions A, B, and C, respectively, deg
δ_p	resultant pitch thrust vector angle, $\tan^{-1} \frac{F_N}{F}$, deg
δ_y	resultant yaw thrust vector angle, $\tan^{-1} \frac{F_S}{F}$, deg

Abbreviations:

A	vane position A
A/B	afterburner
B	vane position B
C	vane position C
HARV	high-alpha research vehicle
max	maximum
mil	military
NPR	nozzle pressure ratio, $p_{t,j}/p_a$
Sta.	model station, in.

Apparatus and Methods

Static Test Facility

This test was conducted in the static test facility of the Langley 16-Foot Transonic Tunnel. A detailed description of this facility is given in reference 21. The test facility completely houses a single-engine cold-air propulsion simulation system and a control room. Testing is conducted by exhausting a high-pressure air jet to atmosphere in a large, vented and acoustically treated room inside the facility. The control room is separated from the test area and is sealed from any jet-induced noise. During testing, all operation of the propulsion simulation system is conducted from the control room, and a closed-circuit television is used to observe the model.

The high-pressure air system of the static test facility uses the same clean, dry air supply available to the 16-Foot Tunnel. The air control system includes valving and filters to ensure air quality and accurate repeatablity of pressure levels. A heat exchanger maintains the compressed air jet at constant

stagnation temperature. This air system is very similar to the high-pressure air system of the 16-Foot Tunnel (ref. 21).

Single-Engine Propulsion Simulation System

A sketch of the single-engine propulsion simulation system with a nozzle–single-vane test configuration installed is presented in figure 2. The propulsion simulator is shown with the military-power nozzle and a single vectoring vane installed in the top mounting bracket. A photograph of the single-engine system with a nozzle–three-vane configuration is presented in figure 3.

An external high-pressure air system provided a continuous flow of clean, dry air maintained at a temperature of approximately 540°R. This high-pressure air was varied during jet simulation up to about 90 psia in the nozzle. The pressurized air was transferred from the supply source to the simulator by six air lines that run through a dolly-mounted support strut and into a high-pressure plenum chamber. The air was then discharged perpendicularly into the model low-pressure plenum through eight multiholed sonic nozzles that were equally spaced around the high-pressure plenum. The high-pressure plenum was separated from the balance system, but the low-pressure plenum was attached to the balance. This particular airflow system was designed to minimize any forces generated by the transfer of axial momentum as the air passed from the nonmetric high-pressure plenum to the metric low-pressure plenum. Two flexible metal bellows sealed the air system between the metric and nonmetric plenums and compensated for forces resulting from pressurization.

From the low-pressure plenum, the air passed through a circular choke plate into an instrumentation section, and then into the exhaust nozzle. The same instrumentation section and choke plate were used for all nozzle configurations tested. The test nozzles were mounted to the instrumentation section at model station 39.235.

Nozzle Geometry

The nozzle design used in this experiment was a 14.25-percent-scale model of the F/A-18 axisymmetric convergent-divergent nozzle with the divergent section of the nozzle removed, thus resulting in a purely convergent nozzle. Eliminating the divergent section allowed easier installation of the vane actuation system and minimized the weight increase that resulted from adding the thrust vectoring vanes to the F/A-18 aircraft. Two nozzle configurations were tested. One configuration represented a maximum afterburner-power (A/B) setting (large throat area), and the other represented a military-power setting (small throat area). Details of the nozzle geometry are presented in figure 4.

Vane Geometry

The three-vane thrust vectoring geometry reported in reference 16 provided the basis for the vane actuation geometry and vane design for the F/A-18 HARV static test hardware. The vane design for the F/A-18 thrust vectoring system consisted of three equally sized vanes placed asymmetrically about the nozzle exit. The vanes were designed for maximum thrust vector angles when installed on the maximum A/B-power nozzle. A larger vane was later proposed for installation in the top vane position (position A). As a result, two different vane sizes were tested, and one of the test objectives was the determination of vane size for the top vane. Sketches of the two vane geometries are presented in figure 5. The original vane is referred to as the *standard* vane, and the oversized vane is referred to as the *large* vane.

Each vane was designed with double curvature, i.e., axial and radial curvature, on the vectoring surface. The vane planform area was 5.337 in^2 for the standard vane and 7.304 in^2 for the large vane. Thus, the large vane was approximately 27 percent greater in planform area than the standard vane. The vanes had clipped corners at the trailing edge. This corner geometry allowed complete closure of any two vanes to angles of 35° without physical interference between the vanes. During thrust vectoring, only one or two vanes were deflected into the jet while the third vane remained retracted (out of the jet flow).

Vane Actuation System

Sketches of the geometries of the simulated vane actuation system are presented in figure 6. The thrust vectoring vanes were initially attached to a mounting plate. The plate was then fastened by two bolts to a mounting bar through a curved, machined slot in the plate, as shown in figure 6. The arrangement of the curved slot and bolt allowed vane deflection from −15° (out of the jet) to 35° (into the jet). When the vane deflection angle was set, an angle block was used to verify the actual inclination of the vane and to ensure repeatability of each vane position. A separate angle block was required for each deflection angle tested.

The vane-mounting hardware was designed to simulate two different vane actuation systems: a translating vane system and a rotating vane system.

One of the test objectives was the evaluation of these two systems. The translating vane system was designed to rotate the vane to set the deflection angle, and then to translate the vane axially and radially into the jet stream. The rotating vane system was designed to simply rotate the vane into the jet flow to set the deflection angle. To simulate the positions of the vane as set by each of the full-scale actuation systems, the position of the mounting bar was adjusted to set each deflection angle.

Figure 6(a) shows the coordinates X and R that defined the position of the mounting bar and vane for each actuation system and each vane deflection angle. The mounting bar was adjusted radially (varying R) by adding or removing thin metal shims. The bar was adjusted axially (varying X) by positioning the bar through a slot in the mounting hardware. The relationship between the vane center of rotation (the coordinates x and r) and the radial and axial position (the coordinates X and R) is defined by the two equations given in figure 6(b). The vane center of rotation was always fixed with respect to the nozzle centerline. Note that several sets of X and R are presented for a vane deflection angle of 25° in the translating vane system. This set of coordinates defines specific points along the path of translation of the vane into the jet after the vane has been rotated to 25°. For the rotating vane system, only one set of X and R values was required to define the position of the deployed vane.

Figure 7 presents sketches detailing the vane positions relative to the nozzle exit for both test nozzles. Photographs of the vanes installed on the military-power nozzle are presented in figure 8. The three thrust vectoring vanes were arranged circumferentially about the nozzle exit and spaced asymmetrically to interface with existing structural hardpoints on the F/A-18 aircraft. The "top" vane (vane A) was located 5° counterclockwise from the vertical centerline of the nozzle. This position did not vary with vane size. The "outboard" vane (vane B) was located 118° counterclockwise from the mounting point of vane A. The "inboard" vane (vane C) was located 138.5° clockwise from the mounting point of vane A. The vane positions were identical for both test nozzles. Note that the vanes were physically closer to the jet plume when actuated on the maximum A/B-power nozzle.

Instrumentation

A six-component strain-gauge balance was used to measure forces and moments on the metric portion of the model. Total pressure in the jet was measured by a nine-probe rake fixed in the instrumentation section. The total pressure rake is shown in figure 2. The nozzle total pressure was computed as the average of the individual total pressures. In addition, a thermocouple was positioned in the rake plane to measure jet total temperature. The measured weight-flow rate of the high-pressure air supplied to the nozzle was calculated from temperature and pressure measurements taken in two calibrated, choked venturi systems located in the external air system. (See ref. 21.)

Data Reduction

Fifty frames of data, acquired at the rate of 10 frames per second over a 5-sec sample interval, were averaged for each measured data parameter at each data point. The averaged values were used in all subsequent computations. Each of the six measured balance components was initially corrected for model weight tares, for balance component interactions, and for jet-off balance interactions that result from the balance installation.

An additional correction was required to remove model pressurization effects (bellows tares). Although the bellows arrangement in the high-pressure air system was designed to eliminate pressure and momentum interactions with the balance, small bellows tares on the six balance components are generated by jet operation. These tares result from a small pressure difference between the ends of the bellows when air-system internal velocities are high and from small differences in the spring constants of the upstream and downstream bellows when the bellows are pressurized. The bellows tares were determined by testing Stratford choke calibration nozzles (ref. 22) with documented performance over the range of expected internal pressures and external forces and moments. Details of the Stratford nozzles used to calibrate the balance–air system are presented in reference 22. The resulting tare factors were then applied to complete the corrections of the six balance components. The procedure for correcting balance measurements is documented in reference 23.

Five computed performance parameters are used to evaluate the results of this experiment: internal thrust ratio F/F_i, resultant thrust ratio F_r/F_i, discharge coefficient w_p/w_i, resultant pitch vector angle δ_p, and resultant yaw vector angle δ_y. All balance data (i.e., thrust parameters and vector angles) except the resultant gross thrust F_r were referenced to the model centerline.

Internal thrust ratio F/F_i is the ratio of the measured nozzle thrust along the body axis to the

ideal isentropic gross thrust of the nozzle. The nozzle internal thrust F is equivalent to the fully corrected axial force measured by the balance. The ideal thrust F_i is computed from the measured weight-flow rate w_p, the average jet total pressure $p_{t,j}$, and the jet total temperature $T_{t,j}$. (See the exact definitions in the *Symbols* section.) The thrust along the body axis F is diminished by any deflection of the exhaust vector away from the axial direction.

The resultant thrust ratio F_r/F_i is the ratio of the nozzle resultant gross thrust F_r to the ideal thrust F_i. Resultant thrust is computed from the fully corrected balance measurements of axial-force, normal-force, and side-force components of the jet resultant force. This thrust parameter is not diminished by actual jet-flow deflection but is indicative of other losses, inherent in the nozzle–vane system, caused by turning the exhaust flow.

The nozzle discharge coefficient w_p/w_i is the ratio of measured weight-flow rate to ideal weight-flow rate. This parameter reflects the ability of a nozzle to pass weight flow. A decrease in discharge coefficient for a given nozzle design reflects momentum and vena contracta losses.

The resultant thrust vector angles reflect the degree of actual jet-flow deflection away from the axial direction. The resultant pitch vector angle δ_p is computed from axial-force and normal-force measurements; the resultant yaw vector angle δ_y is computed from axial-force and side-force measurements.

Results and Discussion

The results of this investigation are presented in both tabular and plotted form. Performance data for each configuration tested are presented in tables. All five computed performance parameters (F/F_i, F_r/F_i, w_p/w_i, δ_p, and δ_y) are tabulated for each jet-on data point; the nozzle pressure ratio (NPR) is also presented. Table 1 provides an index to the tabulated data presented in tables 2–90. Performance parameters for the maximum A/B-power nozzle without vanes are presented in table 2. The performance of the maximum A/B-power nozzle with vane(s) installed is presented in tables 3–68. Performance parameters for the military-power nozzle without vanes are presented in table 69. The performance of the military-power nozzle with vane(s) installed is presented in tables 70–90. Only results for selected configurations will be presented as data plots. Comparison and summary plots for selected configurations are presented in figures 9–19.

Baseline Nozzle Performance

The isolated nozzle performance of the two test nozzles without vectoring vanes installed is presented in figure 9. Axial thrust ratio F/F_i, resultant thrust ratio F_r/F_i, and discharge coefficient w_p/w_i are presented as functions of nozzle pressure ratio NPR. The baseline nozzles without vanes were run at intervals throughout the test to verify the repeatability of the data. All repeat data runs are plotted in the figure. For the baseline nozzles, gross thrust ratio and axial thrust ratios are essentially identical since no vectoring is implemented. The thrust data show typical trends of convergent nozzle performance. Thrust ratios reach a peak when choke flow conditions are established at the nozzle throat (NPR = 1.89), and then they degrade as NPR increases. Thrust losses are caused by flow underexpansion effects.

Discharge coefficient levels differ between the two nozzles because discharge coefficient w_p/w_i is influenced by the nozzle internal geometry upstream of and in the vicinity of the nozzle throat. The maximum A/B-power nozzle achieves a higher level of w_p/w_i than the military-power nozzle because it has a lower internal convergence angle α. (See fig. 4.) The lower convergence angle results in smaller vena contracta losses and, thus, in higher values of discharge coefficient. For both nozzles, w_p/w_i is relatively constant with NPR once the nozzle flow has choked. Such trends are typical for convergent nozzles (ref. 22). Geometric changes downstream of the nozzle throat plane do not generally affect the discharge coefficient. For the F/A-18 nozzles of this investigation, thrust vectoring by vane deflection is always implemented downstream of the nozzle throat and results in insignificant effects on w_p/w_i. Consequently, w_p/w_i is not plotted for the vectoring configurations since trends essentially mirror the baseline nozzle results. However, discharge coefficient data are presented in the tables for each test configuration.

Before continuing with the discussion of the F/A-18 nozzle data, some general performance characteristics of externally mounted thrust vectoring vanes should be noted. Positive deflection of externally mounted vanes produces flow turning but diminishes axial and resultant thrust ratios. The axial thrust is decreased with thrust vectoring because vane deflection diverts flow away from the axial direction. The resultant thrust ratio, however, includes lateral and longitudinal components and is not affected by diverting axial thrust into another plane. Resultant thrust losses occur because the externally mounted vanes deploy into supersonic jet flow. Increased thrust losses were probably caused by additional aerodynamic turning losses (such as shock,

friction, and/or pressure losses). Thrust losses with the external vane thrust vectoring concept were observed in an earlier study (see ref. 16) and were an expected result of the F/A-18 vane investigation. These losses increase with increasing positive deflection angles and with the number of vanes deployed (set at positive deflection angles). Negative vane deflections produce little or no flow turning and, consequently, have essentially no effect on axial or resultant thrust ratio.

Effect of Vane Actuation Geometry

The effects of the two different vane actuation systems on nozzle performance are presented in figure 10. Thrust ratios, resultant pitch vector angle δ_p, and resultant yaw vector angle δ_y are presented as functions of NPR. The open symbols represent the translating vane data and the solid symbols represent the rotating vane data. Results are shown for the three standard-size vanes installed on the maximum A/B-power nozzle. For a given configuration, either one or two of the vanes were deflected into the jet (deployed) while the third vane was installed but positioned away from the jet (retracted). In this report, a geometric vane angle of $-10°$ will always be considered the fully retracted vane position, and a positive vane angle ($>0°$) will be considered a deployed vane setting.

The magnitudes and direction of the resultant thrust vector angles depend on which vane or vanes are deployed and on how many vanes are deployed. Of the data sets for the six vane geometries presented in figure 10, all but one showed larger magnitudes of both δ_p and δ_y for the rotating vane actuation system, especially at low values of NPR. In figure 10(c), the configuration with $\delta_A = 25°$, $\delta_B = -10°$, and $\delta_C = 25°$ results in slightly lower pitch and yaw angles for the rotating vane system at values of NPR > 4. When resultant vector angles were larger, thrust losses were also larger for the rotating vane system. However, the primary objective of the vane actuation study was to determine which actuation geometry generated the largest possible vectoring envelope, not the smallest thrust losses. As mentioned previously, thrust losses were expected for the large vane deflections.

From a full-scale geometry viewpoint, the rotating vane system would probably be the preferred actuation system. The rotating vane actuating mechanism would be simpler (one movement: a rotation) than the translating vane actuating mechanism (two movements: a translation and a rotation). As a result, the full-scale rotating vane hardware would be lighter in total weight. In addition, vane actuation rates would probably be greater for the simpler rotating mechanism. Based on the full-scale application and the generally larger thrust vectoring angles, the rotating vane actuation system was chosen over the translating vane actuation system for the remaining test configurations.

Effect of Top Vane Geometry

The objective of testing two different vane geometries at the top vane position (position A) was to determine which three-vane geometry would produce the largest equal amount of positive and negative pitch vector angles (nose-up and nose-down moments on the aircraft). A balanced pitch vectoring envelope is essential in establishing aircraft stability and post-stall recovery capability. The position of the two lower vanes sets the magnitude of negative pitch vectoring. The size of the top vane was increased in an attempt to raise the maximum levels of positive pitch vectoring. Results are presented in figure 11 for the vanes installed on the maximum A/B-power nozzle and in figure 12 for the vanes installed on the military-power nozzle. The open symbols denote data resulting from testing three standard vanes, and the solid symbols denote data resulting from testing the standard vanes at positions B (outboard) and C (inboard) and the large vane at position A.

For specific cases (illustrated in fig. 11) when vane A was not deployed, the three standard vanes produced a larger magnitude of negative pitch vectoring than the combination of the large and standard vanes (referred to herein as the *large standard combination*). Increased impingement of the vectored jet flow on the retracted large top vane probably restricted the magnitude of the resultant pitch vector angles. Overall, however, the installation of the large vane produced more equally balanced magnitudes of positive and negative resultant pitch vector angles than the use of three standard vanes. For example, at NPR = 3, the large-standard vane combination installed on the maximum A/B-power nozzle resulted in pitch vector angles from $-23°$ to $19°$, whereas the standard vane combinations resulted in pitch vector angles from $-26°$ to $8°$. Thus, the large standard vane combination produced a pitch-thrust vectoring envelope that was less biased toward the negative direction.

The military-power nozzle with vanes installed produced larger resultant vector angles than the maximum A/B-power nozzle with vanes. The military-power nozzle generated a smaller jet diameter such that the deployed vane or vanes affected a larger percentage of the jet plume, and thus it produced proportionally larger amounts of flow turning.

However, the vanes produced the same effects on resultant vector angle regardless of nozzle power-setting geometry. Again, the large–standard vane combination produced a larger positive range of pitch vector angles than the standard vanes and generated a thrust vector envelope that was less biased toward negative pitch vector angles. At NPR = 3, the large standard vane combination installed on the military-power nozzle produced pitch vector angles from $-32°$ to $22°$, whereas the standard vane combinations produced pitch vector angles from $-36°$ to $12°$. Selected geometries of the standard vane combinations without vane A deployed resulted in slightly higher negative pitch vector angles than the large–standard combination. (See fig. 12.)

In summary, the large–standard vane combination generated a more balanced positive and negative pitch vectoring envelope for both nozzle power setting geometries. This vane geometry and arrangement were eventually selected for the F/A-18 HARV flight hardware. The remaining data figures will present results from the large standard vane combinations, not the three standard vanes.

Effects of Parametric Vane Deflections

The remaining configurations were tested to provide a thrust vectoring envelope for each test nozzle. A very detailed matrix of vane deflections was tested for the maximum A/B-power nozzle to completely establish the thrust vectoring capabilities of the nozzle vane system. A coarser vane deflection matrix was tested for the military-power nozzle. The military-power thrust vectoring envelope should equal or surpass the maximum A/B-power envelope because the vanes, which were sized for the maximum A/B-power nozzle, would affect a larger percentage of the jet plume for the military-power nozzle.

To determine the thrust vectoring envelope, at least one vane was always fully retracted with one or two vanes deployed into the jet flow. Three vanes were always installed for the envelope configurations. The matrix of the maximum A/B vane deflection was subdivided as follows: a single vane deployed, two vanes equally deployed, and two vanes deployed with unequal angles. The maximum A/B nozzle results for the parametric vane deflections are presented in figures 13–15. Results for a single vane deployed and two vanes retracted are presented in figure 13. Results for two equally deployed vanes with one vane retracted are presented in figure 14, and results for two unequally deployed vanes with one vane retracted are presented in figure 15. Data are presented as thrust ratios F/F_i and F_r/F_i and resultant thrust vector angles δ_p and δ_y.

Certain trends dominated the vectored-thrust data. Resultant thrust vector angles were always less than the geometric deflection angle of the vane or vanes. In addition, large amounts of flow turning were always accompanied by large thrust losses because the external vanes deflected into supersonic flow. As stated previously, these trends were expected from the results of an earlier study (ref. 16). Flow turning increased with increasing positive vane deflection, as did thrust losses. Because the vanes were arranged asymmetrically about the nozzle exit, pitch vectoring was always coupled with yaw vectoring. However, certain combinations of vane deflections produced pure pitch or pure yaw resultant vector angles. The dominant vectoring direction depended on which vane or vanes were deployed.

The resultant vector angles for the maximum A/B-power nozzle did not always remain constant with NPR, a result which could complicate the in-flight use of this type of vectored-thrust control-power system. Thrust vector angles increased or decreased with increasing NPR depending on which vane or vanes were deployed and on the magnitude of the deployment angle. Generally, vanes deployed to lower angles ($<20°$) produced resultant vector angles that were constant or increased with increasing NPR, whereas vanes deployed to higher angles ($\geq 20°$) produced thrust vector angles that decreased with increasing NPR. For example, single and multiple deployments involving vane A produced pitch vector angles that increased with NPR for vane deployments from $0°$ to $15°$. When vane angles were set to $20°$ or higher, pitch vector angle decreased with increasing NPR. The increase of thrust vector angle with increasing NPR for low vane deployment angles probably reflects a favorable interaction of the deflected vane with the jet plume boundary as the plume expands. The drop in resultant vector angles at higher values of NPR may result from increasing impingement effects of the retracted vane or vanes on the vectored jet plume.

The military-power-nozzle results for the parametric vane deflections are presented in figures 16 and 17. Results for a single vane deployed and two vanes retracted are presented in figure 16. Results for two equally deployed vanes with one vane retracted are presented in figure 17. Data are presented as thrust ratios F/F_i and F_r/F_i and resultant thrust vector angles δ_p and δ_y.

The same trends in performance and thrust vectoring observed for the maximum A/B-power nozzle were also apparent in the military-power-nozzle data. However, for the same vane deployments, resultant thrust vector angles were larger for

the military-power nozzle than for the maximum A/B-power nozzle. As discussed earlier, the vane or vanes deployed on the military-power nozzle affected a larger percentage of the jet plume and thus produced proportionally larger amounts of flow turning. For example, when vane A was deployed to 35° with vanes B and C fully retracted, the maximum pitch vector angle generated was 23°, compared with 21° for the maximum A/B-power nozzle.

One trend that differed between the two nozzle-vane configurations was the effect of increasing NPR on resultant vector angles. For the maximum A/B-power nozzle, the effect of NPR varied with vane deployment angle. For the military-power nozzle, the trend is a predominantly favorable effect; flow turning remains constant or increases with increasing NPR. The increase in vector angle begins to drop off only at the maximum vane deflection angle for the maximum NPR value. The negative impingement effects of the retracted vane or vanes seen for the maximum A/B-power nozzle are apparently reduced for the military-power configurations because the retracted vane or vanes affect a proportionally smaller area of jet flow for the smaller military-power jet plume.

Thrust Vectoring Envelopes

The results of the parametric vane deployments are summarized as thrust vectoring envelopes. Results are presented as δ_p plotted against δ_y up to a maximum vane deployment angle of 30°. The vectoring envelope for the maximum A/B nozzle is presented in figure 18. The military-power envelope is plotted along with the maximum A/B-power envelope in figure 19 so that the magnitudes of thrust vectoring capability can be directly compared. Recall that the operational NPR of the F/A-18 HARV at a free-stream Mach number of 0.3 is approximately 4 for both maximum A/B-power and military-power nozzles.

A separate envelope is presented for each NPR tested. These envelopes illustrated that the net flow turning is always less than the vane deflection angles, as was mentioned previously. The envelopes are also asymmetric, a result of the use of three thrust vectoring vanes positioned asymmetrically around the circumference of the nozzle exit. However, pure pitch or pure yaw vector angles were generated by certain vane deflection combinations, a result indicating that isolated moments could be successfully produced by a three-vane vectoring system. Pitch vectoring capability exceeds the yaw vectoring capability, but this was an anticipated result of the vane geometry. The degrading magnitude of peak resultant vector angle with increasing NPR can be seen by comparing the envelope boundaries for different values of NPR. Finally, the comparison of the maximum A/B-power envelope with the military-power envelope in figure 19 illustrates the increased turning effectiveness of the vanes when actuated on the military-power nozzle.

Conclusions

A static (wind-off) test was conducted in the static test facility of the Langley 16-Foot Transonic Tunnel to evaluate the vectoring capability and isolated nozzle performance of the proposed thrust vectoring system of the F/A-18 high-alpha research vehicle (HARV). The thrust vectoring system consisted of three asymmetrically spaced vanes installed externally on the test nozzle. Two nozzle configurations were tested: a maximum afterburner-power nozzle and a military-power nozzle. Vane size and vane actuation geometry were also investigated. The results of this experiment are summarized as follows:

1. A simple rotating vane actuation system generally produced larger resultant thrust vector angles than a translating–rotating vane concept. The rotating vane system was chosen for the F/A-18 HARV thrust vectoring system.

2. The vane geometry chosen for the three thrust vectoring vanes consisted of a large vane mounted on top of the nozzle and two smaller vanes installed at inboard and outboard positions. This vane arrangement produced more balanced amounts of positive and negative resultant pitch vector angles than an arrangement of three equally sized vanes.

3. Because the externally mounted vanes deployed into supersonic jet flow, effective thrust vectoring always resulted in axial and resultant thrust losses. Thrust losses increased with increased vectoring. Thrust vector angles were always less than the geometric vane deployment angles.

4. Because vectoring was implemented with three vanes arranged asymmetrically about the nozzle exit, pitch and yaw vectoring were always coupled. However, certain combinations of vane deflections successfully produced pure pitch vector angles or pure yaw vector angles.

5. For both nozzles tested, the resultant vector angles showed some variation with nozzle pressure ratio.

6. The thrust vectoring envelope was larger for the military-power nozzle than for the maximum afterburner-power nozzle.

NASA Langley Research Center
Hampton, VA 23665-5225
March 23, 1992

References

1. Herbst, W. B.: Future Fighter Technologies. *J. Aircr.*, vol. 17, no. 8, Aug. 1980, pp. 561 566.

2. Lacey, David W.: Air Combat Advantages From Reaction Control Systems. SAE Tech. Paper Ser. 801177, Oct. 1980.

3. Nelson, B. D.; and Nicolai, L. M.: Application of Multi-Function Nozzles to Advanced Fighters. AIAA-81-2618, Dec. 1981.

4. Kraus, W.; Przibilla, H.; and Haux, U.: Stability and Control for High Angle of Attack Maneuvering. *Criteria for Handling Qualities of Military Aircraft*, AGARD-CP-333, June 1982, pp. 15-1 15-11.

5. Callahan, C. J.: Tactical Aircraft Payoffs for Advanced Exhaust Nozzles. AIAA-86-2660, Oct. 1986.

6. Capone, Francis J.; and Mason, Mary L.: *Multiaxis Aircraft Control Power From Thrust Vectoring at High Angles of Attack*. NASA TM-87741, 1986.

7. Mace, James; and Doane, Paul: Integrated Air Vehicle/Propulsion Technology for a Multirole Fighter A MCAIR Perspective. AIAA-90-2278, July 1990.

8. Herrick, Paul W.: Air-to-Ground Attack Fighter Improvements Through Multi-Function Nozzles. SAE Paper 901002, Apr. 1990.

9. Gallaway, C. R.; and Osborn, R. F.: Aerodynamics Perspective of Supermaneuverability. AIAA-85-4068, Oct. 1985.

10. Nguyen, Luat T.: Flight Dynamics Research for Highly Agile Aircraft. SAE Tech. Paper 892235, Sept. 1989.

11. Mace, J.; Smereczniak, P.; Krekeler, G.; Bowers, D.; MacLean, M.; and Thayer, E.: Advanced Thrust Vectoring Nozzles for Supercruise Fighter Aircraft. AIAA-89-2816, July 1989.

12. Sawyer, Wallace C.; and Jackson, Charlie M., Jr.: Overview of Military Technology at NASA Langley. SAE Paper 892232, Sept. 1989.

13. Gilbert, William P.; Nguyen, Luat T.; and Gera, Joseph: Control Research in the NASA High-Alpha Technology Program. *Aerodynamics of Combat Aircraft Controls and of Ground Effects*, AGARD-CP-465, Apr. 1990, pp. 3-1 3-18.

14. Lacey, David W.; and Murphy, Richard D.: *Jet Engine Thrust Turning by the Use of Small Externally Mounted Vanes*. DTNSRDC-82/080, U.S. Navy, Jan. 1983. (Available from DTIC as AD B070 970L.)

15. Hienz, Egon; and Vedova, Ralph: Requirements, Definition and Preliminary Design for an Axisymmetric Vectoring Nozzle, To Enhance Aircraft Maneuverability. AIAA-84-1212, June 1984.

16. Berrier, Bobby L.; and Mason, Mary L.: *Static Performance of an Axisymmetric Nozzle With Post-Exit Vanes for Multiaxis Thrust Vectoring*. NASA TP-2800, 1988.

17. Powers, Sidney A.; and Schellenger, Harvey G.: The X-31: High Performance at Low Cost. AIAA-89-2122, July Aug. 1989.

18. Carson, George T., Jr.; and Capone, Francis J.: *Static Internal Performance of an Axisymmetric Nozzle With Multiaxis Thrust-Vectoring Capability*. NASA TM-4237, 1991.

19. Berrier, Bobby L.; and Taylor, John G.: *Internal Performance of Two Nozzles Utilizing Gimbal Concepts for Thrust Vectoring*. NASA TP-2991, 1990.

20. Bowers, Albion H.; Noffz, Gregory K.; Grafton, Sue B.; Mason, Mary L.; and Peron, Lee R.: *Multiaxis Thrust Vectoring Using Axisymmetric Nozzles and Posterit Vanes on an F/A-18 Configuration Vehicle*. NASA TM-101741, 1991.

21. Staff of the Propulsion Aerodynamics Branch: *A User's Guide to the Langley 16-Foot Transonic Tunnel Complex, Revision 1*. NASA TM-102750, 1990. (Supersedes NASA TM-83186, compiled by Kathryn H. Peddrew, 1981.)

22. Berrier, Bobby L.; Leavitt, Laurence D.; and Bangert, Linda S.: *Operating Characteristics of the Multiple Critical Venturi System and Secondary Calibration Nozzles Used for Weight-Flow Measurements in the Langley 16-Foot Transonic Tunnel*. NASA TM-86405, 1985.

23. Mercer, Charles E.; Berrier, Bobby L.; Capone, Francis J.; Grayston, Alan M.; and Sherman, C. D.: *Computations for the 16-Foot Transonic Tunnel NASA, Langley Research Center, Revision 1*. NASA TM-86319, 1987. (Supersedes NASA TM-86319, 1984.)

Table 1. Index to Data Tables

(a) Maximum afterburner-power nozzle

Table 1. Concluded

Table 2. Maximum A/B-Power Nozzle Performance
With No Vanes Installed

[δ_p and δ_y are given in degrees]

(a) Run 39

NPR	w_p/w_i	F/F_i	F_r/F_i	δ_p	δ_y
2.0039	0.9548	1.0049	1.0049	0.25	0.16
3.0043	0.9710	0.9959	0.9959	0.25	0.22
4.0013	0.9696	0.9855	0.9855	0.19	0.25
5.0029	0.9682	0.9754	0.9754	0.16	0.25
5.9965	0.9670	0.9669	0.9670	0.19	0.21

(b) Run 241

NPR	w_p/w_i	F/F_i	F_r/F_i	δ_p	δ_y
2.0002	0.9557	1.0082	1.0083	0.50	-0.05
3.0041	0.9714	0.9993	0.9993	0.53	0.01
3.9993	0.9699	0.9868	0.9869	0.43	0.07
4.9997	0.9688	0.9758	0.9759	0.38	0.10
6.0141	0.9668	0.9665	0.9665	0.40	0.10
5.9947	0.9668	0.9667	0.9667	0.36	0.10

Table 3. Maximum A/B-Power Nozzle Performance of Translating Vane Actuation System With Single Standard Vane Installed and Deployed

[δ_p and δ_y are given in degrees]

δ_A = 5.0°, δ_B = off , δ_C = off

NPR	w_p/w_i	F/F_i	F_r/F_i	δ_p	δ_y
2.0049	0.9548	1.0064	1.0065	0.29	0.29
3.0035	0.9707	0.9963	0.9963	0.51	0.24
4.0015	0.9697	0.9832	0.9834	1.05	0.23
5.0047	0.9680	0.9715	0.9721	1.90	0.15
5.9982	0.9667	0.9619	0.9630	2.78	0.04

δ_A = 10.0°, δ_B = off , δ_C = off

NPR	w_p/w_i	F/F_i	F_r/F_i	δ_p	δ_y
2.0071	0.9555	1.0023	1.0024	0.89	0.11
3.0032	0.9710	0.9916	0.9919	1.29	0.13
4.0044	0.9701	0.9775	0.9781	2.13	0.10
5.0058	0.9682	0.9647	0.9661	3.12	0.02
6.0029	0.9668	0.9541	0.9564	4.01	-0.13

δ_A = 15.0°, δ_B = off , δ_C = off

NPR	w_p/w_i	F/F_i	F_r/F_i	δ_p	δ_y
2.0010	0.9548	0.9953	0.9959	2.02	0.02
3.0044	0.9706	0.9848	0.9857	2.43	0.06
4.0010	0.9699	0.9686	0.9703	3.43	-0.07
5.0001	0.9680	0.9548	0.9578	4.55	-0.18
6.0009	0.9667	0.9432	0.9476	5.53	-0.29

δ_A = 20.0°, δ_B = off , δ_C = off

NPR	w_p/w_i	F/F_i	F_r/F_i	δ_p	δ_y
1.9997	0.9551	0.9785	0.9804	3.64	-0.22
3.0031	0.9709	0.9685	0.9711	4.18	-0.16
4.0015	0.9697	0.9511	0.9552	5.26	-0.26
5.0060	0.9681	0.9374	0.9433	6.40	-0.33
5.9999	0.9670	0.9258	0.9333	7.25	-0.46

Table 3. Concluded

δ_A = 25.0°, δ_B = off, δ_C = off
X = 1.758, R = 0.303

NPR	w_p/w_i	F/F_i	F_r/F_i	δ_p	δ_y
2.0018	0.9549	0.9660	0.9696	4.91	-0.37
2.9983	0.9714	0.9539	0.9582	5.42	-0.31
3.9995	0.9696	0.9362	0.9422	6.47	-0.39
4.9997	0.9681	0.9221	0.9302	7.55	-0.44
6.0027	0.9668	0.9105	0.9202	8.32	-0.51

δ_A = 25.0°, δ_B = off, δ_C = off
X = 1.639, R = 0.071

NPR	w_p/w_i	F/F_i	F_r/F_i	δ_p	δ_y
2.0036	0.9547	0.9502	0.9589	7.71	-0.47
3.0097	0.9708	0.9405	0.9503	8.20	-0.49
4.0070	0.9696	0.9250	0.9374	9.32	-0.61
5.0035	0.9679	0.9121	0.9270	10.26	-0.68
5.9993	0.9668	0.9019	0.9185	10.87	-0.73

Table 4. Maximum A/B-Power Nozzle Performance of Translating Vane Actuation System With Three Standard Vanes Installed

[δ_p and δ_y are given in degrees]

(a) One vane deployed; two vanes retracted. $X = 1.639$ in. and $R = 0.071$ in. for 25° deployed vane

δ_A = 25.0°, δ_B = -10.0° , δ_C = -10.0°

NPR	w_p/w_i	F/F_i	F_r/F_i	δ_p	δ_y
2.0026	0.9546	0.9507	0.9581	7.14	-0.35
3.0029	0.9709	0.9405	0.9499	8.03	-0.43
4.0045	0.9699	0.9256	0.9381	9.36	-0.59
5.0019	0.9681	0.9129	0.9281	10.36	-0.70
6.0069	0.9669	0.9028	0.9196	10.95	-0.80

δ_A = -10.0°, δ_B = 25.0° , δ_C = -10.0°

NPR	w_p/w_i	F/F_i	F_r/F_i	δ_p	δ_y
1.9999	0.9550	0.9484	0.9557	-3.26	-6.28
3.0025	0.9705	0.9383	0.9467	-3.72	-6.69
4.0010	0.9698	0.9239	0.9350	-4.62	-7.58
4.9997	0.9684	0.9104	0.9240	-5.22	-8.39
6.0068	0.9669	0.8991	0.9143	-5.62	-8.85

δ_A = -10.0°, δ_B = -10.0° , δ_C = 25.0°

NPR	w_p/w_i	F/F_i	F_r/F_i	δ_p	δ_y
2.0042	0.9550	0.9520	0.9594	-4.84	5.27
3.0029	0.9706	0.9406	0.9493	-5.12	5.87
4.0035	0.9697	0.9257	0.9372	-5.97	6.75
5.0047	0.9681	0.9125	0.9264	-6.67	7.42
5.9930	0.9667	0.9025	0.9174	-7.03	7.69

Table 4. Concluded

(b) Two vanes deployed; one vane retracted. $X = 1.639$ in. and $R = 0.071$ in. for 25° deployed vane

$\delta_A = 25.0°$, $\delta_B = 25.0°$, $\delta_C = -10.0°$

NPR	w_p/w_i	F/F_i	F_r/F_i	δ_p	δ_y
2.0061	0.9535	0.8616	0.8796	5.44	-10.31
3.0008	0.9709	0.8420	0.8625	5.90	-11.13
4.0035	0.9701	0.8300	0.8523	6.03	-11.75
4.9993	0.9683	0.8204	0.8436	6.10	-12.09
6.0099	0.9669	0.8112	0.8347	6.15	-12.26

$\delta_A = -10.0°$, $\delta_B = 25.0°$, $\delta_C = 25.0°$

NPR	w_p/w_i	F/F_i	F_r/F_i	δ_p	δ_y
1.9998	0.9519	0.8558	0.8816	-13.80	-1.72
3.0047	0.9707	0.8333	0.8649	-15.46	-1.61
4.0001	0.9697	0.8224	0.8576	-16.40	-1.61
5.0022	0.9681	0.8114	0.8484	-16.92	-1.63
5.9997	0.9667	0.8019	0.8384	-16.89	-1.75

$\delta_A = 25.0°$, $\delta_B = -10.0°$, $\delta_C = 25.0°$

NPR	w_p/w_i	F/F_i	F_r/F_i	δ_p	δ_y
2.0052	0.9535	0.8700	0.8769	3.26	6.45
3.0063	0.9705	0.8479	0.8566	3.93	7.24
4.0030	0.9699	0.8360	0.8454	4.02	7.53
5.0021	0.9682	0.8274	0.8364	3.92	7.46
6.0028	0.9669	0.8192	0.8277	3.91	7.25

Table 5. Maximum A/B-Power Nozzle Performance of Rotating Vane Actuation System With Single Standard Vane Installed and Deployed

[δ_p and δ_y are given in degrees]

δ_A = 5.0°, δ_B = off , δ_C = off

NPR	w_p/w_i	F/F_i	F_r/F_i	δ_p	δ_y
2.0010	0.9551	1.0052	1.0053	0.80	0.03
3.0039	0.9708	0.9953	0.9954	0.98	0.06
4.0067	0.9697	0.9810	0.9814	1.65	0.04
5.0005	0.9681	0.9684	0.9694	2.61	-0.01
6.0081	0.9668	0.9580	0.9597	3.42	-0.14

δ_A = 10.0°, δ_B = off , δ_C = off

NPR	w_p/w_i	F/F_i	F_r/F_i	δ_p	δ_y
2.0029	0.9541	0.9990	0.9995	1.82	-0.02
3.0044	0.9704	0.9875	0.9881	2.07	0.04
4.0027	0.9690	0.9729	0.9743	3.02	-0.03
4.9994	0.9677	0.9598	0.9624	4.14	-0.15
6.0101	0.9664	0.9493	0.9532	5.13	-0.27

δ_A = 15.0°, δ_B = off , δ_C = off

NPR	w_p/w_i	F/F_i	F_r/F_i	δ_p	δ_y
2.0054	0.9553	0.9827	0.9849	3.77	-0.12
2.9988	0.9703	0.9727	0.9752	4.12	-0.22
4.0049	0.9694	0.9572	0.9610	5.10	-0.26
4.9972	0.9678	0.9435	0.9494	6.35	-0.37
6.0063	0.9665	0.9329	0.9405	7.25	-0.46

δ_A = 20.0°, δ_B = off , δ_C = off

NPR	w_p/w_i	F/F_i	F_r/F_i	δ_p	δ_y
2.0063	0.9553	0.9511	0.9585	7.10	-0.47
3.0113	0.9708	0.9420	0.9502	7.49	-0.47
3.9953	0.9693	0.9315	0.9410	8.14	-0.52
5.0022	0.9679	0.9191	0.9310	9.12	-0.57
6.0041	0.9664	0.9100	0.9236	9.84	-0.68

Table 5. Concluded

δ_A = 25.0°, δ_B = off, δ_C = off

NPR	w_p/w_i	F/F_i	F_r/F_i	δ_p	δ_y
2.0042	0.9551	0.9263	0.9389	9.38	-0.73
3.0055	0.9706	0.9164	0.9301	9.79	-0.77
4.0142	0.9696	0.9079	0.9225	10.17	-0.72
5.0078	0.9679	0.8986	0.9153	10.96	-0.75
5.9929	0.9664	0.8898	0.9084	11.57	-0.84

δ_A = 30.0°, δ_B = off, δ_C = off

NPR	w_p/w_i	F/F_i	F_r/F_i	δ_p	δ_y
2.0042	0.9536	0.8965	0.9158	11.75	-0.91
3.0006	0.9709	0.8858	0.9062	12.13	-0.99
4.0136	0.9694	0.8783	0.8989	12.28	-0.89
4.9953	0.9678	0.8726	0.8948	12.76	-0.91
5.9995	0.9664	0.8639	0.8877	13.25	-1.02

Table 6. Maximum A/B-Power Nozzle Performance of Rotating Vane Actuation System With Two Standard Vanes Installed and Deployed

[δ_p and δ_y are given in degrees]

δ_A = 30.0°, δ_B = 30.0°, δ_C = off°

NPR	w_p/w_i	F/F_i	F_r/F_i	δ_p	δ_y
1.9996	0.9519	0.7081	0.7590	9.94	-18.97
3.0041	0.9701	0.6874	0.7445	10.76	-20.31
4.0058	0.9693	0.6811	0.7406	10.93	-20.83
4.7230	0.9686	0.6797	0.7395	10.85	-20.98
4.7254	0.9685	0.6790	0.7387	10.88	-20.96

δ_A = off°, δ_B = 30.0°, δ_C = 30.0°

NPR	w_p/w_i	F/F_i	F_r/F_i	δ_p	δ_y
2.0002	0.9498	0.7053	0.7874	-26.34	-2.11
3.0050	0.9699	0.6810	0.7736	-28.28	-1.81
4.0018	0.9694	0.6750	0.7703	-28.77	-1.81
5.0009	0.9676	0.6745	0.7679	-28.51	-1.96
6.0011	0.9662	0.6740	0.7650	-28.16	-2.24

δ_A = 30.0°, δ_B = off°, δ_C = 30.0°

NPR	w_p/w_i	F/F_i	F_r/F_i	δ_p	δ_y
2.0045	0.9524	0.7295	0.7491	5.31	12.09
3.0043	0.9700	0.7073	0.7303	5.91	13.26
4.0004	0.9694	0.7001	0.7243	5.96	13.70
4.9991	0.9676	0.6954	0.7202	6.13	13.90
6.0072	0.9662	0.6931	0.7178	6.25	13.82

δ_A = off°, δ_B = 25.0°, δ_C = 25.0°

NPR	w_p/w_i	F/F_i	F_r/F_i	δ_p	δ_y
2.0160	0.9616	0.7839	0.8305	-19.23	-1.65
3.0032	0.9751	0.7649	0.8157	-20.27	-1.60
4.0028	0.9701	0.7589	0.8122	-20.84	-1.52
5.0235	0.9678	0.7560	0.8096	-20.91	-1.66
6.0080	0.9672	0.7516	0.8051	-20.96	-1.77

Table 7. Maximum A/B-Power Nozzle Performance of Rotating Vane Actuation System for Three Standard Vanes Installed With Vane A Deployed and Vanes B and C Fully Retracted

[δ_p and δ_y are given in degrees]

δ_A = 0.0°, δ_B = -10.0° , δ_C = -10.0°

NPR	w_p/w_i	F/F_i	F_r/F_i	δ_p	δ_y
1.9980	0.9547	1.0066	1.0066	0.39	0.08
2.9996	0.9703	0.9966	0.9967	0.48	0.13
3.9999	0.9693	0.9849	0.9849	0.53	0.20
4.9999	0.9677	0.9732	0.9733	1.04	0.14
5.9921	0.9664	0.9642	0.9647	1.70	0.10

δ_A = 5.0°, δ_B = -10.0° , δ_C = -10.0°

NPR	w_p/w_i	F/F_i	F_r/F_i	δ_p	δ_y
2.0007	0.9549	1.0053	1.0054	0.70	0.12
3.0020	0.9702	0.9946	0.9947	0.83	0.13
3.9981	0.9697	0.9807	0.9810	1.44	0.09
4.9996	0.9678	0.9681	0.9690	2.40	0.08
5.9962	0.9664	0.9573	0.9588	3.22	-0.06

δ_A = 10.0°, δ_B = -10.0° , δ_C = -10.0°

NPR	w_p/w_i	F/F_i	F_r/F_i	δ_p	δ_y
1.9994	0.9549	0.9999	1.0003	1.73	0.03
2.9998	0.9707	0.9891	0.9897	2.00	0.04
4.0020	0.9697	0.9725	0.9738	2.93	-0.03
5.0029	0.9678	0.9589	0.9613	4.11	-0.14
6.0030	0.9663	0.9480	0.9518	5.10	-0.21

δ_A = 15.0°, δ_B = -10.0° , δ_C = -10.0°

NPR	w_p/w_i	F/F_i	F_r/F_i	δ_p	δ_y
2.0025	0.9549	0.9812	0.9837	4.09	-0.21
2.9988	0.9708	0.9708	0.9737	4.41	-0.16
4.0042	0.9696	0.9558	0.9601	5.41	-0.22
4.9995	0.9679	0.9426	0.9490	6.64	-0.32
5.9930	0.9665	0.9309	0.9390	7.52	-0.42

Table 7. Continued

δ_A = 17.5°, δ_B = -10.0° , δ_C = -10.0°

NPR	w_p/w_i	F/F_i	F_r/F_i	δ_p	δ_y
1.9993	0.9554	0.9691	0.9731	5.20	-0.31
3.0062	0.9703	0.9578	0.9626	5.67	-0.30
4.0041	0.9695	0.9454	0.9517	6.59	-0.33
4.0006	0.9696	0.9452	0.9515	6.60	-0.31
5.0016	0.9678	0.9329	0.9416	7.77	-0.41
5.9985	0.9663	0.9229	0.9334	8.57	-0.52

δ_A = 20.0°, δ_B = -10.0° , δ_C = -10.0°

NPR	w_p/w_i	F/F_i	F_r/F_i	δ_p	δ_y
1.9997	0.9547	0.9528	0.9605	7.23	-0.31
3.0035	0.9700	0.9418	0.9504	7.72	-0.38
4.0019	0.9692	0.9307	0.9406	8.30	-0.43
5.0003	0.9676	0.9211	0.9330	9.15	-0.54
5.0013	0.9679	0.9213	0.9332	9.14	-0.52
6.0028	0.9664	0.9119	0.9254	9.75	-0.62

δ_A = 22.5°, δ_B = -10.0° , δ_C = -10.0°

NPR	w_p/w_i	F/F_i	F_r/F_i	δ_p	δ_y
2.0051	0.9547	0.9396	0.9503	8.59	-0.50
2.9995	0.9703	0.9276	0.9393	9.04	-0.51
3.9976	0.9697	0.9199	0.9323	9.37	-0.53
5.0002	0.9677	0.9091	0.9238	10.19	-0.65
6.0042	0.9664	0.8993	0.9155	10.76	-0.80

δ_A = 25.0°, δ_B = -10.0° , δ_C = -10.0°

NPR	w_p/w_i	F/F_i	F_r/F_i	δ_p	δ_y
1.9983	0.9544	0.9252	0.9391	9.86	-0.61
2.9992	0.9707	0.9127	0.9278	10.32	-0.65
4.0002	0.9694	0.9063	0.9221	10.60	-0.65
4.9940	0.9678	0.8995	0.9166	11.06	-0.73
4.9940	0.9677	0.8993	0.9165	11.10	-0.75
5.9954	0.9663	0.8903	0.9088	11.54	-0.91

Table 7. Concluded

δ_A = 27.5°, δ_B = -10.0° , δ_C = -10.0°

NPR	w_p/w_i	F/F_i	F_r/F_i	δ_p	δ_y
1.9995	0.9542	0.9062	0.9241	11.28	-0.68
3.0010	0.9703	0.8951	0.9143	11.71	-0.85
4.0007	0.9696	0.8894	0.9088	11.84	-0.77
4.9992	0.9678	0.8791	0.9003	12.42	-0.95
5.9993	0.9663	0.8700	0.8921	12.74	-1.11
6.0037	0.9663	0.8698	0.8921	12.78	-1.11

δ_A = 30.0°, δ_B = -10.0° , δ_C = -10.0°

NPR	w_p/w_i	F/F_i	F_r/F_i	δ_p	δ_y
1.9999	0.9540	0.8910	0.9131	12.59	-0.79
3.0008	0.9704	0.8792	0.9019	12.83	-0.98
3.9971	0.9694	0.8736	0.8961	12.85	-0.87
4.9984	0.9677	0.8636	0.8879	13.38	-1.12
6.0018	0.9663	0.8554	0.8799	13.48	-1.37

δ_A = 35.0°, δ_B = -10.0° , δ_C = -10.0°

NPR	w_p/w_i	F/F_i	F_r/F_i	δ_p	δ_y
1.9995	0.9555	0.8571	0.8862	14.67	-1.18
2.9998	0.9702	0.8424	0.8732	15.20	-1.27
4.0005	0.9694	0.8398	0.8689	14.83	-1.35
4.9982	0.9677	0.8309	0.8604	14.96	-1.61
4.9994	0.9677	0.8311	0.8605	14.94	-1.63
5.9981	0.9662	0.8277	0.8558	14.61	-1.91

Table 8. Maximum A/B-Power Nozzle Performance of Rotating Vane Actuation System for Three Standard Vanes Installed With Vane A Deployed and Vanes B and C Partially Retracted

[δ_p and δ_y are given in degrees]

δ_A = 30.0°, δ_B = -5.0 °, δ_C = -5.0°

NPR	w_p/w_i	F/F_i	F_r/F_i	δ_p	δ_y
1.9979	0.9539	0.8879	0.9096	12.49	-1.03
2.9998	0.9702	0.8773	0.8994	12.66	-1.27
4.0004	0.9693	0.8718	0.8927	12.33	-1.39
4.9972	0.9676	0.8618	0.8832	12.52	-1.74
5.0002	0.9676	0.8618	0.8832	12.53	-1.78
5.9973	0.9661	0.8539	0.8743	12.20	-2.18

δ_A = 25.0°, δ_B = -5.0 °, δ_C = -5.0°

NPR	w_p/w_i	F/F_i	F_r/F_i	δ_p	δ_y
2.0002	0.9545	0.9238	0.9377	9.85	-0.58
2.9980	0.9705	0.9118	0.9269	10.33	-0.72
3.9971	0.9695	0.9045	0.9200	10.51	-0.80
5.0009	0.9677	0.8938	0.9106	10.97	-1.01
5.9941	0.9663	0.8841	0.9012	11.07	-1.51

δ_A = 30.0°, δ_B = 0.0 °, δ_C = 0.0°

NPR	w_p/w_i	F/F_i	F_r/F_i	δ_p	δ_y
2.0002	0.9540	0.8856	0.9040	11.50	-1.43
3.0061	0.9702	0.8714	0.8891	11.33	-1.69
4.0025	0.9694	0.8643	0.8798	10.63	-1.74
4.9984	0.9675	0.8535	0.8681	10.37	-2.02
5.9996	0.9662	0.8435	0.8565	9.76	-2.32

Table 9. Maximum A/B-Power Nozzle Performance of Rotating Vane Actuation System for Three Standard Vanes Installed With Vane B Deployed and Vanes A and C Fully Retracted

[δ_p and δ_y are given in degrees]

δ_A = -10.0°, δ_B = 0.0° , δ_C = -10.0°

NPR	w_p/w_i	F/F_i	F_r/F_i	δ_p	δ_y
2.0032	0.9549	1.0071	1.0071	0.61	0.16
3.0013	0.9702	0.9968	0.9969	0.62	0.14
4.0026	0.9693	0.9852	0.9852	0.40	-0.02
5.0012	0.9677	0.9725	0.9725	0.02	-0.46
5.9952	0.9662	0.9625	0.9627	-0.39	-1.07

δ_A = -10.0°, δ_B = 5.0° , δ_C = -10.0°

NPR	w_p/w_i	F/F_i	F_r/F_i	δ_p	δ_y
2.0003	0.9549	1.0063	1.0064	0.32	-0.17
3.0015	0.9700	0.9937	0.9937	0.27	-0.31
4.0020	0.9694	0.9805	0.9806	-0.20	-0.87
4.9969	0.9675	0.9672	0.9677	-0.76	-1.69
6.0054	0.9661	0.9568	0.9580	-1.33	-2.51

δ_A = -10.0°, δ_B = 10.0° , δ_C = -10.0°

NPR	w_p/w_i	F/F_i	F_r/F_i	δ_p	δ_y
2.0044	0.9553	0.9964	0.9966	-0.34	-1.23
3.0033	0.9705	0.9865	0.9868	-0.49	-1.47
3.9999	0.9694	0.9715	0.9724	-1.13	-2.30
5.0000	0.9676	0.9581	0.9602	-1.78	-3.33
6.0023	0.9662	0.9472	0.9503	-2.34	-4.07

δ_A = -10.0°, δ_B = 15.0° , δ_C = -10.0°

NPR	w_p/w_i	F/F_i	F_r/F_i	δ_p	δ_y
2.0043	0.9554	0.9787	0.9806	-1.51	-3.18
3.0003	0.9704	0.9692	0.9714	-1.67	-3.43
4.0042	0.9695	0.9559	0.9594	-2.33	-4.30
5.0000	0.9677	0.9419	0.9471	-3.06	-5.21
6.0008	0.9662	0.9309	0.9378	-3.61	-5.97

Table 9. Continued

δ_A = -10.0°, δ_B = 17.5° , δ_C = -10.0°

NPR	w_p/w_i	F/F_i	F_r/F_i	δ_p	δ_y
2.0041	0.9548	0.9637	0.9679	-2.42	-4.76
3.0031	0.9708	0.9545	0.9592	-2.70	-4.99
4.0042	0.9695	0.9439	0.9499	-3.23	-5.65
5.0015	0.9676	0.9313	0.9394	-3.83	-6.49
5.9992	0.9662	0.9205	0.9303	-4.38	-7.12

δ_A = -10.0°, δ_B = 20.0° , δ_C = -10.0°

NPR	w_p/w_i	F/F_i	F_r/F_i	δ_p	δ_y
2.0027	0.9547	0.9491	0.9558	-3.37	-5.87
3.0056	0.9705	0.9407	0.9479	-3.54	-6.15
4.0031	0.9695	0.9305	0.9390	-4.00	-6.61
5.0063	0.9676	0.9186	0.9293	-4.62	-7.41
5.9965	0.9661	0.9088	0.9209	-4.99	-7.90

δ_A = -10.0°, δ_B = 22.5° , δ_C = -10.0°

NPR	w_p/w_i	F/F_i	F_r/F_i	δ_p	δ_y
2.0008	0.9538	0.9323	0.9417	-4.09	-7.03
3.0024	0.9707	0.9251	0.9352	-4.22	-7.33
4.0001	0.9695	0.9183	0.9294	-4.58	-7.60
4.9991	0.9675	0.9056	0.9188	-5.17	-8.31
5.9966	0.9662	0.8960	0.9106	-5.60	-8.67

δ_A = -10.0°, δ_B = 25.0° , δ_C = -10.0°

NPR	w_p/w_i	F/F_i	F_r/F_i	δ_p	δ_y
2.0038	0.9550	0.9190	0.9314	-4.75	-8.13
3.0032	0.9707	0.9098	0.9232	-5.10	-8.36
4.0002	0.9695	0.9034	0.9174	-5.29	-8.56
5.0005	0.9679	0.8930	0.9091	-5.82	-9.15
5.9966	0.9662	0.8832	0.9006	-6.23	-9.46

Table 9. Concluded

δ_A = -10.0°, δ_B = 27.5° , δ_C = -10.0°

NPR	w_p/w_i	F/F_i	F_r/F_i	δ_p	δ_y
2.0032	0.9548	0.9046	0.9199	-5.64	-8.87
3.0005	0.9706	0.8947	0.9116	-5.84	-9.44
3.9975	0.9693	0.8901	0.9075	-6.09	-9.49
4.9985	0.9677	0.8788	0.8980	-6.65	-9.93
5.9964	0.9662	0.8683	0.8889	-7.02	-10.25

δ_A = -10.0°, δ_B = 30.0° , δ_C = -10.0°

NPR	w_p/w_i	F/F_i	F_r/F_i	δ_p	δ_y
2.0002	0.9551	0.8897	0.9082	-6.14	-9.90
3.0089	0.9707	0.8829	0.9022	-6.26	-10.15
4.0023	0.9696	0.8760	0.8954	-6.59	-10.04
5.0053	0.9676	0.8654	0.8866	-7.12	-10.43
5.9691	0.9662	0.8558	0.8781	-7.53	-10.65
6.0041	0.9662	0.8550	0.8774	-7.54	-10.65

δ_A = -10.0°, δ_B = 35.0° , δ_C = -10.0°

NPR	w_p/w_i	F/F_i	F_r/F_i	δ_p	δ_y
2.0057	0.9552	0.8564	0.8810	-7.83	-11.21
3.0034	0.9703	0.8442	0.8693	-8.16	-11.31
4.0011	0.9697	0.8375	0.8637	-8.47	-11.48
5.0024	0.9678	0.8313	0.8585	-8.92	-11.56
5.9982	0.9663	0.8242	0.8510	-9.18	-11.29

Table 10. Maximum A/B-Power Nozzle Performance of Rotating Vane Actuation System for Three Standard Vanes Installed With Vane B Deployed and Vanes A and C Partially Retracted

[δ_p and δ_y are given in degrees]

δ_A = -5.0°, δ_B = 30.0° , δ_C = -5.0°

NPR	w_p/w_i	F/F_i	F_r/F_i	δ_p	δ_y
2.0052	0.9539	0.8904	0.9080	-5.98	-9.67
3.0032	0.9706	0.8806	0.8987	-6.29	-9.72
3.9996	0.9694	0.8738	0.8919	-6.64	-9.55
4.9981	0.9677	0.8638	0.8831	-7.30	-9.64
6.0060	0.9662	0.8549	0.8740	-7.53	-9.49
6.0001	0.9661	0.8546	0.8738	-7.50	-9.51

δ_A = -5.0°, δ_B = 25.0° , δ_C = -5.0°

NPR	w_p/w_i	F/F_i	F_r/F_i	δ_p	δ_y
2.0021	0.9548	0.9169	0.9302	-5.15	-8.28
3.0075	0.9706	0.9071	0.9214	-5.41	-8.55
4.0008	0.9695	0.9009	0.9154	-5.62	-8.57
5.0032	0.9678	0.8894	0.9054	-6.24	-8.89
5.9970	0.9662	0.8798	0.8963	-6.51	-8.95

δ_A = 0.0°, δ_B = 30.0° , δ_C = 0.0°

NPR	w_p/w_i	F/F_i	F_r/F_i	δ_p	δ_y
2.0054	0.9538	0.8761	0.8938	-7.26	-8.89
2.9999	0.9702	0.8657	0.8822	-7.18	-8.57
4.0058	0.9693	0.8595	0.8751	-7.10	-8.26
5.0065	0.9676	0.8479	0.8644	-7.47	-8.47
5.9976	0.9661	0.8389	0.8546	-7.35	-8.23

Table 11. Maximum A/B-Power Nozzle Performance of Rotating Vane Actuation System for Three Standard Vanes Installed With Vanes A and B Equally Deployed and Vane C Fully Retracted

[δ_p and δ_y are given in degrees]

δ_A = 25.0°, δ_B = 25.0°, δ_C = -10.0°

NPR	w_p/w_i	F/F_i	F_r/F_i	δ_p	δ_y
2.0047	0.9530	0.7896	0.8179	7.08	-13.50
3.0003	0.9709	0.7732	0.8057	7.86	-14.49
4.0009	0.9693	0.7657	0.7956	7.12	-14.18
5.0012	0.9677	0.7635	0.7886	6.04	-13.27
6.0018	0.9662	0.7627	0.7846	5.34	-12.56

δ_A = 30.0°, δ_B = 30.0°, δ_C = -10.0°

NPR	w_p/w_i	F/F_i	F_r/F_i	δ_p	δ_y
1.9997	0.9519	0.7159	0.7563	8.68	-16.94
3.0090	0.9701	0.6986	0.7355	7.79	-16.65
4.0063	0.9693	0.6956	0.7273	6.28	-15.89
5.0058	0.9678	0.6950	0.7219	5.11	-14.91
6.0097	0.9664	0.6952	0.7190	4.49	-14.14

Table 12. Maximum A/B-Power Nozzle Performance of Rotating Vane Actuation System for Three Standard Vanes Installed With Vanes A and B Equally Deployed and Vane C Partially Retracted

[δ_p and δ_y are given in degrees]

δ_A = 30.0°, δ_B = 30.0°, δ_C = -5.0°

NPR	w_p/w_i	F/F_i	F_r/F_i	δ_p	δ_y
2.0024	0.9510	0.6958	0.7238	5.44	-15.12
3.0064	0.9696	0.6758	0.6993	4.46	-14.27
4.0035	0.9694	0.6714	0.6911	3.29	-13.31
5.0005	0.9676	0.6743	0.6920	2.45	-12.79
5.9987	0.9661	0.6734	0.6897	1.98	-12.33

Table 13. Maximum A/B-Power Nozzle Performance of Rotating Vane Actuation System for Three Standard Vanes Installed With Vanes B and C Equally Deployed and Vane A Fully Retracted

[δ_p and δ_y are given in degrees]

δ_A = -10.0°, δ_B = 25.0°, δ_C = 25.0°

NPR	w_p/w_i	F/F_i	F_r/F_i	δ_p	δ_y
2.0099	0.9533	0.7816	0.8276	-19.10	-2.16
3.0024	0.9705	0.7630	0.8153	-20.54	-2.05
4.0035	0.9694	0.7566	0.8080	-20.46	-2.11
4.9966	0.9676	0.7547	0.8001	-19.29	-2.30
5.9978	0.9662	0.7507	0.7918	-18.41	-2.36

δ_A = -10.0°, δ_B = 30.0°, δ_C = 30.0°

NPR	w_p/w_i	F/F_i	F_r/F_i	δ_p	δ_y
2.0043	0.9488	0.6924	0.7664	-25.23	-3.22
3.0050	0.9698	0.6683	0.7424	-25.67	-3.16
4.0043	0.9692	0.6631	0.7288	-24.35	-3.23
5.0087	0.9676	0.6638	0.7190	-22.38	-3.34
6.0137	0.9662	0.6631	0.7129	-21.30	-3.51
6.0061	0.9663	0.6636	0.7130	-21.22	-3.49

Table 14. Maximum A/B-Power Nozzle Performance of Rotating Vane Actuation System for Three Standard Vanes Installed With Vanes B and C Equally Deployed and Vane A Partially Retracted

[δ_p and δ_y are given in degrees]

δ_A = -5.0°, δ_B = 30.0°, δ_C = 30.0°

NPR	w_p/w_i	F/F_i	F_r/F_i	δ_p	δ_y
2.0001	0.9504	0.6989	0.7556	-22.11	-3.49
3.0155	0.9697	0.6770	0.7304	-21.83	-3.44
3.0062	0.9694	0.6731	0.7281	-22.21	-3.40
4.0063	0.9693	0.6711	0.7183	-20.60	-3.63
4.9975	0.9674	0.6713	0.7125	-19.28	-3.70
5.9989	0.9661	0.6728	0.7101	-18.35	-3.62

Table 15. Maximum A/B-Power Nozzle Performance of Rotating Vane Actuation System for Three Standard Vanes Installed With Vanes A and C Equally Deployed and Vane B Fully Retracted

[δ_p and δ_y are given in degrees]

δ_A = 25.0°, δ_B = -10.0°, δ_C = 25.0°

NPR	w_p/w_i	F/F_i	F_r/F_i	δ_p	δ_y
2.0032	0.9536	0.8086	0.8201	4.13	8.72
3.0013	0.9705	0.7862	0.7988	4.41	9.20
4.0003	0.9696	0.7777	0.7876	3.62	8.33
5.0077	0.9678	0.7733	0.7800	2.74	6.99
6.0039	0.9664	0.7718	0.7767	2.22	6.07

δ_A = 30.0°, δ_B = -10.0°, δ_C = 30.0°

NPR	w_p/w_i	F/F_i	F_r/F_i	δ_p	δ_y
1.9993	0.9513	0.7066	0.7175	3.09	9.51
3.0036	0.9704	0.6839	0.6920	2.20	8.55
4.0060	0.9693	0.6800	0.6861	1.33	7.58
5.0038	0.9677	0.6800	0.6847	0.86	6.64
6.0013	0.9663	0.6799	0.6836	0.59	5.94

Table 16. Maximum A/B-Power Nozzle Performance of Rotating Vane Actuation System for Three Standard Vanes Installed With Vanes A and C Equally Deployed and Vane B Partially Retracted

[δ_p and δ_y are given in degrees]

δ_A = 30.0°, δ_B = -5.0°, δ_C = 30.0°

NPR	w_p/w_i	F/F_i	F_r/F_i	δ_p	δ_y
2.0030	0.9524	0.7195	0.7246	1.88	6.56
2.9998	0.9700	0.6970	0.7002	0.96	5.40
4.0041	0.9692	0.6924	0.6946	0.08	4.49
5.0048	0.9675	0.6920	0.6934	-0.33	3.72
6.0036	0.9664	0.6909	0.6921	-0.49	3.28

Table 17. Maximum A/B-Power Nozzle Performance of Rotating Vane Actuation System for Single Large Vane Installed and Deployed

[δ_p and δ_y are given in degrees]

δ_A = 30.0°, δ_B = off , δ_C = off

NPR	w_p/w_i	F/F_i	F_r/F_i	δ_p	δ_y
2.0013	0.9550	0.8452	0.8843	17.06	-1.15
2.9972	0.9707	0.8309	0.8756	18.35	-1.39
3.9978	0.9695	0.8294	0.8745	18.44	-1.46
5.0009	0.9678	0.8228	0.8707	19.03	-1.52
6.0034	0.9664	0.8157	0.8657	19.51	-1.61

δ_A = 25.0°, δ_B = off , δ_C = off

NPR	w_p/w_i	F/F_i	F_r/F_i	δ_p	δ_y
2.0073	0.9610	0.8974	0.9237	13.65	-1.24
2.9963	0.9746	0.8821	0.9119	14.65	-1.16
4.0134	0.9700	0.8757	0.9068	15.00	-1.14
5.0152	0.9684	0.8668	0.9013	15.85	-1.22
6.0027	0.9670	0.8596	0.8963	16.39	-1.29

Table 18. Maximum A/B-Power Nozzle Performance of Rotating Vane Actuation System With Large Vane and One Standard Vane Installed and Deployed

[δ_p and δ_y are given in degrees]

δ_A = 30.0°, δ_B = 30.0° , δ_C = off

NPR	w_p/w_i	F/F_i	F_r/F_i	δ_p	δ_y
2.0084	0.9498	0.6337	0.7329	20.52	-23.96
2.9996	0.9697	0.6099	0.7194	22.03	-25.49
4.0066	0.9692	0.6017	0.7158	22.50	-26.28
4.1658	0.9692	0.5997	0.7142	22.52	-26.40
4.1683	0.9693	0.6003	0.7148	22.55	-26.35

δ_A = 30.0°, δ_B = off , δ_C = 30.0°

NPR	w_p/w_i	F/F_i	F_r/F_i	δ_p	δ_y
1.9972	0.9499	0.6431	0.6884	15.43	14.79
3.0066	0.9701	0.6183	0.6688	16.30	16.19
4.0015	0.9694	0.6097	0.6620	16.70	16.59
5.0070	0.9675	0.6069	0.6585	16.75	16.41
5.9971	0.9664	0.6051	0.6552	16.69	16.04

δ_A = 25.0°, δ_B = 25.0° , δ_C = off

NPR	w_p/w_i	F/F_i	F_r/F_i	δ_p	δ_y
2.0092	0.9607	0.7473	0.7991	13.33	-16.46
3.0008	0.9751	0.7260	0.7865	14.93	-17.75
4.0158	0.9695	0.7187	0.7834	15.52	-18.42
4.9887	0.9685	0.7163	0.7819	15.68	-18.56

δ_A = 25.0°, δ_B = off , δ_C = 25.0°

NPR	w_p/w_i	F/F_i	F_r/F_i	δ_p	δ_y
2.0166	0.9595	0.7603	0.7832	10.41	9.41
3.0026	0.9746	0.7379	0.7652	11.35	10.57
4.0094	0.9701	0.7286	0.7576	11.60	11.20
5.0022	0.9685	0.7242	0.7544	11.87	11.45
6.0073	0.9668	0.7262	0.7561	11.95	11.22

Table 19. Maximum A/B-Power Nozzle Performance of Rotating Vane Actuation System for Large Vane and Two Standard Vanes Installed With Vane A Deployed and Vanes B and C Fully Retracted

[δ_p and δ_y are given in degrees]

δ_A = 0.0°, δ_B = -10.0° , δ_C = -10.0°

NPR	w_p/w_i	F/F_i	F_r/F_i	δ_p	δ_y
2.0040	0.9548	1.0061	1.0061	0.23	0.16
3.0019	0.9702	0.9958	0.9959	0.32	0.24
4.0002	0.9692	0.9837	0.9837	0.41	0.23
5.0011	0.9675	0.9716	0.9717	1.09	0.21
6.0022	0.9663	0.9611	0.9617	2.03	0.12

δ_A = 5.0°, δ_B = -10.0° , δ_C = -10.0°

NPR	w_p/w_i	F/F_i	F_r/F_i	δ_p	δ_y
2.0044	0.9548	1.0042	1.0042	0.64	0.16
3.0250	0.9707	0.9940	0.9941	0.89	0.17
3.0027	0.9703	0.9934	0.9935	0.88	0.18
3.9980	0.9693	0.9785	0.9789	1.75	0.18
5.0058	0.9676	0.9644	0.9658	3.09	0.05
6.0025	0.9662	0.9530	0.9558	4.39	-0.15

δ_A = 10.0°, δ_B = -10.0° , δ_C = -10.0°

NPR	w_p/w_i	F/F_i	F_r/F_i	δ_p	δ_y
2.0033	0.9553	0.9930	0.9937	2.13	0.11
3.0010	0.9703	0.9825	0.9835	2.56	0.06
4.0005	0.9692	0.9654	0.9678	4.03	-0.08
4.9994	0.9677	0.9505	0.9553	5.77	-0.21
6.0010	0.9662	0.9386	0.9461	7.25	-0.39

δ_A = 15.0°, δ_B = -10.0° , δ_C = -10.0°

NPR	w_p/w_i	F/F_i	F_r/F_i	δ_p	δ_y
2.0024	0.9546	0.9673	0.9718	5.49	-0.22
3.0008	0.9704	0.9570	0.9623	6.04	-0.26
3.9990	0.9695	0.9429	0.9508	7.37	-0.38
5.0014	0.9676	0.9269	0.9392	9.24	-0.52
6.0043	0.9662	0.9167	0.9323	10.49	-0.71

Table 19. Continued

δ_A = 17.5°, δ_B = -10.0° , δ_C = -10.0°

NPR	w_p/w_i	F/F_i	F_r/F_i	δ_p	δ_y
2.0024	0.9545	0.9510	0.9594	7.58	-0.47
3.0023	0.9704	0.9390	0.9489	8.26	-0.49
4.0032	0.9692	0.9261	0.9390	9.51	-0.58
4.9965	0.9676	0.9127	0.9304	11.15	-0.75
5.9963	0.9662	0.9029	0.9238	12.17	-0.94

δ_A = 20.0°, δ_B = -10.0° , δ_C = -10.0°

NPR	w_p/w_i	F/F_i	F_r/F_i	δ_p	δ_y
2.0042	0.9542	0.9282	0.9430	10.16	-0.67
2.9993	0.9706	0.9150	0.9323	11.03	-0.74
4.0000	0.9693	0.9056	0.9256	11.93	-0.78
5.0034	0.9676	0.8943	0.9187	13.21	-0.98
6.0016	0.9663	0.8859	0.9131	13.97	-1.16

δ_A = 22.5°, δ_B = -10.0° , δ_C = -10.0°

NPR	w_p/w_i	F/F_i	F_r/F_i	δ_p	δ_y
2.0070	0.9545	0.9068	0.9280	12.26	-0.83
3.0054	0.9704	0.8937	0.9183	13.28	-0.94
4.0019	0.9693	0.8872	0.9137	13.81	-0.99
5.0051	0.9677	0.8779	0.9081	14.79	-1.13
5.9968	0.9662	0.8702	0.9022	15.24	-1.36

δ_A = 25.0°, δ_B = -10.0° , δ_C = -10.0°

NPR	w_p/w_i	F/F_i	F_r/F_i	δ_p	δ_y
1.9975	0.9540	0.8858	0.9143	14.29	-1.03
3.0023	0.9702	0.8719	0.9045	15.38	-1.19
4.0036	0.9692	0.8672	0.9006	15.62	-1.21
4.9990	0.9676	0.8594	0.8954	16.25	-1.36
5.9988	0.9661	0.8518	0.8888	16.53	-1.61

Table 19. Concluded

δ_A = 27.5°, δ_B = -10.0° , δ_C = -10.0°

NPR	w_p/w_i	F/F_i	F_r/F_i	δ_p	δ_y
2.0033	0.9547	0.8632	0.8999	16.37	-1.27
3.0054	0.9710	0.8507	0.8910	17.25	-1.44
3.9980	0.9693	0.8473	0.8866	17.06	-1.49
5.0011	0.9675	0.8401	0.8810	17.44	-1.69
5.9983	0.9662	0.8327	0.8742	17.63	-2.07

δ_A = 30.0°, δ_B = -10.0° , δ_C = -10.0°

NPR	w_p/w_i	F/F_i	F_r/F_i	δ_p	δ_y
2.0029	0.9545	0.8431	0.8860	17.83	-1.48
3.0012	0.9706	0.8282	0.8736	18.49	-1.58
4.0006	0.9693	0.8267	0.8705	18.19	-1.82
5.0004	0.9675	0.8194	0.8642	18.41	-2.17
5.9989	0.9661	0.8127	0.8573	18.40	-2.58

δ_A = 35.0°, δ_B = -10.0° , δ_C = -10.0°

NPR	w_p/w_i	F/F_i	F_r/F_i	δ_p	δ_y
1.9999	0.9546	0.7926	0.8452	20.06	-3.52
3.0049	0.9709	0.7759	0.8308	20.58	-4.32
4.0045	0.9697	0.7754	0.8273	20.03	-4.27
5.0030	0.9680	0.7694	0.8195	19.72	-4.44
6.0013	0.9664	0.7690	0.8177	19.46	-4.30

Table 20. Maximum A/B-Power Nozzle Performance of Rotating Vane Actuation System for Large Vane and Two Standard Vanes Installed With Vane A Deployed and Vanes B and C Partially Retracted

[δ_p and δ_y are given in degrees]

δ_A = 30.0°, δ_B = -5.0° , δ_C = -5.0°

NPR	w_p/w_i	F/F_i	F_r/F_i	δ_p	δ_y
2.0041	0.9552	0.8384	0.8787	17.31	-2.11
2.9991	0.9704	0.8235	0.8653	17.70	-2.69
4.0016	0.9696	0.8199	0.8576	16.83	-2.76
5.0010	0.9678	0.8123	0.8493	16.72	-3.08
5.9991	0.9663	0.8055	0.8417	16.55	-3.46

δ_A = 30.0°, δ_B = -5.0° , δ_C = -5.0°

NPR	w_p/w_i	F/F_i	F_r/F_i	δ_p	δ_y
1.9984	0.9556	0.8396	0.8775	16.76	-2.33
2.9994	0.9706	0.8246	0.8642	17.18	-2.92
3.9995	0.9696	0.8205	0.8574	16.62	-3.11
4.9976	0.9678	0.8126	0.8490	16.49	-3.49
6.0019	0.9665	0.8066	0.8422	16.29	-3.90

δ_A = 25.0°, δ_B = -5.0° , δ_C = -5.0°

NPR	w_p/w_i	F/F_i	F_r/F_i	δ_p	δ_y
2.0064	0.9547	0.8842	0.9118	14.10	-1.06
3.0075	0.9710	0.8690	0.9005	15.15	-1.34
3.9987	0.9695	0.8639	0.8952	15.11	-1.62
5.0067	0.9678	0.8557	0.8878	15.33	-2.03
6.0001	0.9664	0.8480	0.8797	15.24	-2.44

δ_A = 30.0°, δ_B = 0.0° , δ_C = 0.0°

NPR	w_p/w_i	F/F_i	F_r/F_i	δ_p	δ_y
2.0064	0.9548	0.8286	0.8617	15.57	-3.53
3.0088	0.9707	0.8104	0.8431	15.52	-4.11
4.0048	0.9694	0.8066	0.8342	14.33	-3.79
4.9987	0.9681	0.7990	0.8252	13.97	-3.93
5.9976	0.9663	0.7930	0.8180	13.63	-4.11

Table 21. Maximum A/B-Power Nozzle Performance of Rotating Vane Actuation System for Large Vane and Two Standard Vanes Installed With Vane B Deployed and Vanes A and C Fully Retracted

[δ_p and δ_y are given in degrees]

δ_A = -10.0°, δ_B = 10.0° , δ_C = -10.0°

NPR	w_p/w_i	F/F_i	F_r/F_i	δ_p	δ_y
2.0039	0.9548	0.9968	0.9970	-0.31	-1.05
3.0050	0.9708	0.9862	0.9865	-0.44	-1.30
4.0017	0.9694	0.9721	0.9729	-1.10	-2.17
5.0046	0.9679	0.9581	0.9601	-1.88	-3.19
6.0097	0.9664	0.9467	0.9498	-2.48	-3.95
6.0011	0.9664	0.9469	0.9501	-2.46	-3.96

δ_A = -10.0°, δ_B = 15.0° , δ_C = -10.0°

NPR	w_p/w_i	F/F_i	F_r/F_i	δ_p	δ_y
1.9996	0.9561	0.9798	0.9818	-1.63	-3.21
2.9997	0.9708	0.9706	0.9728	-1.76	-3.41
3.9984	0.9697	0.9561	0.9596	-2.46	-4.25
5.0038	0.9678	0.9422	0.9476	-3.27	-5.17
5.9995	0.9661	0.9316	0.9385	-3.71	-5.89

δ_A = -10.0°, δ_B = 20.0° , δ_C = -10.0°

NPR	w_p/w_i	F/F_i	F_r/F_i	δ_p	δ_y
2.0071	0.9560	0.9497	0.9563	-3.32	-5.86
3.0053	0.9709	0.9411	0.9483	-3.51	-6.14
4.0029	0.9695	0.9315	0.9399	-4.00	-6.55
5.0144	0.9681	0.9182	0.9289	-4.74	-7.37
5.0063	0.9678	0.9186	0.9293	-4.71	-7.38
6.0085	0.9664	0.9083	0.9206	-5.11	-7.90

δ_A = -10.0°, δ_B = 25.0° , δ_C = -10.0°

NPR	w_p/w_i	F/F_i	F_r/F_i	δ_p	δ_y
2.0010	0.9552	0.9198	0.9320	-4.68	-8.07
3.0011	0.9705	0.9108	0.9240	-4.93	-8.41
3.9999	0.9694	0.9048	0.9187	-5.25	-8.51
5.0008	0.9677	0.8937	0.9100	-5.87	-9.20
6.0067	0.9663	0.8839	0.9014	-6.09	-9.57
5.9960	0.9663	0.8845	0.9019	-6.14	-9.51

Table 21. Concluded

δ_A = -10.0°, δ_B = 35.0° , δ_C = -10.0°

NPR	w_p/w_i	F/F_i	F_r/F_i	δ_p	δ_y
1.9967	0.9546	0.8504	0.8753	-7.83	-11.37
3.0031	0.9709	0.8401	0.8655	-7.95	-11.59
4.0075	0.9696	0.8311	0.8571	-8.05	-11.77
5.0048	0.9678	0.8234	0.8496	-8.16	-11.84
6.0047	0.9665	0.8157	0.8414	-8.04	-11.82

δ_A = -10.0°, δ_B = 30.0° , δ_C = -10.0°

NPR	w_p/w_i	F/F_i	F_r/F_i	δ_p	δ_y
2.0023	0.9536	0.8824	0.9017	-6.28	-10.15
3.0079	0.9701	0.8723	0.8926	-6.55	-10.41
3.9993	0.9692	0.8684	0.8889	-6.74	-10.44
5.0082	0.9677	0.8572	0.8798	-7.37	-10.84
5.0040	0.9676	0.8569	0.8792	-7.30	-10.78
5.9979	0.9663	0.8476	0.8706	-7.48	-11.00

Table 22. Maximum A/B-Power Nozzle Performance of Rotating Vane Actuation System for Large Vane and Two Standard Vanes Installed With Vane B Deployed and Vanes A and C Partially Retracted

[δ_p and δ_y are given in degrees]

δ_A = -5.0°, δ_B = 30.0° , δ_C = -5.0°

NPR	w_p/w_i	F/F_i	F_r/F_i	δ_p	δ_y
2.0002	0.9544	0.8835	0.9021	-6.27	-9.91
2.9987	0.9706	0.8713	0.8902	-6.61	-9.92
4.0010	0.9695	0.8680	0.8863	-6.71	-9.64
4.9979	0.9677	0.8575	0.8766	-7.08	-9.78
5.9988	0.9664	0.8476	0.8663	-7.01	-9.73

δ_A = -5.0°, δ_B = 25.0° , δ_C = -5.0°

NPR	w_p/w_i	F/F_i	F_r/F_i	δ_p	δ_y
2.0049	0.9553	0.9169	0.9298	-5.06	-8.11
3.0064	0.9706	0.9081	0.9216	-5.26	-8.37
4.0039	0.9695	0.9032	0.9171	-5.46	-8.39
5.0024	0.9677	0.8921	0.9072	-5.94	-8.71
5.9985	0.9664	0.8816	0.8969	-5.93	-8.85

δ_A = 0.0°, δ_B = -30.0° , δ_C = 0.0°

NPR	w_p/w_i	F/F_i	F_r/F_i	δ_p	δ_y
2.0029	0.9539	0.8783	0.8941	-6.55	-8.67
3.0074	0.9705	0.8666	0.8814	-6.32	-8.47
3.9993	0.9691	0.8591	0.8730	-6.06	-8.30
4.9962	0.9676	0.8482	0.8618	-5.92	-8.34
5.9996	0.9661	0.8382	0.8510	-5.38	-8.39

Table 23. Maximum A/B-Power Nozzle Performance of Rotating Vane Actuation System for Large Vane and Two Standard Vanes Installed With Vane C Deployed and Vanes A and B Fully Retracted

[δ_p and δ_y are given in degrees]

δ_A = -10.0°, δ_B = -10.0° , δ_C = 10.0°

NPR	w_p/w_i	F/F_i	F_r/F_i	δ_p	δ_y
2.0018	0.9553	0.9977	0.9980	-0.69	0.98
3.0017	0.9704	0.9891	0.9894	-0.78	1.24
4.0015	0.9692	0.9733	0.9743	-1.64	2.12
5.0021	0.9678	0.9595	0.9618	-2.57	3.01
6.0040	0.9662	0.9478	0.9512	-3.27	3.65

δ_A = -10.0°, δ_B = -10.0° , δ_C = 15.0°

NPR	w_p/w_i	F/F_i	F_r/F_i	δ_p	δ_y
2.0026	0.9557	0.9815	0.9835	-2.28	2.91
3.0029	0.9703	0.9723	0.9746	-2.44	3.09
4.0033	0.9692	0.9573	0.9611	-3.31	3.90
5.0020	0.9680	0.9435	0.9493	-4.24	4.71
6.0050	0.9661	0.9326	0.9399	-4.89	5.25

δ_A = -10.0°, δ_B = -10.0° , δ_C = 20.0°

NPR	w_p/w_i	F/F_i	F_r/F_i	δ_p	δ_y
2.0049	0.9555	0.9541	0.9600	-4.05	4.93
3.0045	0.9703	0.9444	0.9514	-4.46	5.36
4.0021	0.9692	0.9343	0.9429	-5.09	5.86
5.0048	0.9681	0.9210	0.9322	-6.07	6.55
6.0101	0.9663	0.9108	0.9234	-6.61	6.85
5.9948	0.9662	0.9113	0.9239	-6.61	6.86

δ_A = -10.0°, δ_B = -10.0° , δ_C = 25.0°

NPR	w_p/w_i	F/F_i	F_r/F_i	δ_p	δ_y
2.0056	0.9547	0.9255	0.9376	-5.99	7.06
3.0022	0.9707	0.9151	0.9284	-6.35	7.37
4.0021	0.9696	0.9077	0.9221	-6.78	7.62
4.9958	0.9677	0.8970	0.9135	-7.42	8.09
6.0021	0.9663	0.8866	0.9044	-7.92	8.27

Table 23. Concluded

δ_A = -10.0°, δ_B = -10.0° , δ_C = 35.0°

NPR	w_p/w_i	F/F_i	F_r/F_i	δ_p	δ_y
2.0017	0.9549	0.8564	0.8810	-10.22	9.14
3.0027	0.9708	0.8427	0.8690	-10.80	9.31
4.0012	0.9695	0.8382	0.8638	-10.90	8.97
5.0037	0.9678	0.8268	0.8530	-11.47	8.66
5.9974	0.9662	0.8199	0.8450	-11.52	8.17

δ_A = -10.0°, δ_B = -10.0° , δ_C = 30.0°

NPR	w_p/w_i	F/F_i	F_r/F_i	δ_p	δ_y
2.0047	0.9541	0.9032	0.9195	-7.15	8.18
3.0017	0.9696	0.8910	0.9089	-7.58	8.57
4.0005	0.9691	0.8856	0.9043	-7.94	8.63
5.0004	0.9676	0.8758	0.8963	-8.56	8.90
5.9951	0.9662	0.8655	0.8866	-9.01	8.85

Table 24. Maximum A/B-Power Nozzle Performance of Rotating Vane Actuation System for Large Vane and Two Standard Vanes Installed With Vane C Deployed and Vanes A and B Partially Retracted

[δ_p and δ_y are given in degrees]

δ_A = -5.0°, δ_B = -5.0° , δ_C = 30.0°

NPR	w_p/w_i	F/F_i	F_r/F_i	δ_p	δ_y
2.0034	0.9543	0.8888	0.9077	-8.30	8.37
3.0005	0.9700	0.8771	0.8974	-8.79	8.64
4.0006	0.9693	0.8737	0.8933	-8.84	8.26
5.0006	0.9676	0.8638	0.8838	-9.42	7.93
6.0047	0.9661	0.8542	0.8736	-9.54	7.57
6.0012	0.9662	0.8543	0.8738	-9.55	7.59

δ_A = -5.0°, δ_B = -5.0° , δ_C = 25.0°

NPR	w_p/w_i	F/F_i	F_r/F_i	δ_p	δ_y
1.9985	0.9544	0.9239	0.9352	-5.91	6.71
3.0067	0.9709	0.9146	0.9275	-6.38	7.21
4.0067	0.9694	0.9079	0.9219	-6.88	7.33
5.0030	0.9679	0.8955	0.9113	-7.57	7.63
6.0013	0.9663	0.8852	0.9011	-8.00	7.31

δ_A = 0.0°, δ_B = 0.0° , δ_C = 30.0°

NPR	w_p/w_i	F/F_i	F_r/F_i	δ_p	δ_y
2.0002	0.9547	0.8760	0.8945	-9.28	7.23
3.0043	0.9707	0.8613	0.8785	-9.20	6.76
4.0003	0.9695	0.8541	0.8691	-8.55	6.47
4.9993	0.9678	0.8432	0.8575	-8.71	5.97
6.0076	0.9663	0.8340	0.8464	-8.30	5.32

Table 25. Maximum A/B-Power Nozzle Performance of Rotating Vane Actuation System for Large Vane and Two Standard Vanes Installed With Vanes A and B Equally Deployed and Vane C Fully Retracted

[δ_p and δ_y are given in degrees]

δ_A = 0.0°, δ_B = 0.0° , δ_C = -10.0°

NPR	w_p/w_i	F/F_i	F_r/F_i	δ_p	δ_y
2.0029	0.9559	1.0048	1.0048	-0.20	0.34
3.0042	0.9707	0.9958	0.9958	0.03	0.32
4.0051	0.9695	0.9827	0.9827	0.10	0.11
5.0015	0.9683	0.9697	0.9698	0.60	-0.37
6.0004	0.9665	0.9586	0.9590	1.28	-1.07

δ_A = 5.0°, δ_B = 5.0° , δ_C = -10.0°

NPR	w_p/w_i	F/F_i	F_r/F_i	δ_p	δ_y
2.0008	0.9557	1.0024	1.0024	0.31	-0.07
3.0036	0.9711	0.9917	0.9918	0.57	-0.20
4.0019	0.9695	0.9747	0.9750	1.19	-0.81
5.0072	0.9679	0.9580	0.9591	2.12	-1.74
6.0067	0.9664	0.9455	0.9478	2.95	-2.66

δ_A = 10.0°, δ_B = 10.0° , δ_C = -10.0°

NPR	w_p/w_i	F/F_i	F_r/F_i	δ_p	δ_y
2.0000	0.9557	0.9837	0.9842	1.43	-1.16
3.0013	0.9711	0.9721	0.9730	1.85	-1.60
4.0047	0.9693	0.9525	0.9544	2.59	-2.46
4.9983	0.9683	0.9338	0.9377	3.70	-3.68
6.0468	0.9664	0.9206	0.9269	4.75	-4.72
6.0075	0.9663	0.9213	0.9275	4.73	-4.70

δ_A = 15.0°, δ_B = 15.0° , δ_C = -10.0°

NPR	w_p/w_i	F/F_i	F_r/F_i	δ_p	δ_y
2.0037	0.9555	0.9255	0.9308	3.99	-4.65
3.0019	0.9710	0.9104	0.9179	4.94	-5.46
4.0002	0.9698	0.8908	0.9016	5.99	-6.62
5.0033	0.9678	0.8775	0.8916	6.96	-7.55
5.9955	0.9665	0.8673	0.8837	7.55	-8.18

Table 25. Concluded

δ_A = 20.0°, δ_B = 20.0° , δ_C = -10.0°

NPR	w_p/w_i	F/F_i	F_r/F_i	δ_p	δ_y
2.0014	0.9549	0.8337	0.8576	8.82	-10.44
3.0007	0.9709	0.8125	0.8423	10.15	-11.68
4.0055	0.9692	0.7996	0.8321	10.59	-12.37
5.0016	0.9676	0.7918	0.8220	10.14	-12.07
6.0059	0.9662	0.7876	0.8147	9.59	-11.50
5.9937	0.9662	0.7878	0.8151	9.64	-11.54

δ_A = 25.0°, δ_B = 25.0° , δ_C = -10.0°

NPR	w_p/w_i	F/F_i	F_r/F_i	δ_p	δ_y
2.0018	0.9523	0.7366	0.7892	13.65	-16.63
3.0021	0.9698	0.7146	0.7730	14.71	-17.65
4.0021	0.9694	0.7085	0.7604	13.81	-16.83
5.0009	0.9677	0.7084	0.7519	12.56	-15.52
6.0006	0.9663	0.7095	0.7470	11.67	-14.40

δ_A = 30.0°, δ_B = 30.0° , δ_C = -10.0°

NPR	w_p/w_i	F/F_i	F_r/F_i	δ_p	δ_y
2.0015	0.9468	0.6216	0.6847	16.27	-19.71
2.9999	0.9696	0.5944	0.6524	16.03	-19.26
4.0000	0.9692	0.5902	0.6445	15.21	-19.01
4.9997	0.9679	0.5924	0.6420	14.37	-18.25
6.0060	0.9662	0.5932	0.6398	13.84	-17.77

Table 26. Maximum A/B-Power Nozzle Performance of Rotating Vane Actuation System for Large Vane and Two Standard Vanes Installed With Vanes A and B Equally Deployed and Vane C Partially Retracted

[δ_p and δ_y are given in degrees]

δ_A = 25.0°, δ_B = 25.0° , δ_C = -5.0°

NPR	w_p/w_i	F/F_i	F_r/F_i	δ_p	δ_y
2.0021	0.9528	0.7277	0.7783	13.13	-16.66
3.0041	0.9704	0.7060	0.7521	12.74	-16.14
4.0039	0.9691	0.6994	0.7368	11.37	-14.76
5.0027	0.9676	0.6986	0.7296	10.25	-13.54
5.9993	0.9662	0.6982	0.7258	9.71	-12.76

δ_A = 30.0°, δ_B = 30.0° , δ_C = -5.0°

NPR	w_p/w_i	F/F_i	F_r/F_i	δ_p	δ_y
2.0042	0.9489	0.6236	0.6688	13.59	-16.85
3.0076	0.9699	0.6018	0.6417	12.92	-16.22
3.9979	0.9694	0.5987	0.6356	12.06	-15.94
4.9976	0.9682	0.6007	0.6349	11.36	-15.49
5.9975	0.9663	0.6011	0.6333	10.99	-15.07
5.9989	0.9664	0.6011	0.6332	10.94	-15.04

δ_A = 30.0°, δ_B = 30.0° , δ_C = 0.0°

NPR	w_p/w_i	F/F_i	F_r/F_i	δ_p	δ_y
2.0069	0.9484	0.6095	0.6373	9.68	-14.21
3.0004	0.9704	0.5853	0.6083	8.92	-13.30
4.0031	0.9692	0.5828	0.6034	8.28	-12.71
4.9974	0.9679	0.5830	0.6031	7.96	-12.67
6.0036	0.9662	0.5860	0.6056	7.91	-12.46

Table 27. Maximum A/B-Power Nozzle Performance of Rotating Vane Actuation System for Large Vane and Two Standard Vanes Installed With Vanes B and C Equally Deployed and Vane A Fully Retracted

[δ_p and δ_y are given in degrees]

δ_A = -10.0°, δ_B = 0.0° , δ_C = 0.0°

NPR	w_p/w_i	F/F_i	F_r/F_i	δ_p	δ_y
2.0057	0.9555	1.0055	1.0056	0.48	-0.04
2.9999	0.9711	0.9977	0.9977	0.50	0.04
4.0024	0.9695	0.9839	0.9839	0.05	0.10
5.0028	0.9677	0.9707	0.9708	-0.77	0.14
5.9991	0.9662	0.9595	0.9599	-1.70	0.09

δ_A = -10.0°, δ_B = 5.0° , δ_C = 5.0°

NPR	w_p/w_i	F/F_i	F_r/F_i	δ_p	δ_y
1.9993	0.9556	1.0026	1.0026	-0.10	0.06
2.9992	0.9709	0.9910	0.9910	-0.18	0.06
4.0027	0.9697	0.9745	0.9747	-1.13	0.01
5.0028	0.9679	0.9589	0.9598	-2.40	-0.10
6.0037	0.9663	0.9468	0.9487	-3.60	-0.20

δ_A = -10.0°, δ_B = 10.0° , δ_C = 10.0°

NPR	w_p/w_i	F/F_i	F_r/F_i	δ_p	δ_y
2.0018	0.9557	0.9871	0.9875	-1.53	-0.12
3.0018	0.9711	0.9753	0.9758	-1.95	-0.15
3.9989	0.9696	0.9592	0.9607	-3.24	-0.23
4.9994	0.9683	0.9407	0.9442	-4.88	-0.37
5.0018	0.9679	0.9416	0.9450	-4.84	-0.41
5.9996	0.9665	0.9285	0.9339	-6.10	-0.50

δ_A = -10.0°, δ_B = 15.0° , δ_C = 15.0°

NPR	w_p/w_i	F/F_i	F_r/F_i	δ_p	δ_y
1.9993	0.9552	0.9461	0.9497	-4.99	-0.51
2.9998	0.9706	0.9314	0.9364	-5.91	-0.56
3.9997	0.9694	0.9168	0.9241	-7.18	-0.64
4.9996	0.9678	0.9033	0.9136	-8.57	-0.75
5.9979	0.9664	0.8908	0.9035	-9.58	-0.85

Table 27. Concluded

δ_A = -10.0°, δ_B = 20.0° , δ_C = 20.0°

NPR	w_p/w_i	F/F_i	F_r/F_i	δ_p	δ_y
2.0006	0.9553	0.8605	0.8808	-12.28	-1.24
2.9992	0.9714	0.8452	0.8700	-13.66	-1.26
4.0003	0.9696	0.8344	0.8625	-14.61	-1.33
4.9978	0.9679	0.8265	0.8547	-14.69	-1.46
5.0003	0.9679	0.8268	0.8552	-14.72	-1.49
5.9986	0.9663	0.8197	0.8473	-14.58	-1.64

δ_A = -10.0°, δ_B = 25.0° , δ_C = 25.0°

NPR	w_p/w_i	F/F_i	F_r/F_i	δ_p	δ_y
2.0041	0.9528	0.7805	0.8261	-18.99	-2.34
3.0060	0.9701	0.7613	0.8112	-20.13	-2.05
3.9999	0.9694	0.7557	0.7999	-19.03	-2.30
5.0054	0.9675	0.7531	0.7885	-17.06	-2.49
5.9967	0.9662	0.7502	0.7809	-15.94	-2.62

δ_A = -10.0°, δ_B = 30.0° , δ_C = 30.0°

NPR	w_p/w_i	F/F_i	F_r/F_i	δ_p	δ_y
2.0059	0.9504	0.7037	0.7665	-23.20	-3.17
3.0040	0.9695	0.6787	0.7383	-23.00	-3.22
4.0010	0.9694	0.6749	0.7226	-20.70	-3.41
4.9967	0.9674	0.6748	0.7129	-18.53	-3.54
5.9989	0.9661	0.6727	0.7051	-17.11	-3.55

Table 28. Maximum A/B-Power Nozzle Performance of Rotating Vane Actuation System for Large Vane and Two Standard Vanes Installed With Vanes B and C Equally Deployed and Vane A Partially Retracted

[δ_p and δ_y are given in degrees]

δ_A = -5.0°, δ_B = 25.0° , δ_C = 25.0°

NPR	w_p/w_i	F/F_i	F_r/F_i	δ_p	δ_y
1.9999	0.9534	0.7727	0.8195	-19.36	-2.00
3.0020	0.9707	0.7540	0.7975	-18.90	-2.26
4.0019	0.9695	0.7462	0.7791	-16.54	-2.61
5.0011	0.9679	0.7435	0.7686	-14.46	-2.81
5.9930	0.9663	0.7407	0.7628	-13.50	-3.05
6.0000	0.9663	0.7402	0.7623	-13.51	-3.02

δ_A = -5.0°, δ_B = 30.0° , δ_C = 30.0°

NPR	w_p/w_i	F/F_i	F_r/F_i	δ_p	δ_y
1.9995	0.9486	0.6804	0.7216	-19.13	-3.79
3.0017	0.9699	0.6558	0.6904	-17.85	-3.92
4.0238	0.9695	0.6519	0.6805	-16.15	-4.32
3.9997	0.9693	0.6526	0.6807	-16.03	-4.22
4.9997	0.9677	0.6520	0.6763	-14.87	-4.22
6.0018	0.9662	0.6520	0.6735	-13.93	-4.31
6.0028	0.9662	0.6520	0.6737	-13.97	-4.29

δ_A = 0.0°, δ_B = 30.0° , δ_C = 30.0°

NPR	w_p/w_i	F/F_i	F_r/F_i	δ_p	δ_y
1.9995	0.9476	0.6684	0.6906	-14.01	-4.08
2.9987	0.9701	0.6417	0.6588	-12.35	-4.45
4.0020	0.9694	0.6389	0.6537	-11.31	-4.74
4.9994	0.9677	0.6412	0.6543	-10.46	-4.86
5.9992	0.9663	0.6393	0.6513	-9.88	-4.98

Table 29. Maximum A/B-Power Nozzle Performance of Rotating Vane Actuation System for Large Vane and Two Standard Vanes Installed With Vanes A and C Equally Deployed and Vane B Fully Retracted

[δ_p and δ_y are given in degrees]

δ_A = 0.0°, δ_B = -10.0° , δ_C = 0.0°

NPR	w_p/w_i	F/F_i	F_r/F_i	δ_p	δ_y
1.9969	0.9555	1.0064	1.0064	-0.08	0.05
2.0054	0.9561	1.0061	1.0061	-0.11	0.09
1.9994	0.9558	1.0054	1.0054	-0.11	0.09
2.9975	0.9708	0.9952	0.9952	0.00	0.21
3.9992	0.9696	0.9826	0.9826	0.00	0.40
5.0059	0.9680	0.9696	0.9697	0.30	0.84
5.0028	0.9680	0.9696	0.9697	0.31	0.82
6.0011	0.9665	0.9583	0.9586	0.86	1.19

δ_A = 5.0°, δ_B = -10.0° , δ_C = 5.0°

NPR	w_p/w_i	F/F_i	F_r/F_i	δ_p	δ_y
2.0007	0.9554	1.0015	1.0015	0.26	0.31
3.0002	0.9711	0.9918	0.9918	0.43	0.46
3.9979	0.9695	0.9743	0.9746	0.88	0.92
5.0044	0.9681	0.9576	0.9583	1.62	1.52
5.9965	0.9663	0.9455	0.9469	2.39	2.00

δ_A = 10.0°, δ_B = -10.0° , δ_C = 10.0°

NPR	w_p/w_i	F/F_i	F_r/F_i	δ_p	δ_y
1.9984	0.9559	0.9865	0.9868	1.15	0.99
2.9991	0.9709	0.9734	0.9740	1.50	1.23
4.0005	0.9696	0.9540	0.9551	2.14	1.88
5.0015	0.9679	0.9354	0.9376	3.00	2.62
6.0006	0.9666	0.9217	0.9252	3.85	3.14

δ_A = 15.0°, δ_B = -10.0° , δ_C = 15.0°

NPR	w_p/w_i	F/F_i	F_r/F_i	δ_p	δ_y
1.9956	0.9554	0.9331	0.9357	3.22	2.74
2.0006	0.9557	0.9343	0.9368	3.21	2.78
3.0020	0.9706	0.9167	0.9201	3.64	3.30
3.9987	0.9698	0.8977	0.9027	4.55	3.98
5.0022	0.9678	0.8850	0.8913	5.27	4.36
5.9938	0.9665	0.8767	0.8837	5.68	4.47
6.0013	0.9664	0.8766	0.8836	5.68	4.49

Table 29. Concluded

δ_A = 20.0°, δ_B = -10.0° , δ_C = 20.0°

NPR	w_p/w_i	F/F_i	F_r/F_i	δ_p	δ_y
2.0026	0.9551	0.8534	0.8627	6.16	5.85
2.9999	0.9705	0.8290	0.8416	7.43	6.64
3.9988	0.9697	0.8130	0.8267	7.94	6.88
5.0042	0.9678	0.8035	0.8151	7.60	6.07
6.0003	0.9665	0.7993	0.8090	7.20	5.20

δ_A = 25.0°, δ_B = -10.0° , δ_C = 25.0°

NPR	w_p/w_i	F/F_i	F_r/F_i	δ_p	δ_y
2.0055	0.9531	0.7531	0.7759	10.02	9.84
2.9985	0.9707	0.7298	0.7531	10.60	9.78
4.0024	0.9698	0.7207	0.7377	9.44	8.08
4.9983	0.9678	0.7192	0.7315	8.52	6.23
6.0037	0.9663	0.7191	0.7290	7.93	5.13

δ_A = 30.0°, δ_B = -10.0° , δ_C = 30.0°

NPR	w_p/w_i	F/F_i	F_r/F_i	δ_p	δ_y
2.0000	0.9501	0.6558	0.6723	10.26	7.68
3.0036	0.9697	0.6328	0.6465	10.15	6.17
4.0029	0.9691	0.6280	0.6392	9.48	5.11
5.0015	0.9677	0.6305	0.6403	9.05	4.41
6.0001	0.9661	0.6365	0.6457	9.00	3.69

Table 30. Maximum A/B-Power Nozzle Performance of Rotating Vane Actuation System for Large Vane and Two Standard Vanes Installed With Vanes A and C Equally Deployed and Vane B Partially Retracted

[δ_p and δ_y are given in degrees]

δ_A = 25.0°, δ_B = -5.0° , δ_C = 25.0°

NPR	w_p/w_i	F/F_i	F_r/F_i	δ_p	δ_y
2.0013	0.9531	0.7253	0.7413	9.42	7.48
3.0018	0.9701	0.6998	0.7120	8.77	6.04
3.9985	0.9693	0.6956	0.7035	7.49	4.31
5.0037	0.9678	0.6956	0.7016	6.81	3.22
5.9977	0.9664	0.6963	0.7016	6.53	2.69

δ_A = 30.0°, δ_B = -5.0° , δ_C = 30.0°

NPR	w_p/w_i	F/F_i	F_r/F_i	δ_p	δ_y
2.0055	0.9500	0.6352	0.6432	8.24	3.73
3.0040	0.9705	0.6092	0.6154	7.80	2.50
4.0034	0.9695	0.6043	0.6095	7.28	1.75
5.0065	0.9677	0.6058	0.6105	6.97	1.45
6.0035	0.9664	0.6069	0.6116	7.04	1.29

δ_A = 30.0°, δ_B = 0.0° , δ_C = 30.0°

NPR	w_p/w_i	F/F_i	F_r/F_i	δ_p	δ_y
2.0005	0.9492	0.6180	0.6219	6.47	-0.29
3.0013	0.9696	0.5914	0.5948	6.06	-1.23
4.0037	0.9695	0.5874	0.5904	5.55	-1.60
5.0060	0.9676	0.5900	0.5929	5.41	-1.83
6.0023	0.9663	0.5901	0.5931	5.52	-1.91

Table 31. Maximum A/B-Power Nozzle Performance of Rotating Vane Actuation System for Large Vane and Two Standard Vanes Installed With Vanes A and B Unequally Deployed, $\delta_B = 30°$, and Vane C Fully Retracted

[δ_p and δ_y are given in degrees]

$\delta_A = 5.0°$, $\delta_C = -10.0°$

NPR	w_p/w_i	F/F_i	F_r/F_i	δ_p	δ_y
1.9996	0.9564	0.8634	0.8797	-0.71	-11.04
2.9992	0.9713	0.8513	0.8686	0.48	-11.46
3.9967	0.9699	0.8452	0.8632	1.20	-11.67
5.0044	0.9679	0.8344	0.8540	1.85	-12.16
5.9989	0.9666	0.8293	0.8493	2.46	-12.24

$\delta_A = 10.0°$, $\delta_C = -10.0°$

NPR	w_p/w_i	F/F_i	F_r/F_i	δ_p	δ_y
2.0041	0.9533	0.8446	0.8653	2.96	-12.23
3.0025	0.9695	0.8328	0.8546	4.39	-12.23
4.0052	0.9687	0.8267	0.8491	5.25	-12.18
4.9987	0.9672	0.8169	0.8410	5.92	-12.50
6.0036	0.9658	0.8078	0.8323	6.16	-12.61

$\delta_A = 15.0°$, $\delta_C = -10.0°$

NPR	w_p/w_i	F/F_i	F_r/F_i	δ_p	δ_y
1.9993	0.9525	0.8081	0.8386	7.55	-13.68
2.9984	0.9694	0.7928	0.8260	8.90	-13.86
4.0024	0.9686	0.7828	0.8164	9.43	-13.79
4.9966	0.9672	0.7762	0.8079	9.30	-13.37
5.9933	0.9656	0.7702	0.8005	9.14	-13.12

$\delta_A = 20.0°$, $\delta_C = -10.0°$

NPR	w_p/w_i	F/F_i	F_r/F_i	δ_p	δ_y
2.0036	0.9518	0.7544	0.8019	11.93	-16.27
3.0055	0.9691	0.7304	0.7793	12.88	-16.34
4.0034	0.9685	0.7220	0.7661	12.38	-15.59
5.0027	0.9671	0.7196	0.7579	11.42	-14.65
6.0141	0.9657	0.7179	0.7517	10.69	-13.86
5.9987	0.9656	0.7181	0.7520	10.72	-13.84

Table 31. Concluded

$\delta_A = 25.0°$, $\delta_C = -10.0°$

NPR	w_p/w_i	F/F_i	F_r/F_i	δ_p	δ_y
2.0025	0.9506	0.6907	0.7503	14.71	-18.43
3.0006	0.9689	0.6702	0.7284	14.99	-18.30
4.0003	0.9682	0.6652	0.7156	13.95	-17.19
4.9958	0.9671	0.6661	0.7098	12.86	-16.10
5.9979	0.9656	0.6670	0.7057	12.11	-15.13

Table 32. Maximum A/B-Power Nozzle Performance of Rotating Vane Actuation System for Large Vane and Two Standard Vanes Installed With Vane A Partially Retracted, $\delta_B = 30°$, and Vane C Fully Retracted

[δ_p and δ_y are given in degrees]

δ_A = -5.0°, δ_C = -10.0°

NPR	w_p/w_i	F/F_i	F_r/F_i	δ_p	δ_y
2.0053	0.9565	0.8892	0.9089	-6.15	-10.33
3.0004	0.9707	0.8807	0.8997	-5.86	-10.30
3.9987	0.9698	0.8752	0.8936	-5.72	-10.20
5.0017	0.9679	0.8628	0.8821	-5.81	-10.59
6.0015	0.9665	0.8546	0.8740	-5.52	-10.82

δ_A = 0.0°, δ_C = -10.0°

NPR	w_p/w_i	F/F_i	F_r/F_i	δ_p	δ_y
2.0005	0.9561	0.8847	0.9022	-4.25	-10.49
3.0026	0.9708	0.8713	0.8885	-3.47	-10.80
4.0020	0.9698	0.8664	0.8827	-2.79	-10.69
5.0024	0.9678	0.8544	0.8716	-2.23	-11.21
6.0021	0.9665	0.8443	0.8622	-1.50	-11.58

Table 33. Maximum A/B-Power Nozzle Performance of Rotating Vane Actuation System for Large Vane and Two Standard Vanes Installed With Vanes A and B Unequally Deployed, $\delta_B = 25°$, and Vane C Fully Retracted

[δ_p and δ_y are given in degrees]

$\delta_A = 5.0°$, $\delta_C = -10.0°$

NPR	w_p/w_i	F/F_i	F_r/F_i	δ_p	δ_y
2.0031	0.9583	0.9101	0.9219	-2.60	-8.81
3.0036	0.9710	0.8963	0.9083	-1.57	-9.17
4.0032	0.9694	0.8866	0.8987	-0.56	-9.43
5.0070	0.9679	0.8723	0.8864	0.59	-10.20
5.9980	0.9667	0.8621	0.8777	1.73	-10.66

$\delta_A = 10.0°$, $\delta_C = -10.0°$

NPR	w_p/w_i	F/F_i	F_r/F_i	δ_p	δ_y
2.0050	0.9573	0.8850	0.8978	1.04	-9.63
3.0049	0.9708	0.8689	0.8833	2.40	-10.12
4.0030	0.9696	0.8614	0.8769	3.49	-10.25
5.0102	0.9678	0.8514	0.8694	4.68	-10.78
5.0027	0.9678	0.8509	0.8691	4.74	-10.79
5.9915	0.9666	0.8446	0.8641	5.18	-11.10

$\delta_A = 15.0°$, $\delta_C = -10.0°$

NPR	w_p/w_i	F/F_i	F_r/F_i	δ_p	δ_y
2.0013	0.9575	0.8458	0.8665	5.67	-11.28
3.0022	0.9709	0.8282	0.8525	7.15	-11.82
4.0040	0.9692	0.8166	0.8440	8.17	-12.31
5.0014	0.9676	0.8083	0.8358	8.48	-12.24
5.9965	0.9666	0.8008	0.8277	8.51	-12.11

$\delta_A = 20.0°$, $\delta_C = -10.0°$

NPR	w_p/w_i	F/F_i	F_r/F_i	δ_p	δ_y
2.0016	0.9558	0.7950	0.8318	10.31	-13.93
2.9997	0.9710	0.7726	0.8140	11.51	-14.70
3.9982	0.9694	0.7627	0.8034	11.52	-14.62
5.0082	0.9679	0.7580	0.7935	10.79	-13.71
5.9905	0.9667	0.7600	0.7919	10.24	-12.96

Table 34. Maximum A/B-Power Nozzle Performance of Rotating Vane Actuation System for Large Vane and Two Standard Vanes Installed With Vane A Partially Retracted, $\delta_B = 25°$, and Vane C Fully Retracted

[δ_p and δ_y are given in degrees]

δ_A = -5.0°, δ_C = -10.0°

NPR	w_p/w_i	F/F_i	F_r/F_i	δ_p	δ_y
2.0002	0.9577	0.9227	0.9359	-4.94	-8.34
3.0008	0.9710	0.9105	0.9241	-4.99	-8.50
4.0032	0.9695	0.9042	0.9178	-5.00	-8.55
5.0086	0.9677	0.8933	0.9085	-5.20	-9.19
5.9998	0.9666	0.8832	0.8988	-4.97	-9.52

δ_A = 0.0°, δ_C = -10.0°

NPR	w_p/w_i	F/F_i	F_r/F_i	δ_p	δ_y
2.0024	0.9581	0.9199	0.9325	-4.37	-8.40
3.0013	0.9713	0.9078	0.9205	-4.08	-8.63
3.9997	0.9695	0.9007	0.9132	-3.67	-8.76
5.0057	0.9677	0.8881	0.9016	-3.04	-9.45
6.0028	0.9665	0.8759	0.8902	-2.11	-10.05

Table 35. Maximum A/B-Power Nozzle Performance of Rotating Vane Actuation System for Large Vane and Two Standard Vanes Installed With Vanes A and B Unequally Deployed, $\delta_B = 22.5°$, and Vane C Fully Retracted

[δ_p and δ_y are given in degrees]

δ_A = 10.0°, δ_C = -10.0°

NPR	w_p/w_i	F/F_i	F_r/F_i	δ_p	δ_y
1.9991	0.9540	0.9085	0.9176	0.23	-8.05
2.9982	0.9695	0.8943	0.9045	1.56	-8.50
4.0047	0.9688	0.8829	0.8944	2.69	-8.82
4.9937	0.9672	0.8709	0.8853	4.01	-9.56
6.0024	0.9660	0.8596	0.8763	4.96	-10.10

δ_A = 15.0°, δ_C = -10.0°

NPR	w_p/w_i	F/F_i	F_r/F_i	δ_p	δ_y
1.9983	0.9542	0.8688	0.8838	4.72	-9.48
3.0052	0.9697	0.8520	0.8708	6.22	-10.24
4.0003	0.9686	0.8381	0.8604	7.46	-10.87
4.9961	0.9672	0.8271	0.8511	8.02	-11.17
6.0011	0.9658	0.8194	0.8437	8.26	-11.18

δ_A = 20.0°, δ_C = -10.0°

NPR	w_p/w_i	F/F_i	F_r/F_i	δ_p	δ_y
2.0045	0.9534	0.8086	0.8411	9.99	-12.71
3.0006	0.9695	0.7877	0.8252	11.20	-13.59
4.0035	0.9685	0.7765	0.8149	11.36	-13.89
4.9999	0.9670	0.7712	0.8047	10.61	-13.04
5.9962	0.9657	0.7677	0.7974	9.98	-12.33

Table 36. Maximum A/B-Power Nozzle Performance of Rotating Vane Actuation System for Large Vane and Two Standard Vanes Installed With Vanes A and B Unequally Deployed, $\delta_B = 17.5°$, and Vane C Fully Retracted

[δ_p and δ_y are given in degrees]

$\delta_A = 10.0°$, $\delta_C = -10.0°$

NPR	w_p/w_i	F/F_i	F_r/F_i	δ_p	δ_y
2.0017	0.9551	0.9466	0.9503	0.30	-5.03
2.9998	0.9693	0.9316	0.9361	1.07	-5.56
4.0001	0.9692	0.9175	0.9236	2.12	-6.23
5.0012	0.9672	0.9011	0.9097	3.32	-7.17
6.0212	0.9654	0.8882	0.8994	4.27	-8.01
5.9971	0.9654	0.8883	0.8994	4.28	-7.99

$\delta_A = 15.0°$, $\delta_C = -10.0°$

NPR	w_p/w_i	F/F_i	F_r/F_i	δ_p	δ_y
2.0028	0.9553	0.9098	0.9176	4.06	-6.31
3.0051	0.9701	0.8923	0.9029	5.22	-7.09
4.0040	0.9686	0.8752	0.8894	6.35	-8.11
5.0004	0.9671	0.8616	0.8791	7.30	-8.91
6.0151	0.9660	0.8524	0.8716	7.79	-9.31
6.0052	0.9658	0.8526	0.8720	7.83	-9.35

Table 37. Maximum A/B-Power Nozzle Performance of Rotating Vane Actuation System for Large Vane and Two Standard Vanes Installed With Vanes A and B Unequally Deployed, $\delta_A = 30°$, and Vane C Fully Retracted

[δ_p and δ_y are given in degrees]

δ_B = 5.0°, δ_C = -10.0°

NPR	w_p/w_i	F/F_i	F_r/F_i	δ_p	δ_y
1.9984	0.9564	0.8201	0.8576	15.56	-7.22
3.0009	0.9712	0.8011	0.8407	15.79	-8.34
3.9995	0.9697	0.7996	0.8378	15.27	-8.69
5.0043	0.9680	0.7929	0.8312	15.15	-9.09
5.9970	0.9665	0.7877	0.8245	14.79	-9.14

δ_B = 10.0°, δ_C = -10.0°

NPR	w_p/w_i	F/F_i	F_r/F_i	δ_p	δ_y
2.0006	0.9555	0.7997	0.8396	14.70	-10.36
2.9978	0.9710	0.7822	0.8241	14.77	-11.37
4.0030	0.9696	0.7768	0.8181	14.49	-11.62
5.0010	0.9682	0.7712	0.8088	13.75	-11.33
5.9982	0.9666	0.7655	0.7992	13.08	-10.76

δ_B = 15.0°, δ_C = -10.0°

NPR	w_p/w_i	F/F_i	F_r/F_i	δ_p	δ_y
2.0015	0.9548	0.7668	0.8147	14.47	-14.02
2.0001	0.9555	0.7677	0.8159	14.60	-13.95
2.9976	0.9707	0.7460	0.7962	14.92	-14.63
3.9996	0.9693	0.7373	0.7838	13.98	-14.64
5.0037	0.9682	0.7341	0.7721	12.47	-13.45
6.0075	0.9666	0.7315	0.7642	11.59	-12.50
6.0032	0.9667	0.7315	0.7640	11.54	-12.50

δ_B = 20.0°, δ_C = -10.0°

NPR	w_p/w_i	F/F_i	F_r/F_i	δ_p	δ_y
2.0009	0.9541	0.7263	0.7846	15.11	-17.06
3.0016	0.9701	0.7010	0.7602	15.13	-17.81
4.0022	0.9693	0.6924	0.7416	13.41	-16.73
4.9988	0.9682	0.6919	0.7317	12.07	-15.08
6.0016	0.9666	0.6918	0.7262	11.12	-14.12

Table 37. Concluded

$\delta_B = 25.0°$, $\delta_C = -10.0°$

NPR	w_p/w_i	F/F_i	F_r/F_i	δ_p	δ_y
2.0000	0.9519	0.6718	0.7377	15.54	-19.72
2.9980	0.9708	0.6486	0.7071	14.89	-18.97
3.9983	0.9695	0.6478	0.6968	13.41	-17.55
5.0039	0.9682	0.6500	0.6918	12.22	-16.35
5.9975	0.9665	0.6517	0.6895	11.46	-15.62

Table 38. Maximum A/B-Power Nozzle Performance of Rotating Vane Actuation System for Large Vane and Two Standard Vanes Installed With Vane B Partially Retracted, $\delta_A = 30°$, and Vane C Fully Retracted

[δ_p and δ_y are given in degrees]

δ_B = -5.0°, δ_C = -10.0°

NPR	w_p/w_i	F/F_i	F_r/F_i	δ_p	δ_y
1.9995	0.9570	0.8416	0.8841	17.70	-2.53
2.9989	0.9709	0.8241	0.8681	18.07	-3.13
4.0012	0.9698	0.8214	0.8628	17.54	-3.40
5.0016	0.9678	0.8138	0.8552	17.50	-3.93
6.0036	0.9664	0.8071	0.8486	17.49	-4.45

δ_B = 0.0°, δ_C = -10.0°

NPR	w_p/w_i	F/F_i	F_r/F_i	δ_p	δ_y
2.0007	0.9571	0.8337	0.8734	16.77	-4.72
2.9985	0.9705	0.8136	0.8543	16.96	-5.56
4.0042	0.9697	0.8121	0.8504	16.32	-5.89
4.9985	0.9684	0.8049	0.8439	16.39	-6.40
6.0018	0.9666	0.7987	0.8375	16.27	-6.88

Table 39. Maximum A/B-Power Nozzle Performance of Rotating Vane Actuation System for Large Vane and Two Standard Vanes Installed With Vanes A and B Unequally Deployed, $\delta_A = 25°$, and Vane C Fully Retracted

[δ_p and δ_y are given in degrees]

δ_B = 5.0°, δ_C = -10.0°

NPR	w_p/w_i	F/F_i	F_r/F_i	δ_p	δ_y
2.0080	0.9569	0.8782	0.9031	13.00	-3.75
3.0045	0.9708	0.8567	0.8841	13.47	-4.96
4.0037	0.9697	0.8515	0.8790	13.27	-5.68
5.0007	0.9681	0.8428	0.8715	13.37	-6.46
6.0011	0.9665	0.8343	0.8634	13.21	-7.20

δ_B = 10.0°, δ_C = -10.0°

NPR	w_p/w_i	F/F_i	F_r/F_i	δ_p	δ_y
2.0071	0.9573	0.8581	0.8827	12.09	-6.31
2.9982	0.9708	0.8387	0.8663	12.55	-7.49
3.9992	0.9695	0.8292	0.8583	12.54	-8.42
5.0088	0.9678	0.8231	0.8523	12.29	-8.92
5.9983	0.9665	0.8176	0.8461	12.02	-9.07

δ_B = 15.0°, δ_C = -10.0°

NPR	w_p/w_i	F/F_i	F_r/F_i	δ_p	δ_y
2.0078	0.9576	0.8268	0.8569	11.62	-10.11
3.0022	0.9706	0.8051	0.8397	12.34	-11.28
4.0026	0.9695	0.7933	0.8289	12.32	-11.87
5.0017	0.9677	0.7868	0.8192	11.53	-11.64
6.0086	0.9667	0.7811	0.8101	10.83	-11.16

δ_B = 20.0°, δ_C = -10.0°

NPR	w_p/w_i	F/F_i	F_r/F_i	δ_p	δ_y
2.0049	0.9566	0.7775	0.8211	12.58	-14.35
3.0007	0.9708	0.7579	0.8049	13.25	-15.07
3.9981	0.9693	0.7485	0.7923	12.64	-14.84
5.0051	0.9677	0.7451	0.7814	11.32	-13.74
6.0010	0.9667	0.7436	0.7750	10.51	-12.84

Table 40. Maximum A/B-Power Nozzle Performance of Rotating Vane Actuation System for Large Vane and Two Standard Vanes Installed With Vane B Partially Retracted, $\delta_A = 25°$, and Vane C Fully Retracted

[δ_p and δ_y are given in degrees]

δ_B = -5.0°, δ_C = -10.0°

NPR	w_p/w_i	F/F_i	F_r/F_i	δ_p	δ_y
1.9994	0.9570	0.8907	0.9186	14.12	-1.31
3.0019	0.9709	0.8757	0.9069	15.01	-1.41
3.9977	0.9696	0.8696	0.9009	15.06	-1.70
5.0021	0.9679	0.8607	0.8942	15.61	-2.13
6.0017	0.9666	0.8531	0.8869	15.64	-2.75

δ_B = 0.0°, δ_C = -10.0°

NPR	w_p/w_i	F/F_i	F_r/F_i	δ_p	δ_y
1.9995	0.9570	0.8886	0.9153	13.74	-1.90
2.9994	0.9710	0.8711	0.9006	14.50	-2.50
4.0024	0.9697	0.8645	0.8936	14.31	-3.24
5.0005	0.9679	0.8550	0.8857	14.66	-3.95
6.0021	0.9667	0.8456	0.8767	14.60	-4.80

Table 41. Maximum A/B-Power Nozzle Performance of Rotating Vane Actuation System for Large Vane and Two Standard Vanes Installed With Vanes A and B Unequally Deployed, $\delta_A = 22.5°$, and Vane C Fully Retracted

[δ_p and δ_y are given in degrees]

δ_B = 10.0°, δ_C = -10.0°

NPR	w_p/w_i	F/F_i	F_r/F_i	δ_p	δ_y
2.0027	0.9554	0.8847	0.9040	10.84	-4.94
1.9996	0.9552	0.8839	0.9026	10.71	-4.78
3.0032	0.9707	0.8650	0.8867	11.29	-5.99
3.9962	0.9697	0.8545	0.8779	11.37	-6.98
3.9980	0.9699	0.8541	0.8775	11.39	-6.98
5.0018	0.9682	0.8441	0.8690	11.44	-7.79
6.0038	0.9665	0.8363	0.8614	11.29	-8.25

δ_B = 15.0°, δ_C = -10.0°

NPR	w_p/w_i	F/F_i	F_r/F_i	δ_p	δ_y
2.0026	0.9551	0.8508	0.8731	10.06	-8.39
2.9997	0.9717	0.8314	0.8585	10.98	-9.60
3.9989	0.9693	0.8162	0.8466	11.39	-10.62
5.0029	0.9683	0.8074	0.8364	10.93	-10.73
5.9956	0.9667	0.8016	0.8281	10.36	-10.41

δ_B = 20.0°, δ_C = -10.0°

NPR	w_p/w_i	F/F_i	F_r/F_i	δ_p	δ_y
2.0000	0.9551	0.8082	0.8412	10.76	-12.26
3.0026	0.9709	0.7869	0.8250	11.83	-13.22
4.0033	0.9695	0.7759	0.8139	11.75	-13.46
3.9980	0.9695	0.7755	0.8135	11.73	-13.47
5.0023	0.9682	0.7694	0.8022	10.80	-12.67
5.9935	0.9667	0.7662	0.7951	10.11	-12.01
5.9953	0.9667	0.7662	0.7951	10.12	-12.00

Table 42. Maximum A/B-Power Nozzle Performance of Rotating Vane Actuation System for Large Vane and Two Standard Vanes Installed With Vanes A and B Unequally Deployed, $\delta_A = 17.5°$, and Vane C Fully Retracted

[δ_p and δ_y are given in degrees]

δ_B = 10.0°, δ_C = -10.0°

NPR	w_p/w_i	F/F_i	F_r/F_i	δ_p	δ_y
2.0034	0.9562	0.9396	0.9468	6.54	-2.66
3.0027	0.9706	0.9218	0.9306	7.08	-3.57
4.0018	0.9696	0.9027	0.9138	7.67	-4.60
5.0016	0.9684	0.8888	0.9026	8.40	-5.58
6.0034	0.9660	0.8793	0.8954	8.94	-6.30

δ_B = 15.0°, δ_C = -10.0°

NPR	w_p/w_i	F/F_i	F_r/F_i	δ_p	δ_y
2.0021	0.9562	0.9127	0.9211	5.85	-5.14
2.9989	0.9707	0.8929	0.9042	6.71	-6.14
3.9997	0.9701	0.8744	0.8893	7.61	-7.33
5.0005	0.9685	0.8598	0.8779	8.38	-8.25
6.0048	0.9667	0.8507	0.8703	8.67	-8.69

Table 43. Maximum A/B-Power Nozzle Performance of Rotating Vane Actuation System for Large Vane and Two Standard Vanes Installed With Vanes B and C Unequally Deployed, $\delta_B = 30°$, and Vane A Fully Retracted

[δ_p and δ_y are given in degrees]

δ_A = -10.0°, δ_C = 5.0°

NPR	w_p/w_i	F/F_i	F_r/F_i	δ_p	δ_y
2.0021	0.9564	0.8706	0.8917	-10.46	-6.98
2.9995	0.9710	0.8577	0.8787	-10.85	-6.47
4.0026	0.9700	0.8546	0.8758	-11.08	-6.17
4.9970	0.9683	0.8448	0.8678	-11.91	-5.91
5.9932	0.9666	0.8364	0.8605	-12.38	-5.74

δ_A = -10.0°, δ_C = 10.0°

NPR	w_p/w_i	F/F_i	F_r/F_i	δ_p	δ_y
2.0042	0.9546	0.8575	0.8805	-12.09	-5.33
3.0061	0.9709	0.8457	0.8698	-12.68	-4.81
4.0028	0.9697	0.8414	0.8660	-13.04	-4.33
5.0031	0.9679	0.8331	0.8595	-13.67	-4.19
6.0057	0.9664	0.8244	0.8506	-13.66	-4.19

δ_A = -10.0°, δ_C = 15.0°

NPR	w_p/w_i	F/F_i	F_r/F_i	δ_p	δ_y
1.9988	0.9544	0.8280	0.8591	-15.08	-3.58
3.0058	0.9705	0.8131	0.8463	-15.81	-3.18
4.0060	0.9694	0.8074	0.8408	-15.97	-2.96
4.9996	0.9678	0.8004	0.8321	-15.62	-2.92
6.0063	0.9666	0.7926	0.8228	-15.31	-2.99

δ_A = -10.0°, δ_C = 20.0°

NPR	w_p/w_i	F/F_i	F_r/F_i	δ_p	δ_y
2.0074	0.9540	0.7883	0.8323	-18.58	-2.41
3.0001	0.9706	0.7745	0.8205	-19.15	-2.28
4.0033	0.9694	0.7675	0.8101	-18.53	-2.39
5.0092	0.9678	0.7630	0.7986	-17.01	-2.54
6.0004	0.9664	0.7568	0.7888	-16.18	-2.70

Table 43. Concluded

δ_A = -10.0°, δ_C = 25.0°

NPR	w_p/w_i	F/F_i	F_r/F_i	δ_p	δ_y
2.0088	0.9531	0.7468	0.8060	-22.01	-2.18
3.0049	0.9704	0.7295	0.7868	-21.90	-2.34
3.9988	0.9693	0.7218	0.7697	-20.19	-2.55
5.0029	0.9680	0.7207	0.7576	-17.77	-2.75
5.9950	0.9665	0.7193	0.7510	-16.47	-2.97

Table 44. Maximum A/B-Power Nozzle Performance of Rotating Vane Actuation System for Large Vane and Two Standard Vanes Installed With Vane C Partially Retracted, $\delta_B = 30°$, and Vane A Fully Retracted

[δ_p and δ_y are given in degrees]

δ_A = -10.0°, δ_C = -5.0°

NPR	w_p/w_i	F/F_i	F_r/F_i	δ_p	δ_y
2.0008	0.9573	0.8894	0.9089	-7.22	-9.53
3.0005	0.9710	0.8785	0.8976	-7.18	-9.54
4.0009	0.9699	0.8743	0.8933	-7.56	-9.23
4.9972	0.9680	0.8643	0.8846	-8.21	-9.29
5.9773	0.9666	0.8548	0.8755	-8.50	-9.31
5.9986	0.9666	0.8550	0.8758	-8.51	-9.29

δ_A = -10.0°, δ_C = 0.0°

NPR	w_p/w_i	F/F_i	F_r/F_i	δ_p	δ_y
2.0012	0.9561	0.8861	0.9051	-7.90	-8.82
2.9987	0.9707	0.8736	0.8929	-8.50	-8.49
3.9994	0.9700	0.8685	0.8874	-8.72	-8.12
5.0028	0.9680	0.8572	0.8777	-9.56	-8.02
6.0036	0.9665	0.8483	0.8692	-9.99	-7.84

Table 45. Maximum A/B-Power Nozzle Performance of Rotating Vane Actuation System for Large Vane and Two Standard Vanes Installed With Vanes B and C Unequally Deployed, $\delta_B = 25°$, and Vane A Fully Retracted

[δ_p and δ_y are given in degrees]

δ_A = -10.0°, δ_C = 5.0°

NPR	w_p/w_i	F/F_i	F_r/F_i	δ_p	δ_y
2.0085	0.9593	0.9103	0.9236	-6.84	-7.01
2.0015	0.9576	0.9109	0.9240	-6.85	-6.88
3.0045	0.9708	0.8959	0.9094	-7.41	-6.61
4.0052	0.9694	0.8901	0.9042	-8.09	-6.19
5.0008	0.9676	0.8781	0.8946	-9.39	-5.86
5.9976	0.9664	0.8674	0.8856	-10.30	-5.47

δ_A = -10.0°, δ_C = 10.0°

NPR	w_p/w_i	F/F_i	F_r/F_i	δ_p	δ_y
2.0047	0.9579	0.8924	0.9076	-9.05	-5.38
2.9961	0.9711	0.8793	0.8952	-9.75	-4.82
4.0039	0.9693	0.8736	0.8905	-10.38	-4.27
5.0045	0.9676	0.8632	0.8825	-11.35	-4.05
5.9920	0.9664	0.8532	0.8740	-11.96	-3.83

δ_A = -10.0°, δ_C = 15.0°

NPR	w_p/w_i	F/F_i	F_r/F_i	δ_p	δ_y
2.0022	0.9571	0.8645	0.8858	-12.09	-3.58
2.9981	0.9708	0.8470	0.8704	-12.93	-3.29
4.0020	0.9692	0.8378	0.8635	-13.73	-2.92
5.0020	0.9676	0.8302	0.8561	-13.87	-2.79
6.0002	0.9665	0.8223	0.8481	-13.88	-2.84

δ_A = -10.0°, δ_C = 20.0°

NPR	w_p/w_i	F/F_i	F_r/F_i	δ_p	δ_y
1.9935	0.9564	0.8239	0.8572	-15.87	-2.37
3.0024	0.9709	0.8051	0.8429	-17.09	-2.19
3.9995	0.9693	0.7973	0.8345	-17.04	-2.16
4.9994	0.9678	0.7919	0.8245	-16.01	-2.27
5.9997	0.9666	0.7865	0.8162	-15.33	-2.46

Table 46. Maximum A/B-Power Nozzle Performance of Rotating Vane Actuation System for Large Vane and Two Standard Vanes Installed With Vane C Partially Retracted, $\delta_B = 25°$, and Vane A Fully Retracted

[δ_p and δ_y are given in degrees]

δ_A = -10.0°, δ_C = -5.0°

NPR	w_p/w_i	F/F_i	F_r/F_i	δ_p	δ_y
2.0006	0.9575	0.9205	0.9338	-5.06	-8.30
3.0007	0.9708	0.9090	0.9227	-5.19	-8.43
4.0038	0.9694	0.9034	0.9174	-5.61	-8.37
5.0024	0.9676	0.8930	0.9086	-6.28	-8.65
5.9965	0.9664	0.8821	0.8987	-6.81	-8.75

δ_A = -10.0°, δ_C = 0.0°

NPR	w_p/w_i	F/F_i	F_r/F_i	δ_p	δ_y
2.0001	0.9571	0.9194	0.9327	-5.55	-7.96
3.0031	0.9710	0.9074	0.9211	-6.00	-7.91
4.0005	0.9693	0.9004	0.9139	-6.30	-7.66
5.0045	0.9677	0.8884	0.9037	-7.38	-7.59
5.9948	0.9665	0.8778	0.8944	-8.34	-7.34

Table 47. Maximum A/B-Power Nozzle Performance of Rotating Vane Actuation System for Large Vane and Two Standard Vanes Installed With Vanes B and C Unequally Deployed. $\delta_B = 22.5°$, and Vane A Fully Retracted

[δ_p and δ_y are given in degrees]

δ_A = -10.0°, δ_C = 10.0°

NPR	w_p/w_i	F/F_i	F_r/F_i	δ_p	δ_y
2.0091	0.9562	0.9231	0.9320	-6.63	-4.33
3.0059	0.9711	0.9103	0.9199	-7.31	-4.00
4.0012	0.9696	0.9008	0.9119	-8.23	-3.63
5.0024	0.9678	0.8880	0.9023	-9.62	-3.42
6.0002	0.9665	0.8762	0.8926	-10.52	-3.31

δ_A = -10.0°, δ_C = 15.0°

NPR	w_p/w_i	F/F_i	F_r/F_i	δ_p	δ_y
2.0048	0.9557	0.8948	0.9074	-9.17	-2.74
3.0055	0.9708	0.8797	0.8950	-10.34	-2.50
4.0002	0.9696	0.8686	0.8867	-11.39	-2.29
4.9997	0.9680	0.8597	0.8800	-12.17	-2.16
6.0049	0.9665	0.8500	0.8715	-12.60	-2.17

δ_A = -10.0°, δ_C = 20.0°

NPR	w_p/w_i	F/F_i	F_r/F_i	δ_p	δ_y
2.0025	0.9547	0.8480	0.8727	-13.62	-1.35
3.0054	0.9708	0.8304	0.8600	-15.02	-1.43
4.0017	0.9695	0.8209	0.8527	-15.64	-1.46
5.0012	0.9678	0.8144	0.8443	-15.21	-1.71
6.0075	0.9664	0.8074	0.8355	-14.80	-1.88

Table 48. Maximum A/B-Power Nozzle Performance of Rotating Vane Actuation System for Large Vane and Two Standard Vanes Installed With Vanes B and C Unequally Deployed, $\delta_B = 17.5°$, and Vane A Fully Retracted

[δ_p and δ_y are given in degrees]

δ_A = -10.0°, δ_C = 10.0°

NPR	w_p/w_i	F/F_i	F_r/F_i	δ_p	δ_y
1.9980	0.9562	0.9499	0.9543	-4.62	-2.97
3.0055	0.9708	0.9369	0.9419	-5.23	-2.84
4.0023	0.9694	0.9245	0.9311	-6.30	-2.67
5.0011	0.9681	0.9090	0.9185	-7.86	-2.66
5.9992	0.9665	0.8969	0.9088	-8.91	-2.65

δ_A = -10.0°, δ_C = 15.0°

NPR	w_p/w_i	F/F_i	F_r/F_i	δ_p	δ_y
2.0039	0.9553	0.9257	0.9324	-6.68	-1.57
3.0045	0.9705	0.9091	0.9178	-7.77	-1.46
4.0036	0.9696	0.8954	0.9072	-9.16	-1.38
4.9987	0.9679	0.8830	0.8977	-10.30	-1.44
6.0023	0.9664	0.8719	0.8887	-11.07	-1.52

Table 49. Maximum A/B-Power Nozzle Performance of Rotating Vane Actuation System for Large Vane and Two Standard Vanes Installed With Vanes B and C Unequally Deployed, $\delta_C = 30°$, and Vane A Fully Retracted

[δ_p and δ_y are given in degrees]

δ_A = -10.0°, δ_B = 5.0°

NPR	w_p/w_i	F/F_i	F_r/F_i	δ_p	δ_y
1.9958	0.9562	0.8725	0.8921	-11.14	4.60
2.9996	0.9708	0.8577	0.8790	-11.96	4.24
3.9973	0.9699	0.8553	0.8773	-12.26	3.92
4.9970	0.9678	0.8455	0.8699	-13.18	3.56
6.0048	0.9665	0.8364	0.8616	-13.59	3.01

δ_A = -10.0°, δ_B = 10.0°

NPR	w_p/w_i	F/F_i	F_r/F_i	δ_p	δ_y
2.0022	0.9557	0.8564	0.8790	-12.74	2.81
3.0042	0.9716	0.8414	0.8663	-13.59	2.28
4.0040	0.9695	0.8372	0.8632	-14.03	1.69
5.0026	0.9678	0.8287	0.8561	-14.48	1.30
5.9983	0.9665	0.8195	0.8471	-14.64	0.86

δ_A = -10.0°, δ_B = 15.0°

NPR	w_p/w_i	F/F_i	F_r/F_i	δ_p	δ_y
2.0027	0.9546	0.8276	0.8594	-15.62	0.71
3.0004	0.9704	0.8109	0.8457	-16.51	0.14
4.0032	0.9696	0.8046	0.8398	-16.63	-0.35
5.0054	0.9679	0.7982	0.8303	-15.96	-0.72
6.0044	0.9665	0.7907	0.8195	-15.22	-0.77

δ_A = -10.0°, δ_B = 20.0°

NPR	w_p/w_i	F/F_i	F_r/F_i	δ_p	δ_y
2.0020	0.9535	0.7899	0.8345	-18.78	-0.97
2.9992	0.9708	0.7720	0.8191	-19.50	-1.31
4.0000	0.9697	0.7641	0.8073	-18.76	-1.65
5.0070	0.9681	0.7597	0.7948	-16.98	-2.03
5.9968	0.9664	0.7573	0.7874	-15.76	-2.07

Table 49. Concluded

δ_A = -10.0°, δ_B = 25.0°

NPR	w_p/w_i	F/F_i	F_r/F_i	δ_p	δ_y
2.0030	0.9529	0.7377	0.7986	-22.45	-2.09
3.0039	0.9704	0.7213	0.7804	-22.33	-2.62
4.0024	0.9692	0.7177	0.7658	-20.25	-2.95
5.0100	0.9678	0.7184	0.7546	-17.59	-3.10
6.0060	0.9666	0.7153	0.7465	-16.33	-3.23

Table 50. Maximum A/B-Power Nozzle Performance of Rotating Vane Actuation System for Large Vane and Two Standard Vanes Installed With Vane B Partially Retracted, $\delta_C = 30°$, and Vane A Fully Retracted

[δ_p and δ_y are given in degrees]

δ_A = -10.0°, δ_B = -5.0°

NPR	w_p/w_i	F/F_i	F_r/F_i	δ_p	δ_y
1.9990	0.9566	0.8947	0.9146	-8.51	8.54
3.0015	0.9710	0.8804	0.9011	-8.91	8.65
3.9990	0.9697	0.8761	0.8963	-9.16	8.15
5.0031	0.9680	0.8649	0.8863	-9.96	7.89
6.0107	0.9667	0.8559	0.8778	-10.59	7.37

δ_A = -10.0°, δ_B = 0.0°

NPR	w_p/w_i	F/F_i	F_r/F_i	δ_p	δ_y
1.9971	0.9570	0.8888	0.9087	-9.73	7.18
2.9997	0.9710	0.8736	0.8938	-10.25	6.78
4.0028	0.9698	0.8693	0.8893	-10.53	6.26
4.9968	0.9678	0.8583	0.8804	-11.50	5.87
5.9961	0.9665	0.8487	0.8713	-11.99	5.37

Table 51. Maximum A/B-Power Nozzle Performance of Rotating Vane Actuation System for Large Vane and Two Standard Vanes Installed With Vanes B and C Unequally Deployed, $\delta_C = 25°$, and Vane A Fully Retracted

[δ_p and δ_y are given in degrees]

δ_A = -10.0°, δ_B = 5.0°

NPR	w_p/w_i	F/F_i	F_r/F_i	δ_p	δ_y
2.0073	0.9580	0.9161	0.9284	-7.91	5.06
3.0041	0.9709	0.9017	0.9151	-8.60	4.75
4.0062	0.9692	0.8948	0.9090	-9.24	4.26
5.0048	0.9676	0.8816	0.8986	-10.52	3.77
6.0011	0.9662	0.8709	0.8894	-11.31	3.05

δ_A = -10.0°, δ_B = 10.0°

NPR	w_p/w_i	F/F_i	F_r/F_i	δ_p	δ_y
1.9976	0.9578	0.9004	0.9143	-9.49	3.16
3.0028	0.9709	0.8840	0.8998	-10.40	2.79
3.9987	0.9693	0.8781	0.8950	-10.93	2.25
5.0131	0.9677	0.8677	0.8872	-11.93	1.67
4.9995	0.9677	0.8675	0.8870	-11.91	1.71
5.9922	0.9664	0.8575	0.8781	-12.38	1.25

δ_A = -10.0°, δ_B = 15.0°

NPR	w_p/w_i	F/F_i	F_r/F_i	δ_p	δ_y
1.9997	0.9572	0.8710	0.8911	-12.18	0.88
3.0019	0.9706	0.8510	0.8750	-13.43	0.58
4.0007	0.9692	0.8426	0.8684	-14.01	0.07
5.0073	0.9676	0.8348	0.8608	-14.10	-0.26
5.9992	0.9663	0.8263	0.8523	-14.18	-0.58

δ_A = -10.0°, δ_B = 20.0°

NPR	w_p/w_i	F/F_i	F_r/F_i	δ_p	δ_y
2.0082	0.9574	0.8174	0.8531	-16.61	-1.16
3.0067	0.9709	0.7996	0.8394	-17.67	-1.29
4.0048	0.9695	0.7958	0.8339	-17.35	-1.37
5.0007	0.9678	0.7911	0.8243	-16.24	-1.66
6.0011	0.9665	0.7842	0.8142	-15.51	-1.84

Table 52. Maximum A/B-Power Nozzle Performance of Rotating Vane Actuation System for Large Vane and Two Standard Vanes Installed With Vane B Partially Retracted, $\delta_C = 25°$, and Vane A Fully Retracted

[δ_p and δ_y are given in degrees]

δ_A = -10.0°, δ_B = -5.0°

NPR	w_p/w_i	F/F_i	F_r/F_i	δ_p	δ_y
2.0038	0.9571	0.9296	0.9422	-6.29	7.01
2.9986	0.9711	0.9166	0.9303	-6.52	7.40
4.0081	0.9692	0.9093	0.9235	-6.97	7.31
5.0039	0.9675	0.8974	0.9135	-7.81	7.51
6.0010	0.9662	0.8869	0.9039	-8.56	7.25

δ_A = -10.0°, δ_B = 0.0°

NPR	w_p/w_i	F/F_i	F_r/F_i	δ_p	δ_y
2.0016	0.9572	0.9281	0.9404	-6.69	6.48
3.0012	0.9706	0.9123	0.9256	-7.28	6.52
4.0079	0.9692	0.9051	0.9189	-7.82	6.22
5.0050	0.9675	0.8929	0.9085	-8.90	5.90
6.0019	0.9662	0.8822	0.8991	-9.82	5.36

Table 53. Maximum A/B-Power Nozzle Performance of Rotating Vane Actuation System for Large Vane and Two Standard Vanes Installed With Vanes B and C Unequally Deployed, $\delta_C = 22.5°$, and Vane A Fully Retracted

[δ_p and δ_y are given in degrees]

δ_A = -10.0°, δ_B = 10.0°

NPR	w_p/w_i	F/F_i	F_r/F_i	δ_p	δ_y
2.0070	0.9558	0.9124	0.9227	-8.04	3.02
3.0037	0.9714	0.8991	0.9109	-8.88	2.62
4.0072	0.9694	0.8912	0.9046	-9.67	2.08
5.0089	0.9678	0.8786	0.8947	-10.79	1.50
6.0058	0.9662	0.8677	0.8856	-11.49	1.03

δ_A = -10.0°, δ_B = 15.0°

NPR	w_p/w_i	F/F_i	F_r/F_i	δ_p	δ_y
2.0036	0.9557	0.8892	0.9042	-10.42	0.89
3.0041	0.9717	0.8714	0.8893	-11.49	0.65
4.0048	0.9694	0.8604	0.8811	-12.45	0.14
5.0047	0.9679	0.8501	0.8725	-13.02	-0.18
6.0105	0.9660	0.8401	0.8635	-13.35	-0.46
6.0030	0.9661	0.8405	0.8637	-13.30	-0.47

δ_A = -10.0°, δ_B = 20.0°

NPR	w_p/w_i	F/F_i	F_r/F_i	δ_p	δ_y
2.0062	0.9557	0.8511	0.8752	-13.47	-0.76
3.0011	0.9709	0.8308	0.8601	-14.99	-0.82
4.0061	0.9695	0.8217	0.8529	-15.53	-1.01
5.0019	0.9678	0.8174	0.8468	-15.08	-1.32
6.0048	0.9664	0.8097	0.8377	-14.79	-1.51
5.9983	0.9665	0.8097	0.8377	-14.77	-1.55

Table 54. Maximum A/B-Power Nozzle Performance of Rotating Vane Actuation System for Large Vane and Two Standard Vanes Installed With Vanes B and C Unequally Deployed, $\delta_C = 17.5°$, and Vane A Fully Retracted

[δ_p and δ_y are given in degrees]

δ_A = -10.0°, δ_B = 10.0°

NPR	w_p/w_i	F/F_i	F_r/F_i	δ_p	δ_y
1.9978	0.9558	0.9587	0.9625	-4.59	2.12
3.0059	0.9710	0.9421	0.9467	-5.32	1.93
2.9999	0.9707	0.9420	0.9466	-5.29	1.93
4.0029	0.9692	0.9285	0.9346	-6.39	1.66
4.9976	0.9677	0.9125	0.9216	-7.94	1.50
5.9967	0.9662	0.9005	0.9118	-8.99	1.13

δ_A = -10.0°, δ_B = 15.0°

NPR	w_p/w_i	F/F_i	F_r/F_i	δ_p	δ_y
2.0000	0.9554	0.9346	0.9409	-6.63	0.04
3.0059	0.9712	0.9124	0.9210	-7.82	-0.04
2.9986	0.9711	0.9117	0.9202	-7.80	-0.04
3.9955	0.9695	0.8963	0.9079	-9.18	-0.30
5.0031	0.9678	0.8837	0.8983	-10.34	-0.46
6.0056	0.9663	0.8733	0.8899	-11.07	-0.66

Table 55. Maximum A/B-Power Nozzle Performance of Rotating Vane Actuation System for Large Vane and Two Standard Vanes Installed With Vanes A and C Unequally Deployed, $\delta_A = 30°$, and Vane B Fully Retracted

[δ_p and δ_y are given in degrees]

δ_B = -10.0°, δ_C = 5.0°

NPR	w_p/w_i	F/F_i	F_r/F_i	δ_p	δ_y
2.0011	0.9566	0.8290	0.8617	15.78	1.12
3.0016	0.9705	0.8063	0.8374	15.54	2.00
4.0061	0.9696	0.8013	0.8279	14.42	2.28
5.0037	0.9679	0.7942	0.8194	14.06	2.33
6.0034	0.9667	0.7863	0.8095	13.64	2.00

δ_B = -10.0°, δ_C = 10.0°

NPR	w_p/w_i	F/F_i	F_r/F_i	δ_p	δ_y
1.9994	0.9554	0.8125	0.8378	13.68	3.63
2.9999	0.9710	0.7910	0.8153	13.38	4.40
3.9986	0.9694	0.7845	0.8062	12.55	4.60
5.0013	0.9679	0.7786	0.7976	11.86	4.15
6.0030	0.9662	0.7728	0.7898	11.39	3.58

δ_B = -10.0°, δ_C = 15.0°

NPR	w_p/w_i	F/F_i	F_r/F_i	δ_p	δ_y
1.9993	0.9549	0.7823	0.8055	12.38	6.28
2.9996	0.9704	0.7584	0.7810	12.11	6.84
4.0002	0.9693	0.7504	0.7686	10.95	6.18
4.9994	0.9677	0.7441	0.7579	9.78	4.98
6.0022	0.9662	0.7415	0.7533	9.35	3.98

δ_B = -10.0°, δ_C = 20.0°

NPR	w_p/w_i	F/F_i	F_r/F_i	δ_p	δ_y
2.0020	0.9541	0.7399	0.7646	11.94	8.61
2.9997	0.9707	0.7157	0.7372	11.20	8.44
3.0003	0.9709	0.7148	0.7365	11.26	8.46
4.0013	0.9694	0.7077	0.7228	9.70	6.71
5.0005	0.9678	0.7065	0.7171	8.52	5.06
6.0030	0.9664	0.7057	0.7145	8.01	4.11

Table 55. Concluded

δ_B = -10.0°, δ_C = 25.0°

NPR	w_p/w_i	F/F_i	F_r/F_i	δ_p	δ_y
2.0020	0.9527	0.6836	0.7028	10.63	8.39
3.0031	0.9702	0.6600	0.6746	9.88	6.88
4.0006	0.9692	0.6560	0.6667	8.68	5.55
5.0002	0.9678	0.6579	0.6668	8.21	4.50
5.9965	0.9662	0.6607	0.6682	7.83	3.65

Table 56. Maximum A/B-Power Nozzle Performance of Rotating Vane Actuation System for Large Vane and Two Standard Vanes Installed With Vane C Partially Retracted, $\delta_A = 30°$, and Vane B Fully Retracted

[δ_p and δ_y are given in degrees]

δ_B = -10.0°, δ_C = -5.0°

NPR	w_p/w_i	F/F_i	F_r/F_i	δ_p	δ_y
1.9991	0.9571	0.8424	0.8850	17.80	-1.40
3.0014	0.9703	0.8236	0.8681	18.38	-1.53
4.0022	0.9695	0.8217	0.8627	17.67	-1.50
4.9993	0.9681	0.8138	0.8541	17.60	-1.72
5.9998	0.9667	0.8080	0.8474	17.44	-2.03

δ_B = -10.0°, δ_C = 0.0°

NPR	w_p/w_i	F/F_i	F_r/F_i	δ_p	δ_y
2.0045	0.9569	0.8365	0.8758	17.22	-0.62
3.0035	0.9707	0.8188	0.8579	17.37	-0.30
4.0006	0.9696	0.8142	0.8481	16.25	0.11
5.0060	0.9676	0.8065	0.8394	16.09	0.03
6.0034	0.9662	0.8001	0.8318	15.87	-0.19

Table 57. Maximum A/B-Power Nozzle Performance of Rotating Vane Actuation System for Large Vane and Two Standard Vanes Installed With Vanes A and C Unequally Deployed, $\delta_A = 25°$, and Vane B Fully Retracted

[δ_p and δ_y are given in degrees]

δ_B = -10.0°, δ_C = 5.0°

NPR	w_p/w_i	F/F_i	F_r/F_i	δ_p	δ_y
2.0033	0.9574	0.8802	0.9053	13.51	0.14
2.9988	0.9720	0.8614	0.8868	13.70	0.95
4.0010	0.9690	0.8520	0.8752	13.12	1.68
5.0006	0.9676	0.8420	0.8648	13.04	2.05
6.0031	0.9665	0.8326	0.8541	12.72	2.15

δ_B = -10.0°, δ_C = 10.0°

NPR	w_p/w_i	F/F_i	F_r/F_i	δ_p	δ_y
2.0011	0.9573	0.8646	0.8845	11.98	2.24
3.0028	0.9713	0.8425	0.8621	11.88	3.10
4.0013	0.9693	0.8322	0.8508	11.38	3.86
5.0031	0.9678	0.8242	0.8413	10.93	3.91
6.0004	0.9666	0.8165	0.8325	10.69	3.62

δ_B = -10.0°, δ_C = 15.0°

NPR	w_p/w_i	F/F_i	F_r/F_i	δ_p	δ_y
2.0016	0.9569	0.8425	0.8594	10.64	4.19
3.0014	0.9713	0.8195	0.8374	10.75	5.16
3.9999	0.9693	0.8053	0.8223	10.29	5.65
5.0023	0.9678	0.7974	0.8115	9.51	4.99
6.0011	0.9666	0.7926	0.8046	9.01	4.23

δ_B = -10.0°, δ_C = 20.0°

NPR	w_p/w_i	F/F_i	F_r/F_i	δ_p	δ_y
1.9994	0.9573	0.7927	0.8126	10.43	7.41
3.0029	0.9712	0.7706	0.7906	10.49	7.70
4.0006	0.9694	0.7577	0.7734	9.55	6.67
5.0020	0.9679	0.7513	0.7626	8.46	5.18
6.0018	0.9665	0.7495	0.7588	7.95	4.24

Table 58. Maximum A/B-Power Nozzle Performance of Rotating Vane Actuation System for Large Vane and Two Standard Vanes Installed With Vane C Partially Retracted, $\delta_A = 25°$, and Vane B Fully Retracted

[δ_p and δ_y are given in degrees]

δ_B = -10.0°, δ_C = -5.0°

NPR	w_p/w_i	F/F_i	F_r/F_i	δ_p	δ_y
2.0002	0.9586	0.8878	0.9166	14.37	-1.04
3.0012	0.9717	0.8727	0.9051	15.36	-1.05
4.0017	0.9694	0.8672	0.8993	15.32	-1.02
5.0010	0.9677	0.8572	0.8909	15.76	-1.09
6.0068	0.9665	0.8497	0.8833	15.82	-1.23

δ_B = -10.0°, δ_C = 0.0°

NPR	w_p/w_i	F/F_i	F_r/F_i	δ_p	δ_y
2.0007	0.9576	0.8865	0.9143	14.16	-0.80
2.9995	0.9718	0.8691	0.8992	14.86	-0.51
3.9995	0.9693	0.8624	0.8907	14.48	-0.05
4.9995	0.9678	0.8528	0.8817	14.71	0.14
6.0037	0.9665	0.8438	0.8720	14.61	0.29

Table 59. Maximum A/B-Power Nozzle Performance of Rotating Vane Actuation System for Large Vane and Two Standard Vanes Installed With Vanes A and C Unequally Deployed, $\delta_A = 22.5°$, and Vane B Fully Retracted

[δ_p and δ_y are given in degrees]

δ_B = -10.0°, δ_C = 10.0°

NPR	w_p/w_i	F/F_i	F_r/F_i	δ_p	δ_y
2.0018	0.9549	0.8938	0.9084	10.18	1.43
3.0017	0.9710	0.8743	0.8895	10.41	2.26
3.9976	0.9694	0.8599	0.8752	10.27	3.15
4.9981	0.9677	0.8500	0.8651	10.16	3.55
6.0071	0.9663	0.8413	0.8563	10.18	3.52
6.0044	0.9663	0.8415	0.8566	10.20	3.50

δ_B = -10.0°, δ_C = 15.0°

NPR	w_p/w_i	F/F_i	F_r/F_i	δ_p	δ_y
1.9991	0.9552	0.8693	0.8816	8.85	3.76
3.0001	0.9713	0.8446	0.8585	9.23	4.70
3.9996	0.9695	0.8273	0.8421	9.33	5.47
5.0017	0.9678	0.8175	0.8310	8.98	5.16
5.9985	0.9664	0.8128	0.8243	8.46	4.53

δ_B = -10.0°, δ_C = 20.0°

NPR	w_p/w_i	F/F_i	F_r/F_i	δ_p	δ_y
2.0010	0.9546	0.8216	0.8359	8.28	6.73
3.0037	0.9707	0.7968	0.8135	9.08	7.42
3.0025	0.9703	0.7959	0.8129	9.13	7.48
4.0006	0.9693	0.7824	0.7979	8.95	7.06
5.0014	0.9679	0.7752	0.7871	8.17	5.80
5.9999	0.9664	0.7738	0.7833	7.53	4.84

Table 60. Maximum A/B-Power Nozzle Performance of Rotating Vane Actuation System for Large Vane and Two Standard Vanes Installed With Vanes A and C Unequally Deployed, $\delta_A = 17.5°$, and Vane B Fully Retracted

[δ_p and δ_y are given in degrees]

δ_B = -10.0°, δ_C = 10.0°

NPR	w_p/w_i	F/F_i	F_r/F_i	δ_p	δ_y
1.9977	0.9558	0.9409	0.9466	6.23	1.12
3.0013	0.9711	0.9247	0.9312	6.59	1.58
4.0023	0.9694	0.9079	0.9153	6.93	2.28
4.9985	0.9677	0.8932	0.9023	7.66	2.76
6.0041	0.9663	0.8817	0.8921	8.25	3.02

δ_B = -10.0°, δ_C = 15.0°

NPR	w_p/w_i	F/F_i	F_r/F_i	δ_p	δ_y
2.0010	0.9557	0.9186	0.9229	4.72	2.92
2.9994	0.9709	0.8978	0.9037	5.50	3.59
4.0063	0.9695	0.8783	0.8861	6.26	4.35
3.9991	0.9693	0.8780	0.8859	6.25	4.42
5.0044	0.9678	0.8662	0.8749	6.63	4.68
5.9959	0.9662	0.8597	0.8684	6.82	4.51
5.9956	0.9662	0.8597	0.8685	6.83	4.51

Table 61. Maximum A/B-Power Nozzle Performance of Rotating Vane Actuation System for Large Vane and Two Standard Vanes Installed With Vanes A and C Unequally Deployed, $\delta_C = 30°$, and Vane B Fully Retracted

[δ_p and δ_y are given in degrees]

$\delta_A =$ 5.0°, δ_B = -10.0°

NPR	w_p/w_i	F/F_i	F_r/F_i	δ_p	δ_y
1.9964	0.9560	0.8729	0.8862	-4.33	8.98
3.0008	0.9713	0.8548	0.8670	-3.36	9.05
4.0023	0.9697	0.8479	0.8588	-2.62	8.76
5.0026	0.9681	0.8373	0.8470	-2.02	8.47
6.0067	0.9662	0.8279	0.8363	-1.44	8.02

$\delta_A =$ 10.0°, δ_B = -10.0°

NPR	w_p/w_i	F/F_i	F_r/F_i	δ_p	δ_y
2.0032	0.9544	0.8564	0.8660	-0.89	8.48
3.0046	0.9708	0.8385	0.8483	0.43	8.73
3.9963	0.9694	0.8311	0.8403	1.48	8.36
4.9996	0.9679	0.8220	0.8309	2.19	8.08
5.9926	0.9662	0.8127	0.8206	2.49	7.59

$\delta_A =$ 15.0°, δ_B = -10.0°

NPR	w_p/w_i	F/F_i	F_r/F_i	δ_p	δ_y
2.0028	0.9540	0.8387	0.8487	1.51	8.71
3.0062	0.9708	0.8200	0.8307	2.85	8.78
4.0007	0.9696	0.8103	0.8211	4.00	8.43
4.9900	0.9678	0.8023	0.8117	4.31	7.62
5.9981	0.9661	0.7947	0.8026	4.17	6.91

$\delta_A =$ 20.0°, δ_B = -10.0°

NPR	w_p/w_i	F/F_i	F_r/F_i	δ_p	δ_y
2.0004	0.9543	0.7666	0.7857	8.25	9.74
2.9977	0.9713	0.7433	0.7627	8.93	9.54
4.0000	0.9698	0.7324	0.7472	8.39	7.88
4.9992	0.9678	0.7293	0.7402	7.63	6.26
6.0012	0.9665	0.7283	0.7368	7.08	5.15

Table 61. Concluded

$\delta_A = 25.0°$, $\delta_B = -10.0°$

NPR	w_p/w_i	F/F_i	F_r/F_i	δ_p	δ_y
1.9989	0.9529	0.7007	0.7203	10.27	8.80
3.0006	0.9700	0.6765	0.6925	10.18	7.10
4.0005	0.9693	0.6734	0.6851	9.07	5.63
4.9979	0.9678	0.6735	0.6832	8.45	4.72
5.9926	0.9664	0.6787	0.6870	7.94	4.14
5.9979	0.9663	0.6786	0.6869	7.97	4.10

Table 62. Maximum A/B-Power Nozzle Performance of Rotating Vane Actuation System for Large Vane and Two Standard Vanes Installed With Vane A Partially Retracted, $\delta_C = 30°$, and Vane B Fully Retracted

[δ_p and δ_y are given in degrees]

δ_A = -5.0°, δ_B = -10.0°

NPR	w_p/w_i	F/F_i	F_r/F_i	δ_p	δ_y
2.0057	0.9562	0.8914	0.9120	-8.11	9.24
3.0031	0.9709	0.8769	0.8982	-8.32	9.47
4.0043	0.9695	0.8714	0.8914	-8.22	9.11
5.0050	0.9678	0.8594	0.8798	-8.55	9.09
6.0047	0.9663	0.8513	0.8702	-8.45	8.60

δ_A = 0.0°, δ_B = -10.0°

NPR	w_p/w_i	F/F_i	F_r/F_i	δ_p	δ_y
2.0059	0.9560	0.8860	0.9045	-7.30	9.10
3.0006	0.9706	0.8701	0.8876	-6.65	9.35
4.0034	0.9695	0.8636	0.8790	-5.89	9.04
5.0035	0.9677	0.8534	0.8680	-5.77	8.84
6.0034	0.9661	0.8440	0.8568	-5.32	8.40

Table 63. Maximum A/B-Power Nozzle Performance of Rotating Vane Actuation System for Large Vane and Two Standard Vanes Installed With Vanes A and C Unequally Deployed, $\delta_C = 25°$, and Vane B Fully Retracted

[δ_p and δ_y are given in degrees]

$\delta_A =$ 5.0°, $\delta_B =$ -10.0°

NPR	w_p/w_i	F/F_i	F_r/F_i	δ_p	δ_y
2.0009	0.9570	0.9224	0.9325	-4.68	7.04
3.0015	0.9712	0.9053	0.9147	-3.91	7.25
4.0004	0.9694	0.8949	0.9035	-3.04	7.34
5.0007	0.9678	0.8799	0.8884	-2.15	7.66
6.0003	0.9664	0.8681	0.8758	-1.33	7.51

$\delta_A =$ 10.0°, $\delta_B =$ -10.0°

NPR	w_p/w_i	F/F_i	F_r/F_i	δ_p	δ_y
2.0013	0.9574	0.9027	0.9100	-1.88	6.98
3.0027	0.9717	0.8837	0.8910	-0.78	7.28
4.0027	0.9695	0.8734	0.8805	0.34	7.29
5.0024	0.9678	0.8615	0.8686	1.38	7.17
5.9942	0.9665	0.8528	0.8597	1.72	7.07

$\delta_A =$ 15.0°, $\delta_B =$ -10.0°

NPR	w_p/w_i	F/F_i	F_r/F_i	δ_p	δ_y
2.0015	0.9569	0.8661	0.8736	1.96	7.27
2.9964	0.9722	0.8466	0.8554	3.27	7.54
4.0031	0.9694	0.8330	0.8428	4.49	7.52
5.0026	0.9679	0.8233	0.8322	4.92	6.82
5.9992	0.9666	0.8161	0.8239	4.99	6.17

$\delta_A =$ 20.0°, $\delta_B =$ -10.0°

NPR	w_p/w_i	F/F_i	F_r/F_i	δ_p	δ_y
2.0022	0.9571	0.8085	0.8235	7.17	8.37
2.9961	0.9719	0.7841	0.8011	8.06	8.76
4.0000	0.9693	0.7690	0.7833	7.86	7.73
5.0077	0.9679	0.7634	0.7737	7.08	6.13
5.0010	0.9677	0.7633	0.7736	7.12	6.18
5.9998	0.9667	0.7665	0.7749	6.70	5.18

Table 64. Maximum A/B-Power Nozzle Performance of Rotating Vane Actuation System for Large Vane and Two Standard Vanes Installed With Vane A Partially Retracted, $\delta_C = 25°$, and Vane B Fully Retracted

[δ_p and δ_y are given in degrees]

δ_A = -5.0°, δ_B = -10.0°

NPR	w_p/w_i	F/F_i	F_r/F_i	δ_p	δ_y
2.0048	0.9578	0.9293	0.9420	-6.24	7.16
3.0019	0.9706	0.9169	0.9308	-6.56	7.51
4.0067	0.9691	0.9101	0.9244	-6.75	7.57
4.9986	0.9673	0.8980	0.9140	-7.22	8.03
6.0080	0.9662	0.8879	0.9039	-7.38	7.98

δ_A = 0.0°, δ_B = -10.0°

NPR	w_p/w_i	F/F_i	F_r/F_i	δ_p	δ_y
2.0039	0.9584	0.9288	0.9410	-6.00	7.06
2.9999	0.9708	0.9148	0.9273	-5.96	7.35
4.0056	0.9691	0.9060	0.9180	-5.55	7.46
5.0016	0.9675	0.8930	0.9051	-5.23	7.83
6.0089	0.9663	0.8815	0.8925	-4.65	7.74

Table 65. Maximum A/B-Power Nozzle Performance of Rotating Vane Actuation System for Large Vane and Two Standard Vanes Installed With Vanes A and C Unequally Deployed, $\delta_C = 22.5°$, and Vane B Fully Retracted

[δ_p and δ_y are given in degrees]

δ_A = 10.0°, δ_B = -10.0°

NPR	w_p/w_i	F/F_i	F_r/F_i	δ_p	δ_y
2.0018	0.9559	0.9184	0.9239	-1.59	6.01
3.0034	0.9708	0.9014	0.9070	-0.70	6.33
4.0029	0.9692	0.8893	0.8951	0.46	6.49
5.0012	0.9679	0.8746	0.8809	1.38	6.68
5.9981	0.9662	0.8627	0.8692	2.01	6.68

δ_A = 15.0°, δ_B = -10.0°

NPR	w_p/w_i	F/F_i	F_r/F_i	δ_p	δ_y
2.0021	0.9557	0.8814	0.8876	2.77	6.21
2.9997	0.9707	0.8598	0.8675	3.83	6.65
4.0000	0.9695	0.8444	0.8537	5.05	6.84
5.0009	0.9680	0.8335	0.8426	5.46	6.46
6.0004	0.9657	0.8268	0.8349	5.40	5.88

δ_A = 20.0°, δ_B = -10.0°

NPR	w_p/w_i	F/F_i	F_r/F_i	δ_p	δ_y
2.0075	0.9553	0.8248	0.8377	6.98	7.31
2.9979	0.9709	0.8017	0.8172	8.02	7.91
4.0013	0.9693	0.7870	0.8018	8.26	7.42
5.0000	0.9679	0.7805	0.7917	7.61	6.06
5.9918	0.9663	0.7778	0.7869	7.11	5.11

Table 66. Maximum A/B-Power Nozzle Performance of Rotating Vane Actuation System for Large Vane and Two Standard Vanes Installed With Vanes A and C Unequally Deployed, $\delta_C = 17.5°$, and Vane B Fully Retracted

[δ_p and δ_y are given in degrees]

$\delta_A = 10.0°$, $\delta_B = -10.0°$

NPR	w_p/w_i	F/F_i	F_r/F_i	δ_p	δ_y
2.0056	0.9559	0.9543	0.9563	-0.41	3.76
3.0024	0.9709	0.9398	0.9422	0.08	4.10
4.0038	0.9693	0.9237	0.9266	0.84	4.52
4.9971	0.9679	0.9060	0.9100	1.47	5.18
6.0013	0.9663	0.8939	0.8985	2.09	5.40

$\delta_A = 15.0°$, $\delta_B = -10.0°$

NPR	w_p/w_i	F/F_i	F_r/F_i	δ_p	δ_y
2.0021	0.9555	0.9185	0.9221	3.31	3.82
3.0053	0.9706	0.9011	0.9058	3.86	4.39
4.0070	0.9694	0.8822	0.8888	4.92	4.99
5.0044	0.9679	0.8697	0.8772	5.52	5.14
5.9982	0.9661	0.8623	0.8699	5.67	5.01

Table 67. Maximum A/B-Power Nozzle Performance of Rotating Vane Actuation System for Large Vane and Two Standard Vanes Installed With Three Vanes Equally Deployed

[δ_p and δ_y are given in degrees]

δ_A = 5.0°, δ_B = 5.0° , δ_C = 5.0°

NPR	w_p/w_i	F/F_i	F_r/F_i	δ_p	δ_y
2.0113	0.9570	1.0020	1.0020	0.25	-0.03
2.0058	0.9568	1.0010	1.0010	0.23	-0.03
3.0007	0.9711	0.9883	0.9883	0.29	-0.03
4.0022	0.9696	0.9703	0.9703	0.24	-0.20
5.0025	0.9686	0.9517	0.9518	0.32	-0.46
6.0054	0.9663	0.9388	0.9389	0.49	-0.73

δ_A = 10.0°, δ_B = 10.0° , δ_C = 10.0°

NPR	w_p/w_i	F/F_i	F_r/F_i	δ_p	δ_y
1.9985	0.9557	0.9738	0.9738	0.45	-0.37
3.0009	0.9711	0.9567	0.9568	0.56	-0.45
4.0019	0.9700	0.9362	0.9364	0.78	-0.69
5.0027	0.9686	0.9111	0.9114	1.08	-1.07
6.0033	0.9667	0.8961	0.8966	1.32	-1.33

δ_A = 15.0°, δ_B = 15.0° , δ_C = 15.0°

NPR	w_p/w_i	F/F_i	F_r/F_i	δ_p	δ_y
1.9991	0.9558	0.8832	0.8837	0.91	-1.81
3.0055	0.9717	0.8506	0.8514	1.25	-2.19
4.0016	0.9699	0.8121	0.8132	1.36	-2.69
5.0055	0.9686	0.7876	0.7891	1.47	-3.23
5.9991	0.9667	0.7763	0.7778	1.40	-3.33

δ_A = 20.0°, δ_B = 20.0° , δ_C = 20.0°

NPR	w_p/w_i	F/F_i	F_r/F_i	δ_p	δ_y
2.0019	0.9558	0.6930	0.6961	0.40	-5.38
2.9977	0.9726	0.6606	0.6639	0.75	-5.68
3.9997	0.9694	0.6526	0.6562	0.89	-5.99
5.0007	0.9676	0.6469	0.6509	1.10	-6.26
6.0037	0.9664	0.6448	0.6490	1.45	-6.32

Table 67. Concluded

δ_A = 25.0°, δ_B = 25.0° , δ_C = 25.0°

NPR	w_p/w_i	F/F_i	F_r/F_i	δ_p	δ_y
2.0056	0.9420	0.5079	0.5181	2.45	-11.09
3.0039	0.9692	0.4696	0.4805	2.41	-12.01
4.0003	0.9697	0.4646	0.4753	2.11	-12.02
5.0045	0.9682	0.4663	0.4766	2.28	-11.74
5.9984	0.9663	0.4765	0.4859	2.21	-11.04

δ_A = 30.0°, δ_B = 30.0° , δ_C = 30.0°

NPR	w_p/w_i	F/F_i	F_r/F_i	δ_p	δ_y
2.0016	0.8769	0.2704	0.2997	7.74	-24.59
3.0021	0.9357	0.2458	0.2805	10.02	-27.47
4.0028	0.9526	0.2382	0.2711	10.75	-26.99
5.0041	0.9614	0.2363	0.2691	11.17	-26.90
6.0065	0.9637	0.2377	0.2681	11.01	-25.85

C-2

Table 68. Maximum A/B-Power Nozzle Performance of Rotating Vane Actuation System for Large Vane and Two Standard Vanes Installed With Three Vanes Partially Retracted

[δ_p and δ_y are given in degrees]

δ_A = -5.0°, δ_B = -5.0° , δ_C = -5.0°

NPR	w_p/w_i	F/F_i	F_r/F_i	δ_p	δ_y
2.0035	0.9569	1.0079	1.0079	0.33	0.09
3.0078	0.9708	0.9977	0.9977	0.40	0.13
4.0025	0.9699	0.9852	0.9852	0.29	0.15
5.0022	0.9688	0.9720	0.9720	0.24	0.15
6.0034	0.9662	0.9621	0.9622	0.39	0.03

δ_A = 0.0°, δ_B = 0.0° , δ_C = 0.0°

NPR	w_p/w_i	F/F_i	F_r/F_i	δ_p	δ_y
2.0025	0.9565	1.0068	1.0068	0.31	0.04
3.0026	0.9715	0.9975	0.9975	0.39	0.08
4.0001	0.9701	0.9825	0.9825	0.37	0.01
5.0000	0.9686	0.9677	0.9677	0.55	-0.15
5.9995	0.9662	0.9560	0.9561	0.76	-0.37

Table 69. Military-Power Nozzle Performance
With No Vanes Installed

[δ_p and δ_y are given in degrees]

(a) Run 1

NPR	w_p/w_i	F/F_i	F_r/F_i	δ_p	δ_y
2.0030	0.8856	1.0021	1.0021	0.17	-0.14
2.9973	0.9291	1.0007	1.0007	0.33	-0.01
4.0022	0.9361	0.9894	0.9894	0.40	0.00
4.9924	0.9365	0.9788	0.9788	0.36	0.03
5.9988	0.9285	0.9681	0.9681	0.32	0.06

(b) Run 2

NPR	w_p/w_i	F/F_i	F_r/F_i	δ_p	δ_y
1.9996	0.8862	0.9998	0.9999	0.00	-0.15
3.0044	0.9283	0.9978	0.9978	0.30	-0.09
3.9989	0.9358	0.9884	0.9884	0.36	0.00
4.9862	0.9312	0.9776	0.9776	0.38	0.01
6.0022	0.9286	0.9682	0.9682	0.34	0.05

(c) Run 18

NPR	w_p/w_i	F/F_i	F_r/F_i	δ_p	δ_y
2.0026	0.8865	0.9994	0.9994	-0.08	-0.23
3.0007	0.9285	0.9985	0.9985	0.11	-0.08
3.9962	0.9361	0.9892	0.9892	0.19	-0.02
5.0077	0.9287	0.9770	0.9770	0.21	0.06
6.0006	0.9286	0.9690	0.9691	0.17	0.07

(d) Run 250

NPR	w_p/w_i	F/F_i	F_r/F_i	δ_p	δ_y
2.0008	0.8863	0.9992	0.9992	0.06	-0.14
2.9941	0.9272	1.0001	1.0001	0.39	-0.11
4.0025	0.9336	0.9885	0.9885	0.42	-0.10
4.9867	0.9320	0.9781	0.9781	0.45	-0.04
6.0000	0.9285	0.9681	0.9681	0.41	-0.03

Table 69. Concluded

(e) Run 370

NPR	w_p/w_i	F/F_i	F_r/F_i	δ_p	δ_y
2.0004	0.8861	0.9992	0.9992	-0.10	-0.23
3.0034	0.9280	0.9989	0.9989	0.25	-0.09
4.0104	0.9340	0.9889	0.9889	0.29	-0.05
4.0009	0.9355	0.9904	0.9904	0.28	-0.05
4.9808	0.9335	0.9792	0.9792	0.22	-0.01
5.9982	0.9282	0.9694	0.9694	0.22	0.05

Table 70. Military-Power Nozzle Performance of Translating Vane Actuation System With Single Standard Vane Installed and Deployed

[δ_p and δ_y are given in degrees]

δ_A = 10.0°, δ_B = off , δ_C = off

NPR	w_p/w_i	F/F_i	F_r/F_i	δ_p	δ_y
2.0012	0.8859	0.9997	0.9997	0.19	-0.22
2.9939	0.9274	0.9985	0.9985	0.43	-0.03
4.0061	0.9359	0.9879	0.9880	0.62	-0.05
5.0126	0.9286	0.9733	0.9734	0.99	0.00
6.0042	0.9284	0.9620	0.9624	1.58	0.00

δ_A = 15.0°, δ_B = off , δ_C = off

NPR	w_p/w_i	F/F_i	F_r/F_i	δ_p	δ_y
2.0100	0.8867	0.9975	0.9975	0.31	-0.16
2.9928	0.9279	0.9950	0.9951	0.71	-0.08
4.0070	0.9358	0.9825	0.9827	1.20	-0.08
4.9825	0.9360	0.9681	0.9686	1.92	-0.09
5.0240	0.9287	0.9665	0.9670	1.95	-0.08
5.9990	0.9286	0.9537	0.9547	2.71	-0.10

δ_A = 17.5°, δ_B = off , δ_C = off

NPR	w_p/w_i	F/F_i	F_r/F_i	δ_p	δ_y
2.0069	0.8868	0.9856	0.9859	1.22	-0.16
3.0014	0.9273	0.9849	0.9853	1.65	-0.08
3.9970	0.9359	0.9709	0.9717	2.39	-0.14
5.0278	0.9318	0.9518	0.9535	3.44	-0.19
5.9995	0.9285	0.9371	0.9399	4.35	-0.29

Table 70. Concluded

δ_A = 25.0°, δ_B = off, δ_C = off
X = 1.757, R = 0.611

NPR	w_p/w_i	F/F_i	F_r/F_i	δ_p	δ_y
2.0022	0.8864	0.9737	0.9745	2.39	-0.24
3.0063	0.9285	0.9686	0.9699	2.93	-0.21
3.9999	0.9360	0.9552	0.9572	3.65	-0.25
5.0203	0.9299	0.9355	0.9388	4.80	-0.30
5.9997	0.9286	0.9216	0.9262	5.69	-0.34

δ_A = 25.0°, δ_B = off, δ_C = off
X = 1.590, R = 0.310

NPR	w_p/w_i	F/F_i	F_r/F_i	δ_p	δ_y
2.0004	0.8860	0.9454	0.9512	6.30	-0.78
2.9950	0.9282	0.9379	0.9451	7.02	-0.63
4.0054	0.9358	0.9292	0.9374	7.55	-0.58
4.9790	0.9324	0.9147	0.9252	8.60	-0.63
6.0093	0.9283	0.9013	0.9143	9.64	-0.69

δ_A = 25.0°, δ_B = off, δ_C = off
X = 1.359, R = 0.072

NPR	w_p/w_i	F/F_i	F_r/F_i	δ_p	δ_y
2.0032	0.8865	0.9223	0.9371	10.15	-0.89
3.0041	0.9277	0.9155	0.9328	11.01	-0.96
4.0037	0.9357	0.9089	0.9278	11.55	-0.86
4.9972	0.9287	0.8950	0.9177	12.73	-1.06
5.9952	0.9285	0.8837	0.9095	13.64	-1.09

Table 71. Military-Power Nozzle Performance of Translating Vane Actuation System With Three Standard Vanes Installed

[δ_p and δ_y are given in degrees]

(a) One vane deployed; two vanes retracted. $X = 1.359$ in. and $R = 0.072$ in. for 25° deployed vane

δ_A = 25.0°, δ_B = -10.0° , δ_C = -10.0°

NPR	w_p/w_i	F/F_i	F_r/F_i	δ_p	δ_y
2.0033	0.8861	0.9217	0.9372	10.40	-0.97
3.0030	0.9286	0.9171	0.9349	11.18	-0.90
4.0075	0.9360	0.9094	0.9289	11.74	-0.94
5.0104	0.9337	0.8949	0.9182	12.88	-1.07
5.9930	0.9285	0.8824	0.9085	13.73	-1.14

δ_A = -10.0°, δ_B = 25.0° , δ_C = -10.0°

NPR	w_p/w_i	F/F_i	F_r/F_i	δ_p	δ_y
2.0066	0.8870	0.9112	0.9298	-5.81	-9.99
3.0002	0.9280	0.9060	0.9261	-6.07	-10.36
4.0049	0.9360	0.8980	0.9197	-6.52	-10.75
5.0063	0.9367	0.8854	0.9104	-7.37	-11.40
5.9989	0.9286	0.8736	0.9014	-8.31	-11.76

δ_A = -10.0°, δ_B = -10.0° , δ_C = 25.0°

NPR	w_p/w_i	F/F_i	F_r/F_i	δ_p	δ_y
2.0032	0.8872	0.9147	0.9328	-7.70	8.37
3.0103	0.9288	0.9065	0.9272	-8.16	9.11
4.0027	0.9361	0.8991	0.9213	-8.62	9.31
5.0588	0.9288	0.8842	0.9101	-9.65	9.90
4.9805	0.9368	0.8862	0.9122	-9.68	9.90
5.9995	0.9287	0.8746	0.9036	-10.65	10.14

Table 71. Concluded

(b) Two vanes deployed; one vane retracted. $X = 1.359$ in. and $R = 0.072$ in. for 25° deployed vane

$\delta_A = 25.0°$, $\delta_B = 25.0°$, $\delta_C = -10.0°$

NPR	w_p/w_i	F/F_i	F_r/F_i	δ_p	δ_y
2.0080	0.8840	0.7421	0.7936	8.34	-19.28
3.0071	0.9250	0.7199	0.7725	8.04	-19.92
4.0094	0.9358	0.7137	0.7628	7.08	-19.62
5.0224	0.9314	0.7120	0.7564	6.41	-18.80
5.9998	0.9284	0.7100	0.7512	5.69	-18.30

$\delta_A = -10.0°$, $\delta_B = 25.0°$, $\delta_C = 25.0°$

NPR	w_p/w_i	F/F_i	F_r/F_i	δ_p	δ_y
2.0013	0.8789	0.7094	0.8243	-30.45	-3.87
3.0080	0.9268	0.6825	0.8051	-31.85	-4.30
4.0046	0.9355	0.6761	0.7922	-31.22	-4.31
5.0304	0.9339	0.6764	0.7801	-29.63	-4.67
5.9991	0.9285	0.6743	0.7691	-28.48	-4.68

$\delta_A = 25.0°$, $\delta_B = -10.0°$, $\delta_C = 25.0°$

NPR	w_p/w_i	F/F_i	F_r/F_i	δ_p	δ_y
2.0028	0.8855	0.7605	0.7776	3.80	11.45
3.0122	0.9255	0.7373	0.7528	3.68	11.07
4.0064	0.9357	0.7294	0.7418	3.06	10.06
5.0030	0.9351	0.7245	0.7339	2.37	8.85
6.0036	0.9285	0.7221	0.7291	1.55	7.82

Table 72. Military-Power Nozzle Performance of Rotating Vane Actuation System With Single Standard Vane Installed and Deployed

[δ_p and δ_y are given in degrees]

δ_A = 10.0°, δ_B = off , δ_C = off

NPR	w_p/w_i	F/F_i	F_r/F_i	δ_p	δ_y
2.0043	0.8864	0.9982	0.9982	-0.02	-0.08
3.0056	0.9273	0.9966	0.9966	0.32	-0.04
4.0117	0.9345	0.9865	0.9866	0.51	0.00
5.0112	0.9287	0.9715	0.9717	1.09	0.04
6.0095	0.9285	0.9580	0.9585	1.90	0.01
6.0042	0.9284	0.9584	0.9589	1.91	0.01

δ_A = 15.0°, δ_B = off , δ_C = off

NPR	w_p/w_i	F/F_i	F_r/F_i	δ_p	δ_y
2.0031	0.8865	0.9879	0.9880	0.97	-0.32
3.0128	0.9263	0.9847	0.9851	1.57	-0.04
4.0009	0.9358	0.9752	0.9757	1.92	-0.05
5.0003	0.9287	0.9566	0.9580	3.03	-0.08
6.0017	0.9284	0.9408	0.9436	4.38	-0.20

δ_A = 17.5°, δ_B = off , δ_C = off

NPR	w_p/w_i	F/F_i	F_r/F_i	δ_p	δ_y
2.0054	0.8865	0.9774	0.9781	2.13	-0.24
2.9950	0.9279	0.9745	0.9756	2.78	-0.12
4.0052	0.9357	0.9640	0.9655	3.17	-0.18
5.0012	0.9287	0.9452	0.9480	4.40	-0.25
5.9983	0.9285	0.9296	0.9342	5.69	-0.30

δ_A = 20.0°, δ_B = off , δ_C = off

NPR	w_p/w_i	F/F_i	F_r/F_i	δ_p	δ_y
2.0047	0.8863	0.9683	0.9697	3.08	-0.25
2.9929	0.9282	0.9619	0.9638	3.63	-0.27
4.0041	0.9358	0.9515	0.9541	4.22	-0.28
4.9991	0.9300	0.9326	0.9369	5.52	-0.29
6.0056	0.9286	0.9168	0.9234	6.85	-0.39

Table 72. Concluded

δ_A = 25.0°, δ_B = off , δ_C = off

NPR	w_p/w_i	F/F_i	F_r/F_i	δ_p	δ_y
2.0025	0.8863	0.9316	0.9370	6.13	-0.70
2.9905	0.9284	0.9247	0.9318	7.06	-0.59
4.0044	0.9358	0.9140	0.9225	7.75	-0.56
5.0061	0.9288	0.9024	0.9127	8.60	-0.60
5.9969	0.9285	0.8907	0.9039	9.79	-0.68

δ_A = 30.0°, δ_B = off , δ_C = off

NPR	w_p/w_i	F/F_i	F_r/F_i	δ_p	δ_y
2.0010	0.8858	0.8663	0.8845	11.60	-1.05
3.0019	0.9285	0.8568	0.8782	12.63	-1.03
4.0083	0.9359	0.8544	0.8769	12.96	-1.01
4.9802	0.9342	0.8544	0.8769	12.98	-1.04
4.9854	0.9348	0.8541	0.8769	13.04	-1.03
6.0115	0.9285	0.8464	0.8709	13.60	-1.01

δ_A = off, δ_B = 25.0°, δ_C = off

NPR	w_p/w_i	F/F_i	F_r/F_i	δ_p	δ_y
1.9938	0.8882	0.8939	0.9062	-4.86	-8.16
3.0089	0.9285	0.8854	0.8994	-5.10	-8.78
4.0100	0.9318	0.8785	0.8933	-5.37	-9.04
5.0001	0.9288	0.8753	0.8907	-5.46	-9.21
6.0153	0.9291	0.8666	0.8841	-6.07	-9.77

δ_A = off, δ_B = 30.0°, δ_C = off

NPR	w_p/w_i	F/F_i	F_r/F_i	δ_p	δ_y
2.0002	0.8908	0.8536	0.8760	-6.85	-11.14
3.0074	0.9285	0.8445	0.8683	-6.86	-11.67
4.0163	0.9289	0.8429	0.8663	-6.89	-11.53
5.0058	0.9290	0.8458	0.8679	-6.82	-11.12
6.0037	0.9284	0.8404	0.8639	-7.09	-11.46

Table 73. Military-Power Nozzle Performance of Rotating Vane Actuation System With Two Standard Vanes Installed and Deployed

[δ_p and δ_y are given in degrees]

δ_A = off, δ_B = 25.0° , δ_C = 25.0°

NPR	w_p/w_i	F/F_i	F_r/F_i	δ_p	δ_y
1.9951	0.8883	0.7612	0.7966	-17.04	-1.84
3.0088	0.9265	0.7318	0.7757	-19.31	-1.74
4.0175	0.9299	0.7140	0.7696	-21.86	-1.82
5.0112	0.9291	0.7101	0.7704	-22.76	-1.95
5.9985	0.9284	0.7093	0.7716	-23.11	-1.92

Table 74. Military-Power Nozzle Performance of Rotating Vane Actuation System With Three Standard Vanes Installed and Deployed

[δ_p and δ_y are given in degrees]

(a) One vane deployed and two vanes retracted

δ_A = 30.0°, δ_B = -10.0° , δ_C = -10.0°

NPR	w_p/w_i	F/F_i	F_r/F_i	δ_p	δ_y
2.0003	0.8857	0.8677	0.8859	11.62	-0.63
3.0027	0.9279	0.8583	0.8793	12.53	-0.82
4.0085	0.9354	0.8558	0.8779	12.84	-0.98
5.0089	0.9285	0.8536	0.8761	12.99	-0.91
6.0036	0.9286	0.8461	0.8708	13.64	-0.93

δ_A = -10.0°, δ_B = 30.0° , δ_C = -10.0°

NPR	w_p/w_i	F/F_i	F_r/F_i	δ_p	δ_y
2.0029	0.8859	0.8496	0.8720	-6.73	-11.26
3.0029	0.9282	0.8424	0.8663	-7.11	-11.60
3.9992	0.9360	0.8421	0.8655	-6.90	-11.53
4.9700	0.9345	0.8444	0.8670	-6.80	-11.33
5.0393	0.9286	0.8421	0.8647	-6.78	-11.36
5.0053	0.9350	0.8442	0.8667	-6.82	-11.28
6.0050	0.9284	0.8387	0.8627	-7.12	-11.65

δ_A = -10.0°, δ_B = -10.0° , δ_C = 30.0°

NPR	w_p/w_i	F/F_i	F_r/F_i	δ_p	δ_y
2.0055	0.8853	0.8531	0.8782	-9.69	9.92
3.0062	0.9278	0.8434	0.8711	-10.12	10.55
3.9997	0.9356	0.8420	0.8689	-9.68	10.71
4.9997	0.9284	0.8445	0.8698	-9.35	10.41
5.9996	0.9284	0.8401	0.8663	-9.65	10.54

Table 74. Concluded

(b) Two vanes deployed and one vane retracted

δ_A = 30.0°, δ_B = 30.0°, δ_C = -10.0°

NPR	w_p/w_i	F/F_i	F_r/F_i	δ_p	δ_y
2.0013	0.8844	0.6227	0.6837	11.57	-22.02
3.0093	0.9269	0.6100	0.6763	12.15	-23.16
3.9973	0.9356	0.6101	0.6680	11.09	-21.84
4.9973	0.9355	0.6148	0.6624	9.24	-20.12
6.0007	0.9284	0.6206	0.6607	7.77	-18.72

δ_A = -10.0°, δ_B = 30.0°, δ_C = 30.0°

NPR	w_p/w_i	F/F_i	F_r/F_i	δ_p	δ_y
2.0004	0.8833	0.5891	0.7162	-34.57	-3.28
3.0134	0.9265	0.5817	0.7121	-35.15	-2.93
4.0002	0.9357	0.5830	0.7028	-33.84	-3.49
5.0116	0.9341	0.5887	0.6917	-31.55	-3.33
5.9936	0.9284	0.5930	0.6813	-29.37	-3.35

δ_A = 30.0°, δ_B = -10.0°, δ_C = 30.0°

NPR	w_p/w_i	F/F_i	F_r/F_i	δ_p	δ_y
2.0045	0.8848	0.6440	0.6676	4.03	14.79
2.9989	0.9281	0.6179	0.6426	4.90	15.26
4.0074	0.9348	0.6181	0.6355	3.76	12.96
4.9811	0.9341	0.6240	0.6354	2.41	10.61
5.0413	0.9285	0.6240	0.6354	2.44	10.64
6.0086	0.9284	0.6313	0.6397	1.50	9.18

Table 75. Military-Power Nozzle Performance of Rotating Vane Actuation System With Single Large Vane Installed and Deployed

[δ_p and δ_y are given in degrees]

δ_A = 25.0°, δ_B = off , δ_C = off

NPR	w_p/w_i	F/F_i	F_r/F_i	δ_p	δ_y
2.0042	0.8872	0.8947	0.9101	10.47	-1.20
3.0059	0.9271	0.8843	0.9021	11.34	-1.11
4.0017	0.9303	0.8722	0.8931	12.36	-1.09
4.9951	0.9290	0.8622	0.8861	13.28	-1.17
6.0127	0.9295	0.8533	0.8808	14.30	-1.22

δ_A = 30.0°, δ_B = off , δ_C = off

NPR	w_p/w_i	F/F_i	F_r/F_i	δ_p	δ_y
2.0127	0.8919	0.8188	0.8553	16.74	-1.53
3.0264	0.9260	0.8048	0.8445	17.58	-1.59
3.9935	0.9314	0.8020	0.8435	17.99	-1.59
5.0082	0.9287	0.8016	0.8442	18.21	-1.59
5.9926	0.9285	0.7988	0.8441	18.80	-1.57

Table 76. Military-Power Nozzle Performance of Rotating Vane Actuation System With Large Vane and One Standard Vane Installed and Deployed

[δ_p and δ_y are given in degrees]

δ_A = 25.0°, δ_B = 25.0° , δ_C = off

NPR	w_p/w_i	F/F_i	F_r/F_i	δ_p	δ_y
2.0022	0.8876	0.7409	0.7724	9.36	-13.74
3.0003	0.9255	0.7093	0.7524	11.84	-15.91
4.0080	0.9295	0.6822	0.7395	14.15	-18.46
5.0190	0.9299	0.6717	0.7378	15.29	-19.93
6.0172	0.9291	0.6707	0.7399	15.79	-20.32

δ_A = 25.0°, δ_B = off , δ_C = 25.0°

NPR	w_p/w_i	F/F_i	F_r/F_i	δ_p	δ_y
2.0112	0.8908	0.7664	0.7765	6.18	6.92
3.0207	0.9257	0.7326	0.7477	7.87	8.54
4.0038	0.9328	0.7042	0.7262	9.78	10.42
5.0103	0.9296	0.6915	0.7177	10.69	11.54
6.0023	0.9288	0.6874	0.7155	11.15	11.94

Table 77. Military-Power Nozzle Performance of Rotating Vane Actuation System for Large Vane and Two Standard Vanes Installed With Vane A Deployed and Vanes B and C Fully Retracted

[δ_p and δ_y are given in degrees]

δ_A = 10.0°, δ_B = -10.0° , δ_C = -10.0°

NPR	w_p/w_i	F/F_i	F_r/F_i	δ_p	δ_y
2.0016	0.8860	0.9973	0.9973	0.27	-0.21
3.0014	0.9282	0.9967	0.9967	0.69	-0.20
4.0037	0.9358	0.9861	0.9862	0.92	-0.15
5.0024	0.9283	0.9684	0.9689	1.75	-0.12
6.0004	0.9284	0.9529	0.9541	2.86	-0.16

δ_A = 15.0°, δ_B = -10.0° , δ_C = -10.0°

NPR	w_p/w_i	F/F_i	F_r/F_i	δ_p	δ_y
2.0069	0.8864	0.9844	0.9848	1.58	-0.31
3.0113	0.9263	0.9809	0.9816	2.23	-0.28
3.0044	0.9268	0.9819	0.9825	2.14	-0.24
4.0049	0.9359	0.9693	0.9704	2.82	-0.24
5.0016	0.9285	0.9472	0.9499	4.30	-0.34
6.0038	0.9285	0.9286	0.9338	5.99	-0.44

δ_A = 20.0°, δ_B = -10.0° , δ_C = -10.0°

NPR	w_p/w_i	F/F_i	F_r/F_i	δ_p	δ_y
3.0063	0.9248	0.9297	0.9362	6.75	-0.45
4.0049	0.9349	0.9171	0.9258	7.84	-0.62
4.9997	0.9284	0.8999	0.9121	9.34	-0.73
5.9970	0.9283	0.8856	0.9022	10.97	-0.86

δ_A = 25.0°, δ_B = -10.0° , δ_C = -10.0°

NPR	w_p/w_i	F/F_i	F_r/F_i	δ_p	δ_y
1.9960	0.8853	0.8867	0.9019	10.51	-0.62
3.0060	0.9245	0.8759	0.8948	11.74	-0.96
4.0020	0.9349	0.8655	0.8877	12.80	-1.16
5.0013	0.9285	0.8554	0.8808	13.72	-1.23
5.9986	0.9282	0.8461	0.8754	14.83	-1.24

Table 77. Concluded

δ_A = 30.0°, δ_B = -10.0° , δ_C = -10.0°

NPR	w_p/w_i	F/F_i	F_r/F_i	δ_p	δ_y
2.0110	0.8875	0.8161	0.8531	16.90	-1.29
2.9988	0.9291	0.8011	0.8431	18.09	-1.62
3.9973	0.9361	0.7992	0.8435	18.61	-1.44
4.9858	0.9303	0.7974	0.8428	18.84	-1.48
5.9901	0.9285	0.7940	0.8415	19.28	-1.64

δ_A = 35.0°, δ_B = -10.0° , δ_C = -10.0°

NPR	w_p/w_i	F/F_i	F_r/F_i	δ_p	δ_y
2.0002	0.8881	0.7475	0.8088	22.27	-3.15
2.9926	0.9252	0.7350	0.7990	22.91	-3.27
2.9990	0.9255	0.7352	0.7997	23.00	-3.17
4.0014	0.9355	0.7375	0.8001	22.60	-3.48
4.9983	0.9288	0.7410	0.8002	21.94	-3.73
6.0032	0.9283	0.7419	0.7987	21.43	-4.07

Table 78. Military-Power Nozzle Performance of Rotating Vane Actuation System for Large Vane and Two Standard Vanes Installed With Vane A Deployed and Vanes B and C Partially Retracted

[δ_p and δ_y are given in degrees]

δ_A = 30.0°, δ_B = -5.0° , δ_C = -5.0°

NPR	w_p/w_i	F/F_i	F_r/F_i	δ_p	δ_y
2.0001	0.8863	0.8153	0.8541	17.27	-1.59
2.9898	0.9278	0.8005	0.8432	18.22	-1.82
3.9865	0.9319	0.7958	0.8399	18.57	-1.87
4.0082	0.9290	0.7946	0.8387	18.58	-1.90
4.9994	0.9283	0.7936	0.8369	18.40	-2.09
5.0001	0.9286	0.7932	0.8363	18.37	-2.06
6.0005	0.9282	0.7898	0.8335	18.51	-2.36

δ_A = 25.0°, δ_B = -5.0° , δ_C = -5.0°

NPR	w_p/w_i	F/F_i	F_r/F_i	δ_p	δ_y
2.0020	0.8858	0.8860	0.9026	10.97	-0.92
3.0018	0.9238	0.8754	0.8946	11.87	-0.91
3.9972	0.9337	0.8643	0.8872	12.99	-1.20
5.0001	0.9284	0.8542	0.8798	13.80	-1.26
6.0021	0.9283	0.8453	0.8745	14.79	-1.35

δ_A = 30.0°, δ_B = 0.0° , δ_C = 0.0°

NPR	w_p/w_i	F/F_i	F_r/F_i	δ_p	δ_y
2.0008	0.8860	0.8164	0.8546	17.06	-2.17
3.0019	0.9257	0.7977	0.8380	17.68	-2.52
3.9993	0.9355	0.7890	0.8288	17.59	-3.01
4.9969	0.9286	0.7812	0.8169	16.71	-3.31
6.0024	0.9282	0.7733	0.8073	16.32	-3.73

Table 79. Military-Power Nozzle Performance of Rotating Vane Actuation System for Large Vane and Two Standard Vanes Installed With Vane B Deployed and Vanes A and C Fully Retracted

[δ_p and δ_y are given in degrees]

δ_A = -10.0°, δ_B = 10.0° , δ_C = -10.0°

NPR	w_p/w_i	F/F_i	F_r/F_i	δ_p	δ_y
2.0010	0.8866	0.9975	0.9976	0.05	-0.46
3.0013	0.9258	0.9928	0.9928	0.17	-0.50
3.9999	0.9354	0.9833	0.9834	0.07	-0.72
5.0015	0.9282	0.9662	0.9665	-0.30	-1.26
5.9996	0.9282	0.9530	0.9538	-0.90	-2.07

δ_A = -10.0°, δ_B = 15.0° , δ_C = -10.0°

NPR	w_p/w_i	F/F_i	F_r/F_i	δ_p	δ_y
1.9994	0.8859	0.9872	0.9876	-0.58	-1.52
3.0004	0.9249	0.9795	0.9800	-0.63	-1.73
4.0001	0.9355	0.9699	0.9706	-0.73	-1.98
4.9979	0.9283	0.9515	0.9529	-1.30	-2.87
6.0017	0.9283	0.9364	0.9393	-2.12	-3.96

δ_A = -10.0°, δ_B = 20.0° , δ_C = -10.0°

NPR	w_p/w_i	F/F_i	F_r/F_i	δ_p	δ_y
2.0014	0.8862	0.9436	0.9480	-2.64	-4.84
3.0007	0.9276	0.9377	0.9426	-2.71	-5.16
3.9995	0.9342	0.9291	0.9345	-2.87	-5.44
4.9986	0.9297	0.9160	0.9229	-3.41	-6.18
5.9995	0.9284	0.9026	0.9123	-4.26	-7.22

δ_A = -10.0°, δ_B = 25.0° , δ_C = -10.0°

NPR	w_p/w_i	F/F_i	F_r/F_i	δ_p	δ_y
2.0015	0.8864	0.9077	0.9178	-4.44	-7.30
3.0066	0.9258	0.8997	0.9109	-4.69	-7.74
4.0020	0.9352	0.8945	0.9066	-4.84	-8.05
5.0012	0.9285	0.8894	0.9020	-4.86	-8.29
6.0002	0.9283	0.8796	0.8947	-5.55	-9.01

Table 79. Concluded

δ_A = -10.0°, δ_B = 30.0° , δ_C = -10.0°

NPR	w_p/w_i	F/F_i	F_r/F_i	δ_p	δ_y
2.0005	0.8856	0.8695	0.8885	-6.50	-10.03
2.9915	0.9294	0.8608	0.8816	-6.68	-10.63
3.9998	0.9359	0.8578	0.8787	-6.59	-10.74
4.9802	0.9333	0.8562	0.8766	-6.55	-10.61
6.0020	0.9282	0.8491	0.8714	-6.91	-11.11

δ_A = -10.0°, δ_B = 35.0° , δ_C = -10.0°

NPR	w_p/w_i	F/F_i	F_r/F_i	δ_p	δ_y
2.0000	0.8862	0.8001	0.8348	-10.35	-13.24
2.9945	0.9267	0.7948	0.8308	-10.22	-13.78
3.9996	0.9352	0.8002	0.8326	-9.12	-13.41
4.9984	0.9288	0.8041	0.8338	-8.69	-12.82
6.0007	0.9286	0.7998	0.8301	-9.12	-12.78

Table 80. Military-Power Nozzle Performance of Rotating Vane Actuation System for Large Vane and Two Standard Vanes Installed With Vane B Deployed and Vanes A and C Partially Retracted

[δ_p and δ_y are given in degrees]

δ_A = -5.0°, δ_B = 30.0° , δ_C = -5.0°

NPR	w_p/w_i	F/F_i	F_r/F_i	δ_p	δ_y
2.0003	0.8851	0.8445	0.8687	-7.90	-11.18
2.9974	0.9253	0.8368	0.8623	-7.84	-11.72
4.0028	0.9355	0.8374	0.8621	-7.50	-11.66
4.9916	0.9300	0.8392	0.8622	-7.34	-11.20
5.0033	0.9284	0.8385	0.8616	-7.33	-11.21
5.9988	0.9282	0.8336	0.8572	-7.64	-11.25

δ_A = -5.0°, δ_B = 25.0° , δ_C = -5.0°

NPR	w_p/w_i	F/F_i	F_r/F_i	δ_p	δ_y
1.9998	0.8862	0.9039	0.9152	-4.82	-7.63
2.9987	0.9258	0.8958	0.9079	-4.85	-8.06
4.0029	0.9343	0.8908	0.9037	-4.94	-8.35
4.9985	0.9288	0.8840	0.8979	-5.23	-8.65
5.9984	0.9283	0.8751	0.8911	-5.75	-9.28

δ_A = 0.0°, δ_B = 30.0° , δ_C = 0.0°

NPR	w_p/w_i	F/F_i	F_r/F_i	δ_p	δ_y
1.9980	0.8860	0.8432	0.8674	-7.64	-11.33
2.9847	0.9278	0.8364	0.8618	-7.46	-11.91
2.9989	0.9256	0.8344	0.8592	-7.61	-11.63
4.0031	0.9350	0.8325	0.8560	-7.29	-11.43
4.9993	0.9285	0.8314	0.8524	-6.72	-10.92
5.9974	0.9284	0.8244	0.8453	-6.75	-10.94

Table 81. Military-Power Nozzle Performance of Rotating Vane Actuation System for Large Vane and Two Standard Vanes Installed With Vane C Deployed and Vanes A and B Fully Retracted

[δ_p and δ_y are given in degrees]

δ_A = -10.0°, δ_B = -10.0° , δ_C = 10.0°

NPR	w_p/w_i	F/F_i	F_r/F_i	δ_p	δ_y
1.9987	0.8862	0.9990	0.9991	-0.19	0.06
3.0121	0.9252	0.9933	0.9933	-0.05	0.23
2.9975	0.9248	0.9933	0.9933	-0.07	0.28
3.9984	0.9343	0.9831	0.9832	-0.18	0.48
4.9998	0.9282	0.9685	0.9687	-0.60	0.99
5.9996	0.9281	0.9555	0.9562	-1.30	1.70

δ_A = -10.0°, δ_B = -10.0° , δ_C = 15.0°

NPR	w_p/w_i	F/F_i	F_r/F_i	δ_p	δ_y
2.0029	0.8861	0.9871	0.9874	-0.98	0.97
3.0028	0.9273	0.9806	0.9811	-1.11	1.38
4.0038	0.9355	0.9699	0.9706	-1.32	1.66
5.0017	0.9283	0.9521	0.9537	-2.04	2.55
6.0008	0.9282	0.9371	0.9401	-2.95	3.52

δ_A = -10.0°, δ_B = -10.0° , δ_C = 20.0°

NPR	w_p/w_i	F/F_i	F_r/F_i	δ_p	δ_y
2.0052	0.8861	0.9556	0.9586	-3.14	3.28
3.0069	0.9270	0.9466	0.9503	-3.28	3.86
4.0038	0.9348	0.9376	0.9418	-3.48	4.16
5.0026	0.9282	0.9231	0.9291	-4.24	5.00
6.0027	0.9280	0.9087	0.9177	-5.29	6.05

δ_A = -10.0°, δ_B = -10.0° , δ_C = 25.0°

NPR	w_p/w_i	F/F_i	F_r/F_i	δ_p	δ_y
2.0037	0.8861	0.9104	0.9207	-5.78	6.37
3.0017	0.9232	0.8997	0.9115	-6.14	6.92
3.9896	0.9314	0.8938	0.9062	-6.24	7.20
5.0029	0.9282	0.8867	0.9000	-6.48	7.50
6.0051	0.9282	0.8778	0.8943	-7.37	8.28

Table 81. Concluded

δ_A = -10.0°, δ_B = -10.0° , δ_C = 30.0°

NPR	w_p/w_i	F/F_i	F_r/F_i	δ_p	δ_y
2.0035	0.8849	0.8634	0.8846	-8.66	9.25
3.0006	0.9256	0.8506	0.8747	-9.29	9.95
4.0034	0.9353	0.8473	0.8713	-9.18	10.04
5.0081	0.9284	0.8477	0.8709	-8.96	9.94
5.9973	0.9281	0.8428	0.8674	-9.38	10.14

δ_A = -10.0°, δ_B = -10.0° , δ_C = 35.0°

NPR	w_p/w_i	F/F_i	F_r/F_i	δ_p	δ_y
2.0026	0.8874	0.8085	0.8435	-12.09	11.62
2.9918	0.9262	0.7991	0.8347	-12.07	12.04
3.9970	0.9352	0.8044	0.8371	-11.43	11.58
5.0040	0.9281	0.8089	0.8390	-10.90	11.14
6.0035	0.9282	0.8037	0.8351	-11.56	11.02

Table 82. Military-Power Nozzle Performance of Rotating Vane Actuation System for Large Vane and Two Standard Vanes Installed With Vane C Deployed and Vanes A and B Partially Retracted

[δ_p and δ_y are given in degrees]

δ_A = -5.0°, δ_B = -5.0° , δ_C = 30.0°

NPR	w_p/w_i	F/F_i	F_r/F_i	δ_p	δ_y
2.0047	0.8856	0.8514	0.8754	-9.28	9.88
3.0042	0.9235	0.8410	0.8671	-9.84	10.29
4.0055	0.9352	0.8412	0.8672	-9.77	10.32
5.0037	0.9282	0.8423	0.8667	-9.44	10.01
6.0057	0.9279	0.8372	0.8620	-9.79	9.87

δ_A = -5.0°, δ_B = -5.0° , δ_C = 25.0°

NPR	w_p/w_i	F/F_i	F_r/F_i	δ_p	δ_y
1.9980	0.8862	0.9108	0.9216	-5.98	6.50
3.0083	0.9225	0.8978	0.9103	-6.33	7.16
4.0106	0.9350	0.8928	0.9063	-6.62	7.43
5.0087	0.9282	0.8852	0.8994	-6.79	7.69
6.0078	0.9281	0.8755	0.8922	-7.50	8.29

δ_A = 0.0°, δ_B = 0.0° , δ_C = 30.0°

NPR	w_p/w_i	F/F_i	F_r/F_i	δ_p	δ_y
2.0060	0.8857	0.8487	0.8732	-10.12	9.29
2.9964	0.9259	0.8387	0.8646	-10.56	9.48
4.0026	0.9350	0.8355	0.8607	-10.46	9.33
5.0031	0.9283	0.8337	0.8557	-9.93	8.59
6.0031	0.9280	0.8266	0.8485	-10.30	8.18

Table 83. Military-Power Nozzle Performance of Rotating Vane Actuation System for Large Vane and Two Standard Vanes Installed With Vanes A and B Equally Deployed and Vane C Fully Retracted

[δ_p and δ_y are given in degrees]

δ_A = 0.0°, δ_B = 0.0° , δ_C = -10.0°

NPR	w_p/w_i	F/F_i	F_r/F_i	δ_p	δ_y
2.0029	0.8860	0.9967	0.9967	-0.26	0.01
3.0006	0.9277	0.9988	0.9988	0.02	0.12
3.9801	0.9343	0.9889	0.9889	0.09	0.14
3.9909	0.9306	0.9874	0.9874	0.12	0.15
5.0064	0.9283	0.9769	0.9769	0.08	0.18
5.9993	0.9282	0.9670	0.9670	0.03	0.09

δ_A = 5.0°, δ_B = 5.0° , δ_C = -10.0°

NPR	w_p/w_i	F/F_i	F_r/F_i	δ_p	δ_y
2.0002	0.8860	0.9976	0.9976	-0.25	0.08
2.9965	0.9263	0.9961	0.9961	0.05	0.11
3.9927	0.9317	0.9857	0.9857	0.09	0.10
5.0039	0.9284	0.9726	0.9726	0.19	-0.09
6.0041	0.9283	0.9597	0.9597	0.43	-0.52

δ_A = 10.0°, δ_B = 10.0° , δ_C = -10.0°

NPR	w_p/w_i	F/F_i	F_r/F_i	δ_p	δ_y
2.0023	0.8862	0.9924	0.9924	-0.30	-0.31
3.0049	0.9260	0.9899	0.9899	0.11	-0.35
3.9991	0.9286	0.9777	0.9777	0.28	-0.50
5.0042	0.9282	0.9585	0.9587	0.73	-1.15
6.0083	0.9281	0.9381	0.9391	1.46	-2.10

δ_A = 15.0°, δ_B = 15.0° , δ_C = -10.0°

NPR	w_p/w_i	F/F_i	F_r/F_i	δ_p	δ_y
2.0032	0.8863	0.9707	0.9711	0.49	-1.69
3.0051	0.9262	0.9575	0.9582	0.98	-1.99
3.9964	0.9303	0.9400	0.9412	1.46	-2.47
5.0024	0.9282	0.9090	0.9121	2.69	-3.93
6.0037	0.9282	0.8828	0.8892	4.23	-5.45

Table 83. Concluded

δ_A = 20.0°, δ_B = 20.0° , δ_C = -10.0°

NPR	w_p/w_i	F/F_i	F_r/F_i	δ_p	δ_y
2.0035	0.8863	0.8668	0.8741	3.75	-6.44
2.9978	0.9245	0.8481	0.8580	4.91	-7.25
3.9994	0.9282	0.8109	0.8281	6.99	-9.44
5.0011	0.9282	0.7838	0.8097	9.07	-11.54
6.0056	0.9282	0.7688	0.8016	10.31	-13.07

δ_A = 25.0°, δ_B = 25.0° , δ_C = -10.0°

NPR	w_p/w_i	F/F_i	F_r/F_i	δ_p	δ_y
2.0069	0.8853	0.7250	0.7649	11.00	-15.34
2.9962	0.9241	0.6959	0.7461	12.98	-17.25
4.0065	0.9272	0.6685	0.7315	14.91	-19.58
5.0007	0.9282	0.6601	0.7251	15.19	-20.04
6.0036	0.9280	0.6566	0.7138	14.26	-18.90

δ_A = 30.0°, δ_B = 30.0° , δ_C = -10.0°

NPR	w_p/w_i	F/F_i	F_r/F_i	δ_p	δ_y
2.0033	0.8848	0.5599	0.6688	21.51	-27.53
2.9958	0.9289	0.5391	0.6469	22.07	-27.68
3.9976	0.9356	0.5420	0.6329	20.44	-25.36
4.9884	0.9363	0.5516	0.6273	18.10	-23.35
6.0001	0.9285	0.5573	0.6239	16.52	-22.14

Table 84. Military-Power Nozzle Performance of Rotating Vane Actuation System for Large Vane and Two Standard Vanes Installed With Vanes A and B Equally Deployed and Vane C Partially Retracted

[δ_p and δ_y are given in degrees]

δ_A = 25.0°, δ_B = 25.0° , δ_C = -5.0°

NPR	w_p/w_i	F/F_i	F_r/F_i	δ_p	δ_y
2.0033	0.8853	0.7307	0.7710	11.20	-15.22
3.0057	0.9244	0.6969	0.7473	12.94	-17.32
4.0002	0.9286	0.6688	0.7287	14.41	-19.18
5.0050	0.9283	0.6557	0.7107	13.77	-18.72
6.0107	0.9281	0.6507	0.6956	12.42	-17.07

δ_A = 30.0°, δ_B = 30.0° , δ_C = -5.0°

NPR	w_p/w_i	F/F_i	F_r/F_i	δ_p	δ_y
2.0025	0.8853	0.5339	0.6207	19.60	-25.36
3.0034	0.9243	0.5108	0.5850	17.94	-24.46
4.0043	0.9270	0.5166	0.5720	15.81	-20.90
4.9999	0.9282	0.5251	0.5732	14.55	-19.43
5.9997	0.9280	0.5349	0.5775	13.36	-18.28

δ_A = 30.0°, δ_B = 30.0° , δ_C = 0.0°

NPR	w_p/w_i	F/F_i	F_r/F_i	δ_p	δ_y
2.0060	0.8861	0.5197	0.5884	16.63	-23.71
2.9976	0.9240	0.4982	0.5471	13.65	-20.95
3.9885	0.9316	0.5007	0.5373	12.00	-18.05
5.0087	0.9284	0.5090	0.5389	10.76	-16.25
6.0039	0.9281	0.5175	0.5459	9.96	-15.96

Table 85. Military-Power Nozzle Performance of Rotating Vane Actuation System for Large Vane and Two Standard Vanes Installed With Vanes B and C Equally Deployed and Vane A Fully Retracted

[δ_p and δ_y are given in degrees]

δ_A = -10.0°, δ_B = 0.0° , δ_C = 0.0°

NPR	w_p/w_i	F/F_i	F_r/F_i	δ_p	δ_y
2.0004	0.8857	0.9993	0.9993	0.10	-0.13
2.9978	0.9262	0.9979	0.9979	0.29	-0.07
4.0008	0.9308	0.9869	0.9869	0.40	0.02
4.9902	0.9305	0.9769	0.9769	0.34	0.02
5.0005	0.9282	0.9759	0.9759	0.34	0.02
5.9954	0.9279	0.9664	0.9664	0.18	0.00

δ_A = -10.0°, δ_B = 5.0° , δ_C = 5.0°

NPR	w_p/w_i	F/F_i	F_r/F_i	δ_p	δ_y
2.0011	0.8862	0.9970	0.9970	0.09	-0.23
3.0003	0.9258	0.9973	0.9973	0.32	-0.03
4.0040	0.9306	0.9862	0.9863	0.32	-0.02
5.0006	0.9288	0.9733	0.9733	0.01	-0.04
6.0065	0.9282	0.9597	0.9597	-0.64	-0.11

δ_A = -10.0°, δ_B = 10.0° , δ_C = 10.0°

NPR	w_p/w_i	F/F_i	F_r/F_i	δ_p	δ_y
2.0030	0.8861	0.9931	0.9931	-0.25	-0.09
2.9988	0.9275	0.9902	0.9902	-0.27	-0.19
3.9847	0.9312	0.9782	0.9782	-0.40	-0.16
3.9918	0.9318	0.9781	0.9781	-0.43	-0.16
4.9996	0.9283	0.9602	0.9604	-1.27	-0.27
5.9980	0.9280	0.9426	0.9435	-2.51	-0.35

δ_A = -10.0°, δ_B = 15.0° , δ_C = 15.0°

NPR	w_p/w_i	F/F_i	F_r/F_i	δ_p	δ_y
2.0036	0.8863	0.9645	0.9652	-1.92	-0.70
2.9940	0.9253	0.9558	0.9567	-2.39	-0.60
4.0003	0.9333	0.9404	0.9418	-3.09	-0.56
5.0017	0.9283	0.9142	0.9175	-4.81	-0.76
6.0012	0.9278	0.8934	0.8997	-6.77	-0.85

Table 85. Concluded

δ_A = -10.0°, δ_B = 20.0° , δ_C = 20.0°

NPR	w_p/w_i	F/F_i	F_r/F_i	δ_p	δ_y
1.9997	0.8858	0.8768	0.8860	-8.08	-1.64
3.0047	0.9271	0.8609	0.8720	-9.04	-1.44
4.0088	0.9285	0.8313	0.8488	-11.53	-1.63
5.0000	0.9282	0.8107	0.8355	-13.88	-1.69
6.0015	0.9281	0.7992	0.8296	-15.49	-1.66

δ_A = -10.0°, δ_B = 25.0° , δ_C = 25.0°

NPR	w_p/w_i	F/F_i	F_r/F_i	δ_p	δ_y
1.9988	0.8846	0.7467	0.7908	-19.15	-1.95
2.9940	0.9237	0.7209	0.7719	-20.89	-1.80
4.0122	0.9281	0.7062	0.7663	-22.77	-1.95
4.9959	0.9281	0.7039	0.7665	-23.23	-2.13
5.9981	0.9280	0.7030	0.7609	-22.41	-2.25

δ_A = -10.0°, δ_B = 30.0° , δ_C = 30.0°

NPR	w_p/w_i	F/F_i	F_r/F_i	δ_p	δ_y
2.0050	0.8835	0.6238	0.7307	-31.24	-3.76
2.9926	0.9278	0.6126	0.7237	-32.05	-3.50
3.9956	0.9353	0.6106	0.7112	-30.67	-4.13
5.0058	0.9285	0.6122	0.6919	-27.55	-4.08
5.9914	0.9284	0.6173	0.6801	-24.51	-4.46

Table 86. Military-Power Nozzle Performance of Rotating Vane Actuation System for Large Vane and Two Standard Vanes Installed With Vanes B and C Equally Deployed and Vane A Partially Retracted

[δ_p and δ_y are given in degrees]

δ_A = -5.0°, δ_B = 25.0° , δ_C = 25.0°

NPR	w_p/w_i	F/F_i	F_r/F_i	δ_p	δ_y
2.0010	0.8842	0.7480	0.7904	-18.81	-1.48
3.0035	0.9248	0.7229	0.7734	-20.78	-1.60
4.0031	0.9291	0.7082	0.7669	-22.50	-1.99
5.0018	0.9282	0.7012	0.7580	-22.24	-2.29
5.9970	0.9279	0.6983	0.7444	-20.13	-2.46

δ_A = -5.0°, δ_B = 30.0° , δ_C = 30.0°

NPR	w_p/w_i	F/F_i	F_r/F_i	δ_p	δ_y
2.0003	0.8835	0.5995	0.7166	-33.13	-2.98
2.9931	0.9272	0.5835	0.6884	-31.93	-3.39
3.9964	0.9300	0.5794	0.6520	-27.08	-4.10
5.0016	0.9284	0.5878	0.6413	-23.22	-4.50
6.0054	0.9280	0.5946	0.6374	-20.75	-4.26

δ_A = 0.0°, δ_B = 30.0° , δ_C = 30.0°

NPR	w_p/w_i	F/F_i	F_r/F_i	δ_p	δ_y
2.0004	0.8831	0.5817	0.6640	-28.65	-3.79
3.0104	0.9214	0.5555	0.6077	-23.47	-5.08
4.0043	0.9276	0.5574	0.5913	-18.93	-5.14
4.9990	0.9281	0.5670	0.5924	-16.11	-5.19
6.0042	0.9281	0.5742	0.5951	-14.46	-4.99
6.0020	0.9280	0.5745	0.5953	-14.43	-4.97

Table 87. Military-Power Nozzle Performance of Rotating Vane Actuation System for Large Vane and Two Standard Vanes Installed With Vanes A and C Equally Deployed and Vane B Fully Retracted

[δ_p and δ_y are given in degrees]

δ_A = 0.0°, δ_B = -10.0° , δ_C = 0.0°

NPR	w_p/w_i	F/F_i	F_r/F_i	δ_p	δ_y
2.0008	0.8862	0.9976	0.9976	-0.30	-0.23
3.0043	0.9233	0.9968	0.9968	0.02	-0.04
4.0081	0.9275	0.9872	0.9872	0.10	0.03
5.0037	0.9281	0.9768	0.9768	0.10	0.12
6.0027	0.9280	0.9670	0.9670	0.05	0.23

δ_A = 5.0°, δ_B = -10.0° , δ_C = 5.0°

NPR	w_p/w_i	F/F_i	F_r/F_i	δ_p	δ_y
1.9988	0.8859	0.9996	0.9996	-0.32	0.00
3.0006	0.9251	0.9973	0.9973	-0.04	0.08
3.9982	0.9291	0.9866	0.9867	0.08	0.16
5.0011	0.9282	0.9738	0.9738	0.10	0.36
6.0022	0.9281	0.9605	0.9606	0.27	0.65

δ_A = 10.0°, δ_B = -10.0° , δ_C = 10.0°

NPR	w_p/w_i	F/F_i	F_r/F_i	δ_p	δ_y
2.0013	0.8862	0.9947	0.9947	-0.26	-0.10
2.9991	0.9265	0.9920	0.9920	-0.03	0.35
3.9862	0.9308	0.9800	0.9801	0.10	0.56
4.0067	0.9279	0.9787	0.9787	0.12	0.56
5.0027	0.9283	0.9602	0.9604	0.38	1.01
6.0008	0.9281	0.9412	0.9418	0.91	1.65

δ_A = 15.0°, δ_B = -10.0° , δ_C = 15.0°

NPR	w_p/w_i	F/F_i	F_r/F_i	δ_p	δ_y
2.0006	0.8857	0.9684	0.9685	0.34	1.00
3.0038	0.9226	0.9562	0.9565	0.75	1.38
3.9960	0.9274	0.9405	0.9412	1.16	1.85
5.0026	0.9285	0.9100	0.9118	2.22	2.81
6.0098	0.9279	0.8842	0.8875	3.38	3.63

Table 87. Concluded

δ_A = 20.0°, δ_B = -10.0° , δ_C = 20.0°

NPR	w_p/w_i	F/F_i	F_r/F_i	δ_p	δ_y
2.0002	0.8856	0.8809	0.8839	2.98	3.68
3.0050	0.9267	0.8627	0.8669	3.77	4.17
4.0051	0.9278	0.8283	0.8350	5.00	5.32
5.0052	0.9282	0.7977	0.8083	6.54	6.67
6.0023	0.9280	0.7816	0.7947	7.47	7.33

δ_A = 25.0°, δ_B = -10.0° , δ_C = 25.0°

NPR	w_p/w_i	F/F_i	F_r/F_i	δ_p	δ_y
2.0063	0.8851	0.7541	0.7676	6.92	8.31
3.0216	0.9229	0.7221	0.7402	8.55	9.52
2.9976	0.9273	0.7231	0.7410	8.58	9.39
4.0147	0.9283	0.6953	0.7188	9.98	11.00
3.9967	0.9293	0.6966	0.7202	10.00	10.99
5.0019	0.9281	0.6824	0.7048	10.07	10.63
6.0043	0.9280	0.6782	0.6947	9.14	8.70

δ_A = 30.0°, δ_B = -10.0° , δ_C = 30.0°

NPR	w_p/w_i	F/F_i	F_r/F_i	δ_p	δ_y
2.0029	0.8851	0.5797	0.6143	13.63	14.20
3.0006	0.9281	0.5414	0.5716	14.30	12.59
4.0015	0.9356	0.5416	0.5596	12.22	8.21
5.0149	0.9332	0.5509	0.5643	11.12	5.83
5.9983	0.9289	0.5612	0.5720	10.10	4.86

Table 88. Maximum A/B-Power Nozzle Performance of Rotating Vane Actuation System for Large Vane and Two Standard Vanes Installed With Vanes A and C Equally Deployed and Vane B Partially Retracted

[δ_p and δ_y are given in degrees]

δ_A = 25.0°, δ_B = -5.0° , δ_C = 25.0°

NPR	w_p/w_i	F/F_i	F_r/F_i	δ_p	δ_y
2.0004	0.8852	0.7615	0.7750	6.61	8.46
3.0025	0.9259	0.7295	0.7458	8.18	8.86
4.0042	0.9275	0.6923	0.7077	8.44	8.61
5.0067	0.9282	0.6738	0.6824	6.95	5.88
6.0030	0.9280	0.6712	0.6764	6.07	3.69

δ_A = 30.0°, δ_B = -5.0° , δ_C = 30.0°

NPR	w_p/w_i	F/F_i	F_r/F_i	δ_p	δ_y
2.0026	0.8850	0.5456	0.5660	11.70	10.32
3.0018	0.9246	0.5175	0.5292	10.30	6.47
4.0105	0.9276	0.5197	0.5272	9.03	3.45
3.9899	0.9285	0.5199	0.5277	9.19	3.52
5.0085	0.9280	0.5296	0.5358	8.47	2.04
6.0077	0.9278	0.5395	0.5446	7.70	1.69

δ_A = 30.0°, δ_B = 0.0° , δ_C = 30.0°

NPR	w_p/w_i	F/F_i	F_r/F_i	δ_p	δ_y
2.0058	0.8832	0.5387	0.5440	6.88	4.18
2.9885	0.9216	0.5107	0.5141	6.51	1.22
2.9851	0.9257	0.5106	0.5140	6.51	1.30
3.9971	0.9278	0.5098	0.5127	6.04	-0.85
5.0035	0.9278	0.5155	0.5181	5.47	-1.79
6.0073	0.9279	0.5229	0.5253	5.03	-2.18

Table 89. Military-Power Nozzle Performance of Rotating Vane Actuation System for Large Vane and Two Standard Vanes Installed With Three Vanes Equally Deployed

[δ_p and δ_y are given in degrees]

δ_A = 5.0°, δ_B = 5.0° , δ_C = 5.0°

NPR	w_p/w_i	F/F_i	F_r/F_i	δ_p	δ_y
2.0075	0.8867	0.9978	0.9978	-0.06	0.01
3.0091	0.9278	0.9966	0.9966	0.13	0.04
4.0017	0.9355	0.9868	0.9868	0.11	0.03
4.9986	0.9293	0.9717	0.9717	0.02	0.00
6.0020	0.9285	0.9568	0.9568	-0.19	-0.09

δ_A = 10.0°, δ_B = 10.0° , δ_C = 10.0°

NPR	w_p/w_i	F/F_i	F_r/F_i	δ_p	δ_y
2.0031	0.8866	0.9901	0.9902	-0.08	-0.18
3.0121	0.9268	0.9862	0.9862	0.09	-0.15
2.9903	0.9287	0.9865	0.9865	0.08	-0.10
3.9969	0.9354	0.9743	0.9743	0.09	-0.13
4.0043	0.9353	0.9733	0.9733	0.09	-0.13
5.0018	0.9319	0.9504	0.9504	0.18	-0.22
6.0059	0.9282	0.9259	0.9259	0.24	-0.46

δ_A = 15.0°, δ_B = 15.0° , δ_C = 15.0°

NPR	w_p/w_i	F/F_i	F_r/F_i	δ_p	δ_y
2.0033	0.8866	0.9509	0.9510	-0.69	-0.69
3.0045	0.9290	0.9370	0.9371	-0.69	-0.58
3.9999	0.9355	0.9074	0.9075	-0.68	-0.66
5.0006	0.9339	0.8536	0.8539	-0.49	-1.29
5.9983	0.9285	0.8065	0.8070	0.03	-1.92

δ_A = 20.0°, δ_B = 20.0° , δ_C = 20.0°

NPR	w_p/w_i	F/F_i	F_r/F_i	δ_p	δ_y
2.0048	0.8861	0.7900	0.7910	-0.75	-2.78
3.0046	0.9285	0.7484	0.7498	0.02	-3.57
3.9986	0.9355	0.6646	0.6671	0.79	-4.91
5.0193	0.9314	0.6241	0.6278	0.79	-6.21
6.0025	0.9281	0.6122	0.6163	0.88	-6.54

Table 89. Concluded

$\delta_A = 25.0°$, $\delta_B = 25.0°$, $\delta_C = 25.0°$

NPR	w_p/w_i	F/F_i	F_r/F_i	δ_p	δ_y
2.0016	0.8822	0.5114	0.5181	-0.98	-9.16
3.0068	0.9262	0.4477	0.4578	0.34	-12.08
4.0039	0.9347	0.4342	0.4454	1.43	-12.83
4.9959	0.9341	0.4335	0.4446	1.51	-12.71
6.0046	0.9282	0.4369	0.4475	1.04	-12.49

Table 90. Military-Power Nozzle Performance of Rotating Vane Actuation System for Large Vane and Two Standard Vanes Installed With Three Vanes Partially Retracted

[δ_p and δ_y are given in degrees]

δ_A = -5.0°, δ_B = -5.0° , δ_C = -5.0°

NPR	w_p/w_i	F/F_i	F_r/F_i	δ_p	δ_y
2.0026	0.8856	0.9995	0.9995	-0.08	-0.14
3.0007	0.9288	0.9989	0.9989	0.19	0.00
4.0075	0.9352	0.9883	0.9883	0.23	0.00
4.9938	0.9296	0.9764	0.9764	0.22	0.06
5.9982	0.9284	0.9669	0.9669	0.18	0.09

δ_A = 0.0°, δ_B = 0.0° , δ_C = 0.0°

NPR	w_p/w_i	F/F_i	F_r/F_i	δ_p	δ_y
2.0030	0.8859	1.0012	1.0012	-0.09	-0.05
3.0004	0.9270	0.9988	0.9988	0.16	0.01
3.9990	0.9355	0.9887	0.9887	0.19	0.04
4.9972	0.9304	0.9765	0.9765	0.15	0.08
5.9995	0.9282	0.9662	0.9662	0.06	0.06

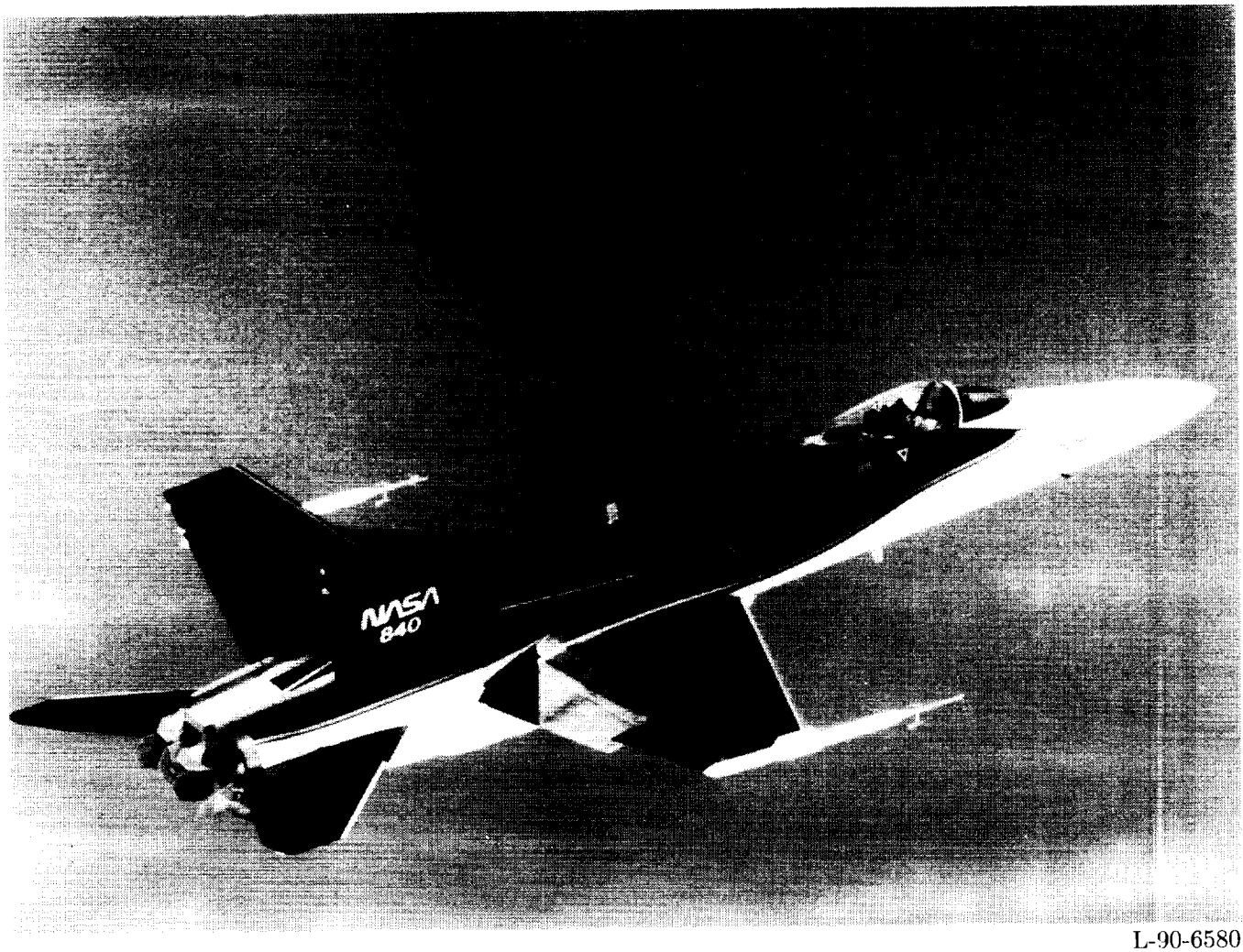

L-90-6580

Figure 1. Artist's concept of the F/A-18 high-alpha research vehicle (HARV) with thrust vectoring control system.

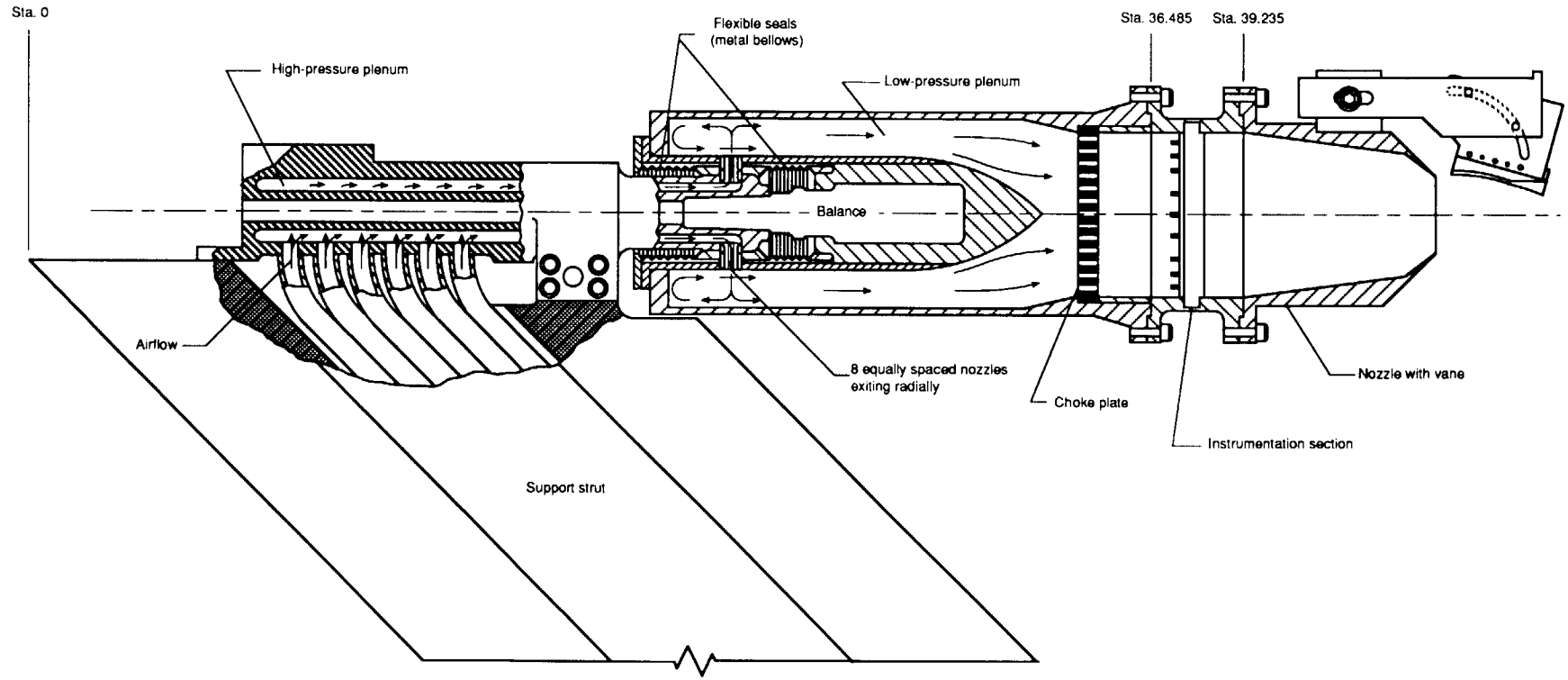

Figure 2. Sketch of single-engine propulsion simulation system with a nozzle single-vane test configuration installed. All dimensions are given in inches.

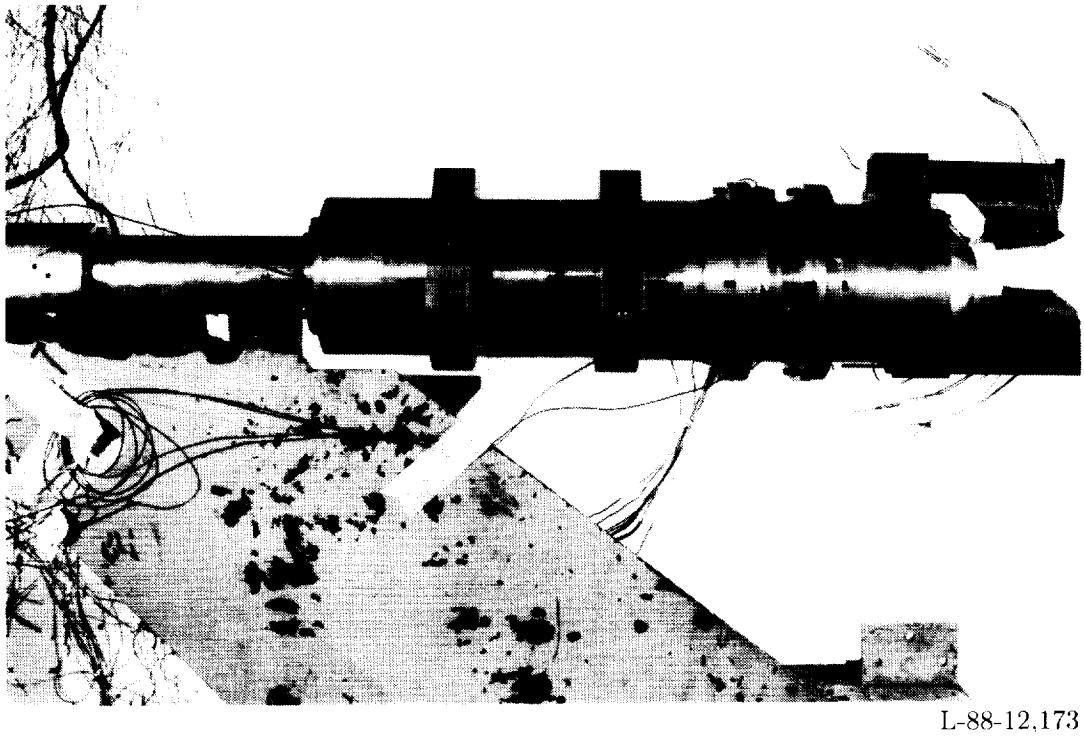

L-88-12,173

Figure 3. Photograph of single-engine propulsion simulation system with typical nozzle–three-vane configuration installed.

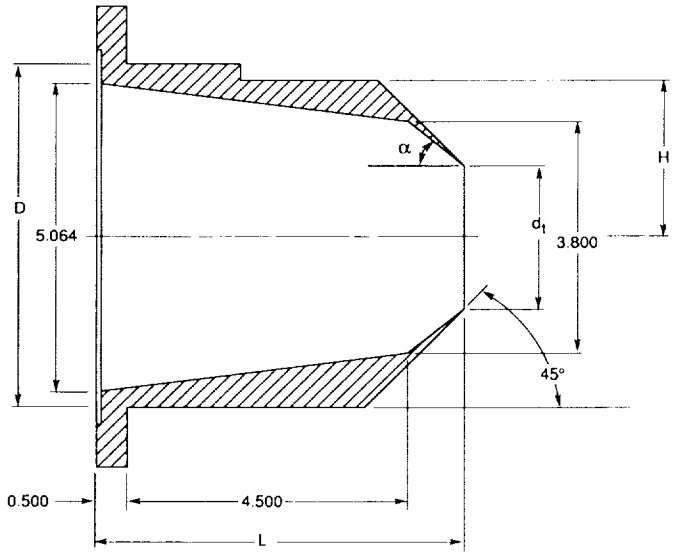

Configuration	d_t	H	D	L	A_t, in^2	α, deg
Mil	2.386	2.593	5.640	5.934	4.475	37.124
Max A/B	3.000	2.900	6.100	6.108	7.140	19.850

Figure 4. Sketch showing important geometry details of axisymmetric convergent test nozzle. All dimensions are given in inches unless otherwise noted.

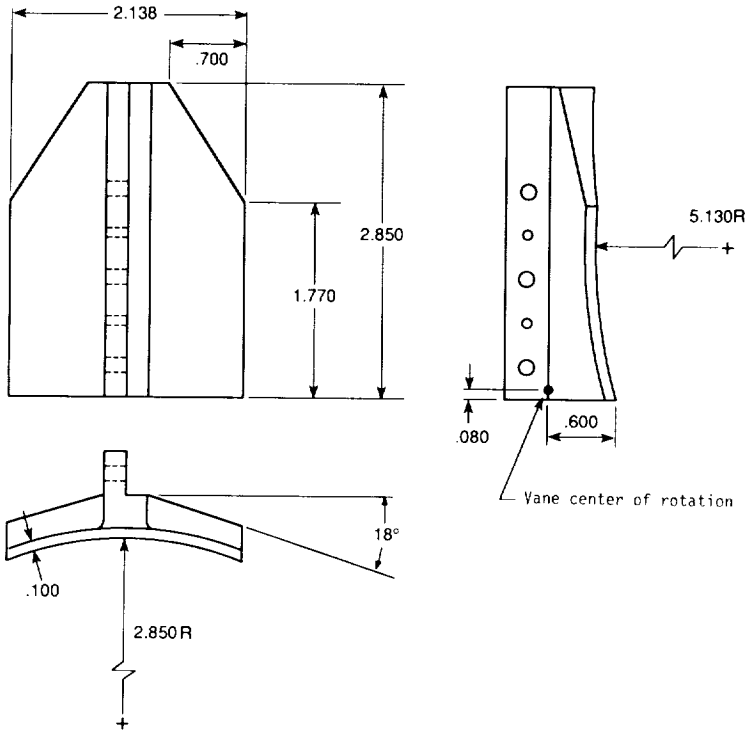

(a) Standard vane. Vane planform area, 5.337 in^2.

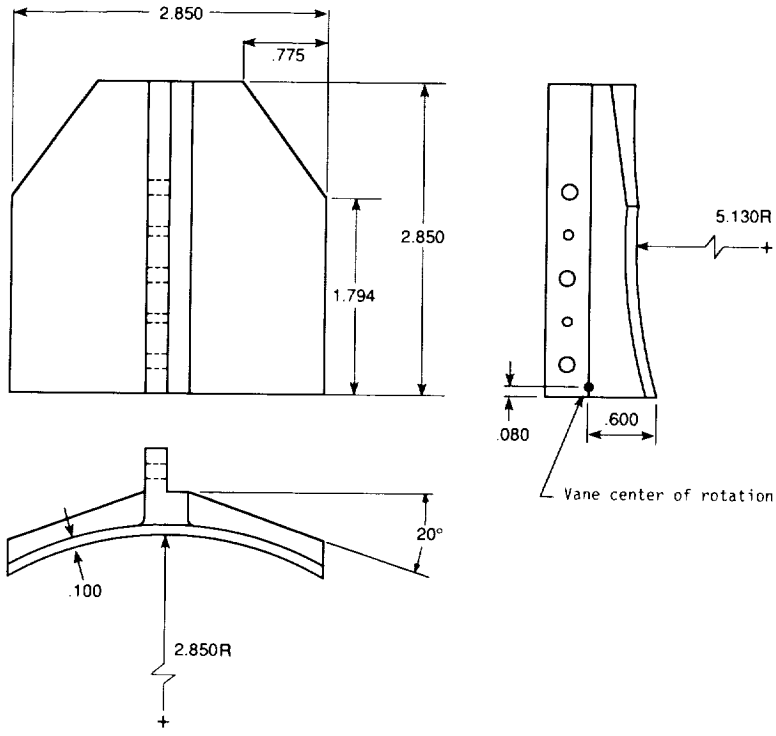

(b) Large vane. Vane planform area, 7.304 in^2.

Figure 5. Sketches showing geometry of thrust vectoring vanes. All dimensions are given in inches unless otherwise noted.

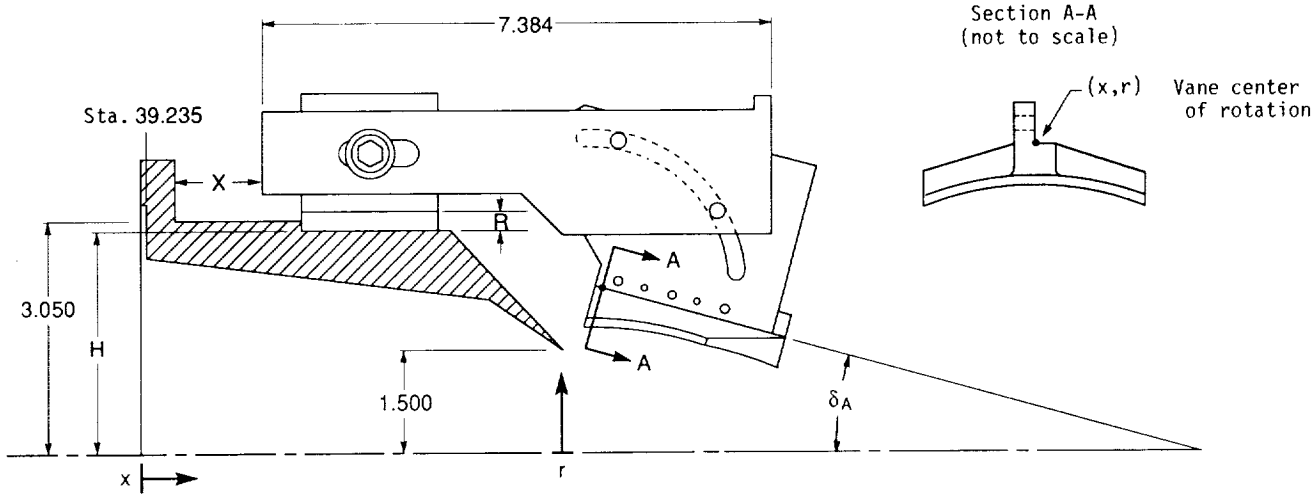

(a) Nozzle and vane geometry.

Rotating vane system

δ_A, deg	Max A/B		Mil	
	H = 2.900		H = 2.593	
	X	R	X	R
-10.0	1.817	0.518	1.818	0.825
-5.0	1.799	0.474	1.800	0.781
0.0	1.777	0.432	1.778	0.740
5.0	1.751	0.392	1.752	0.700
7.5	1.737	0.373	1.738	0.681
10.0	1.723	0.355	1.724	0.662
12.5	1.707	0.337	1.708	0.645
15.0	1.690	0.320	1.691	0.628
17.5	1.673	0.304	1.674	0.611
20.0	1.656	0.288	1.657	0.596
22.5	1.637	0.274	1.638	0.581
25.0	1.618	0.260	1.619	0.567
27.5	1.598	0.247	1.599	0.554
30.0	1.578	0.235	1.579	0.542
35.0	1.536	0.213	1.537	0.520

Translating vane system

δ_A, deg	Max A/B		Mil	
	H = 2.900		H = 2.593	
	X	R	X	R
-10.0	1.771	0.305	1.770	0.612
-5.0	1.769	0.304	1.768	0.612
0.0	1.767	0.304	1.766	0.611
5.0	1.765	0.303	1.764	0.611
10.0	1.763	0.303	1.762	0.610
12.5	1.762	0.303	1.761	0.610
15.0	1.761	0.303	1.761	0.610
17.5	1.760	0.303	1.760	0.610
20.0	1.759	0.303	1.759	0.610
22.5	1.759	0.303	1.758	0.611
25.0	1.758	0.303	1.757	0.611
25.0	1.736	0.252	1.719	0.524
25.0	1.720	0.216	1.682	0.453
25.0	1.702	0.181	1.640	0.381
25.0	1.683	0.145	1.590	0.310
25.0	1.663	0.110	1.533	0.239
25.0	1.639	0.071	1.467	0.168
25.0			1.389	0.096
25.0			1.359	0.072

(b) Tables and equations defining vane center of rotation. $x = X + 5.204$; $r = H + R - 1.000$.

Figure 6. Geometry of vane actuation systems. All dimensions are given in inches unless otherwise noted.

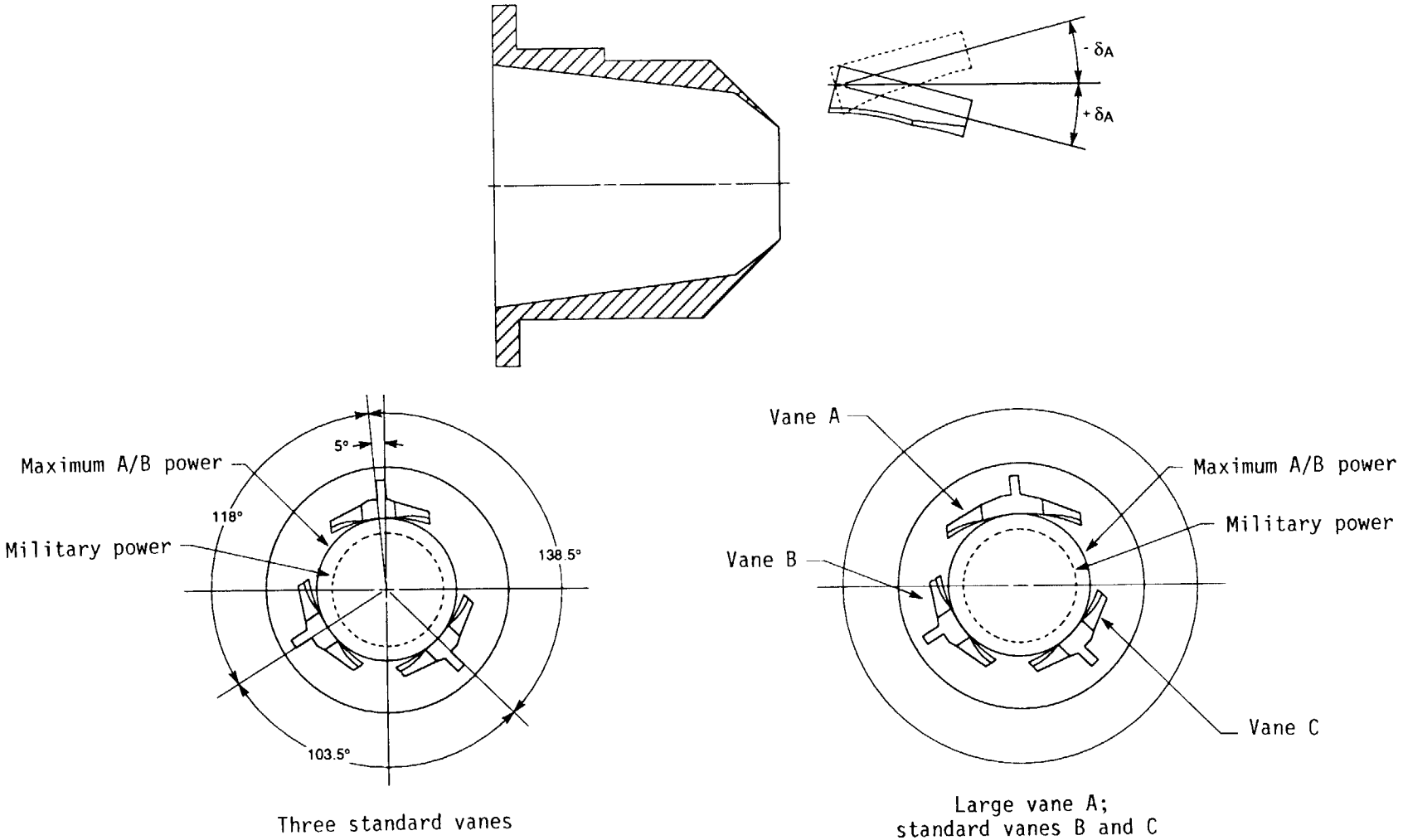

Figure 7. Sketches showing thrust vectoring vane positions relative to nozzle exit. Vanes are shown undeflected and with supports omitted for clarity.

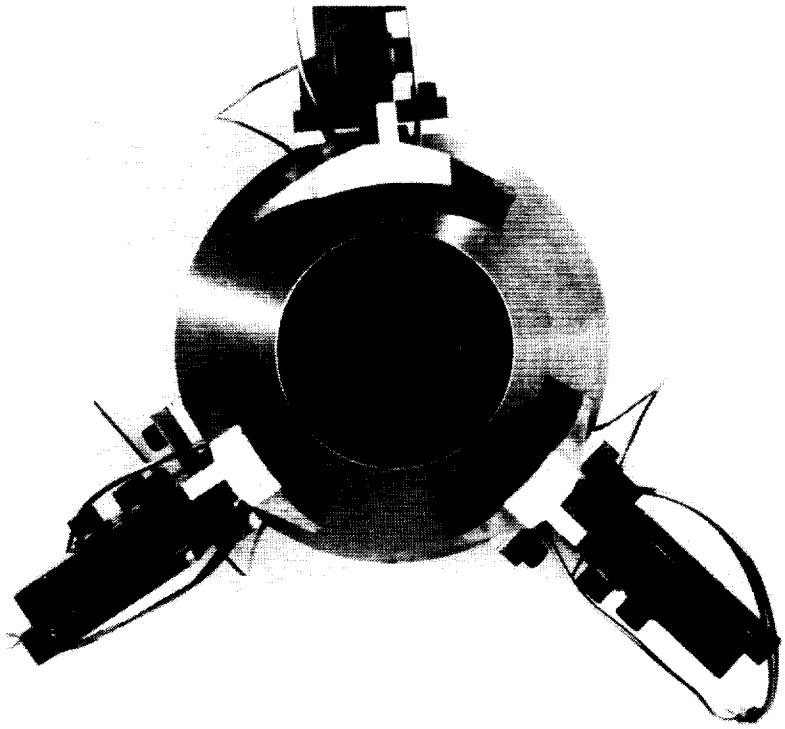

L-88-12,174

(a) Three vanes fully retracted. $\delta_A = \delta_B = \delta_C = -10°$.

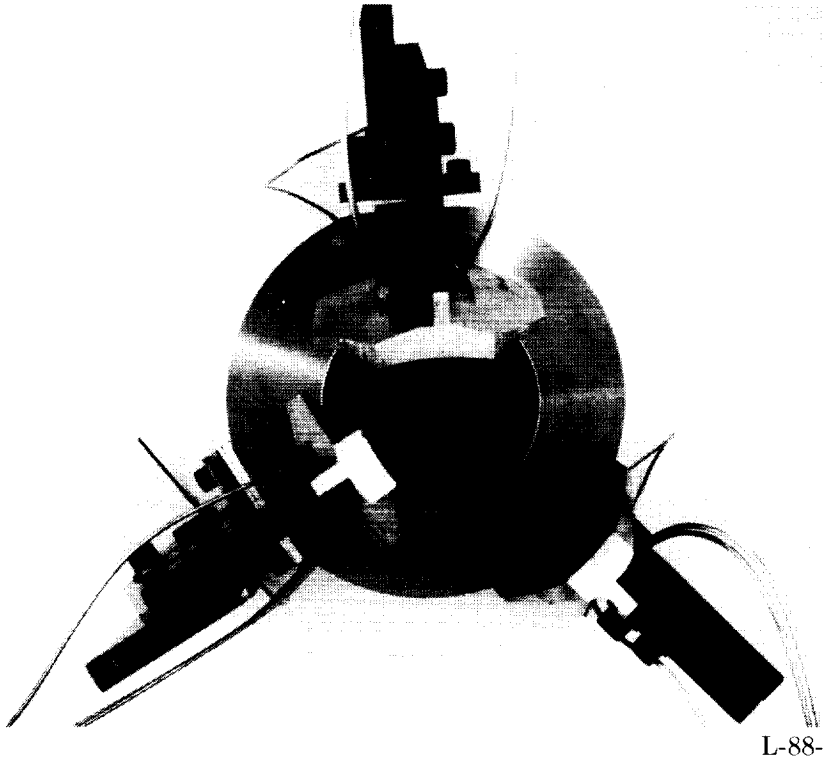

L-88-12,177

(b) Two vanes deployed; one vane retracted. $\delta_A = 25°$; $\delta_B = 25°$; $\delta_C = -10°$.

Figure 8. Thrust vectoring vanes installed on military-power nozzle.

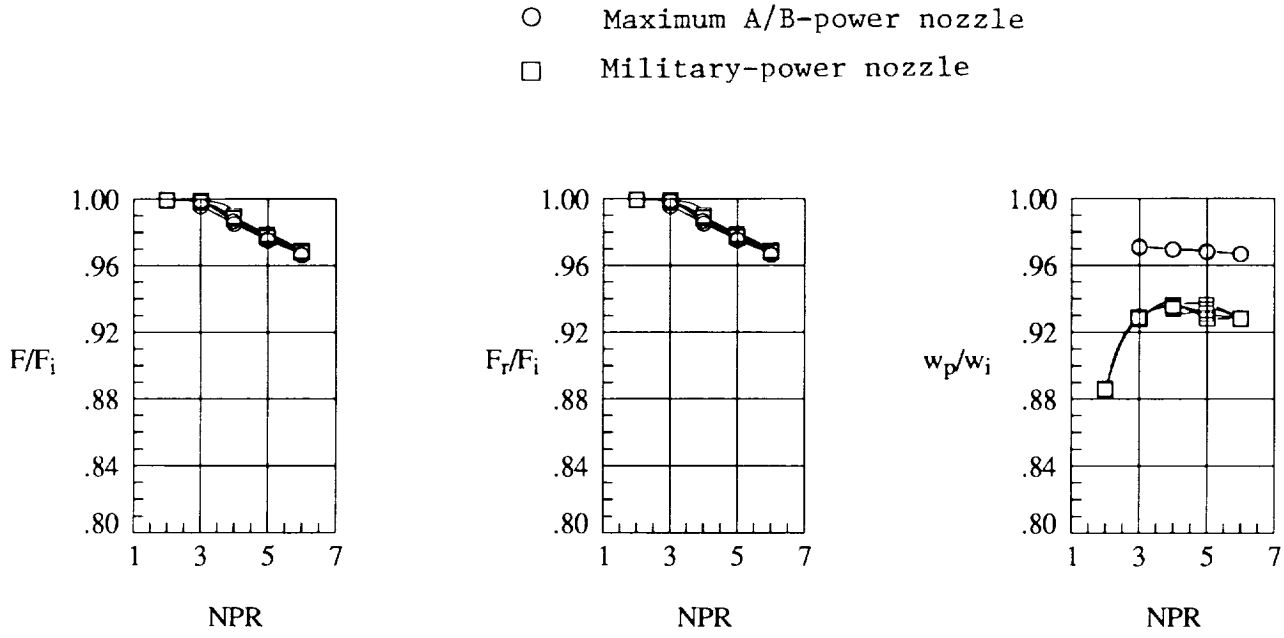

Figure 9. Baseline nozzle internal performance with vanes off.

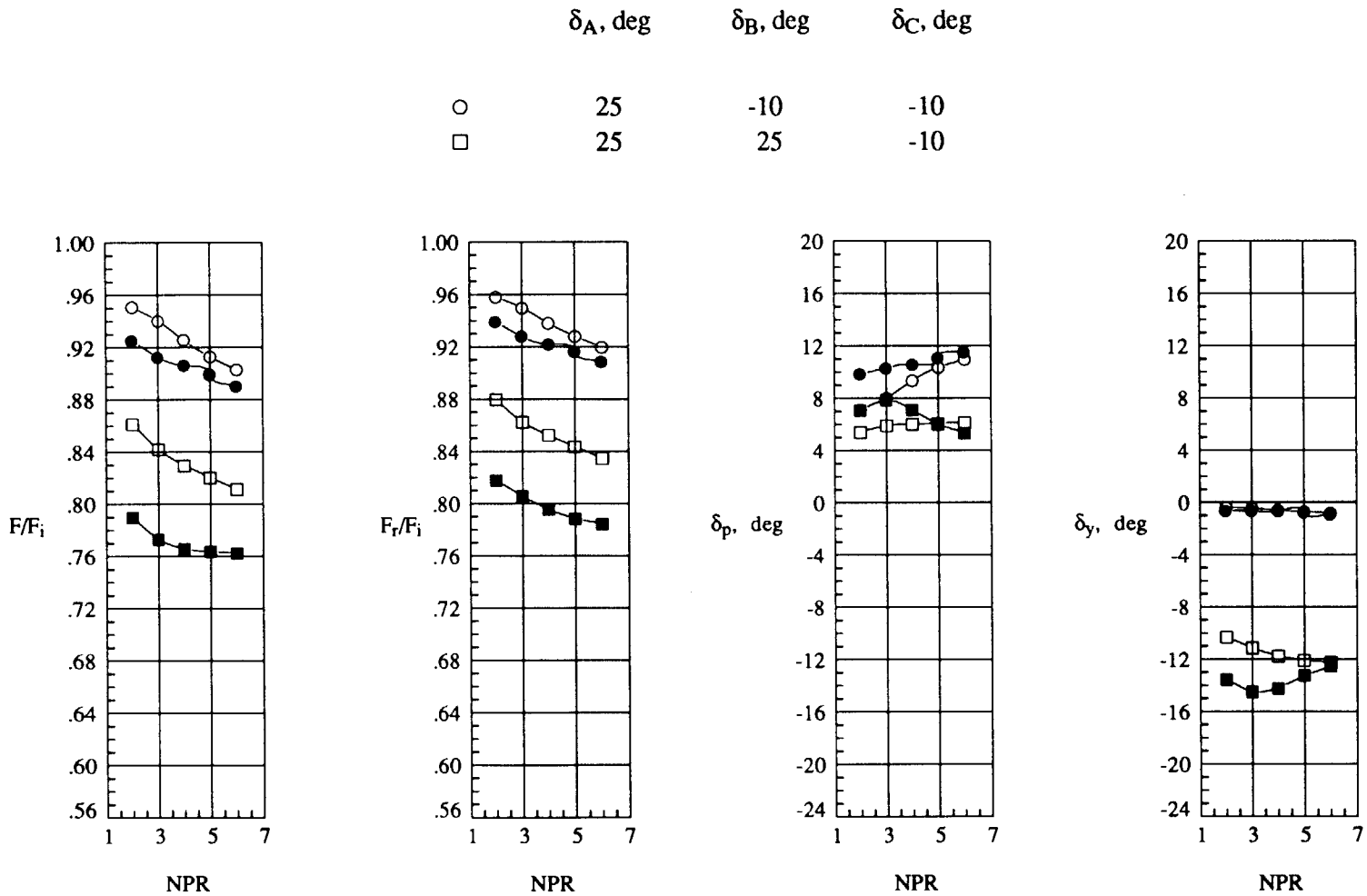

(a) Vanes A and B deployed; vane C retracted.

Figure 10. Effect of vane actuation system on performance of maximum A/B-power nozzle with three equivalent vanes installed. Open symbols denote translating vane system; solid symbols denote rotating vane system.

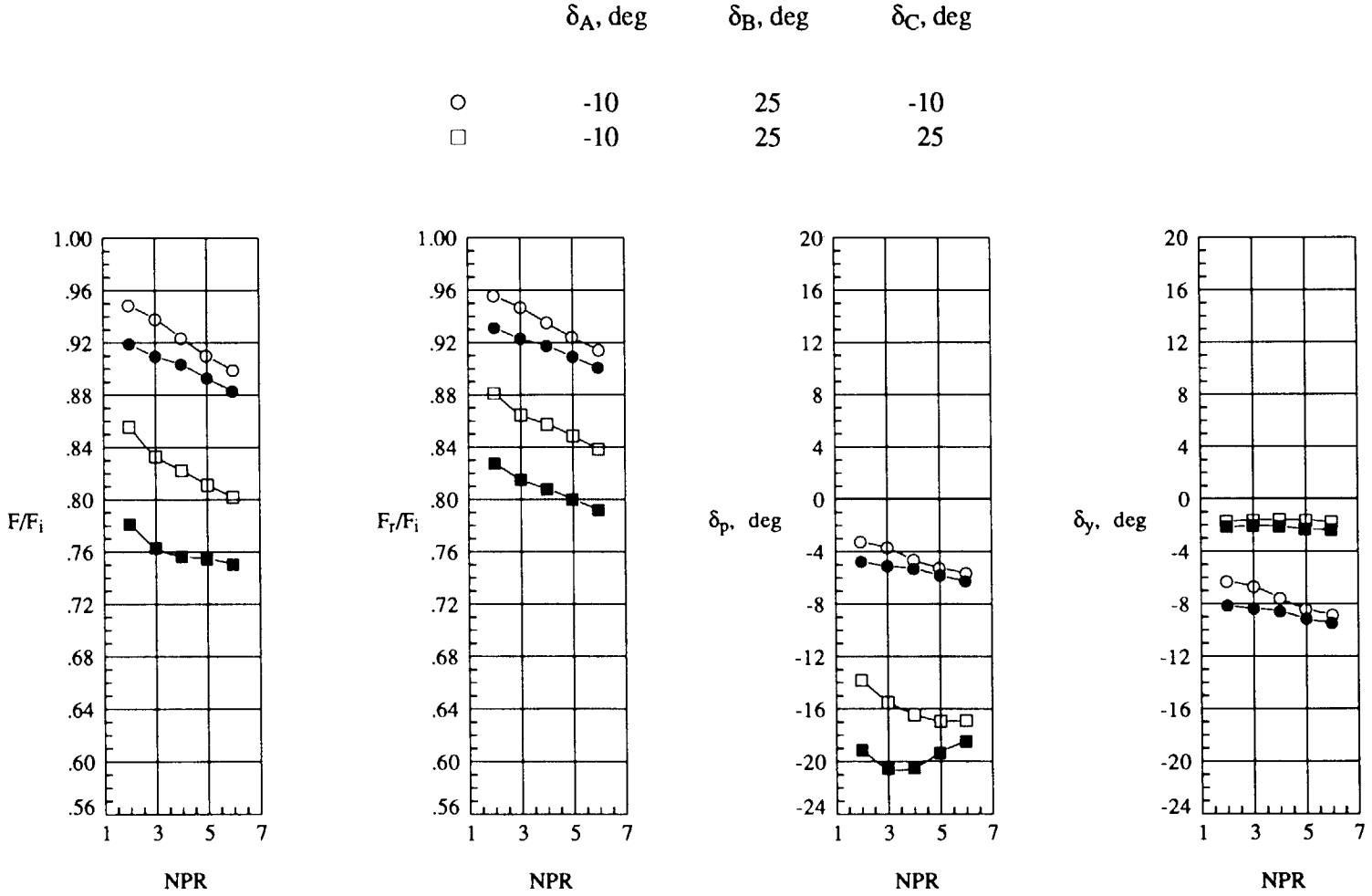

(b) Vanes B and C deployed; vane A retracted.

Figure 10. Continued.

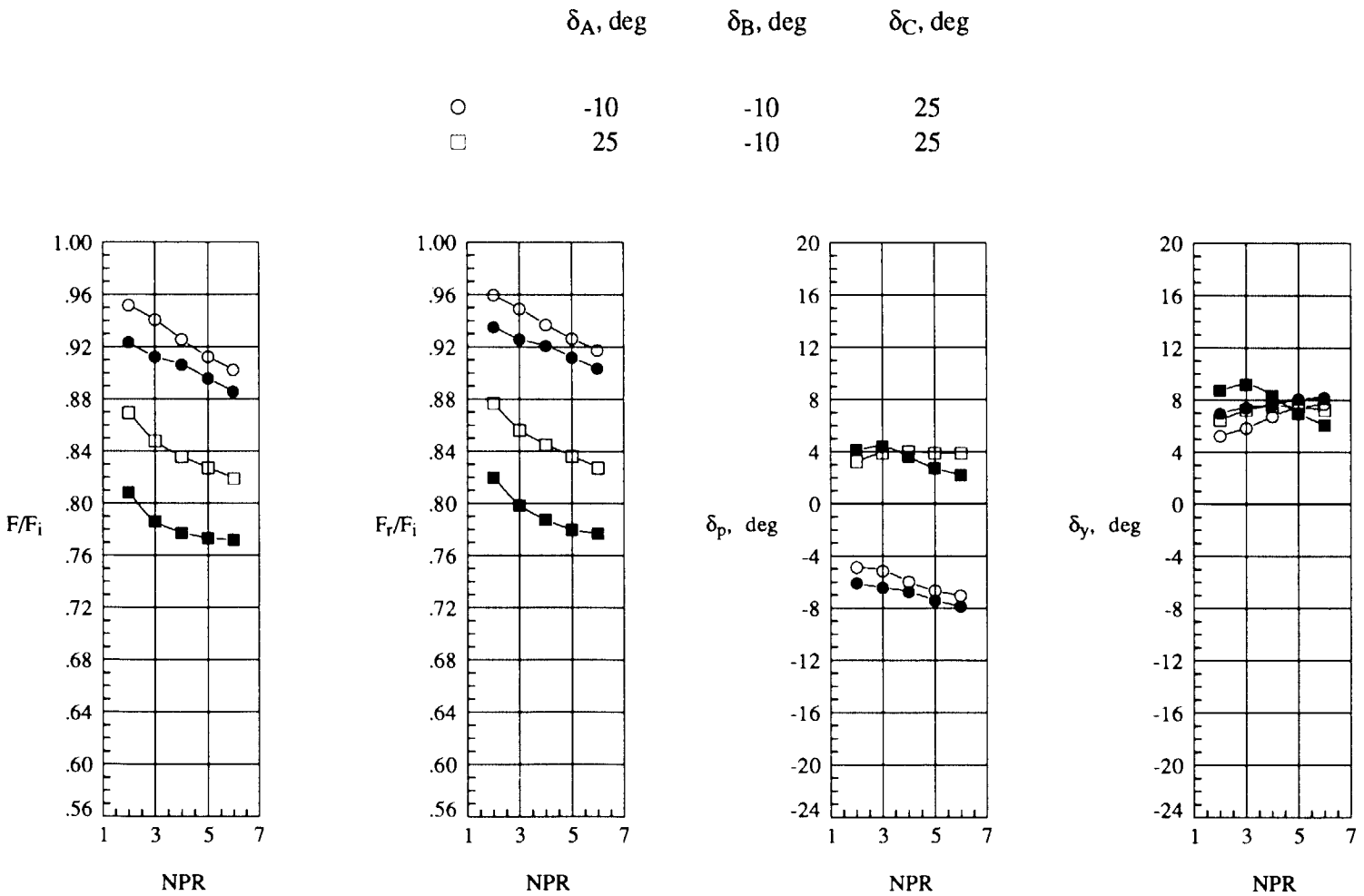

(c) Vanes A and C deployed; vane B retracted.

Figure 10. Concluded.

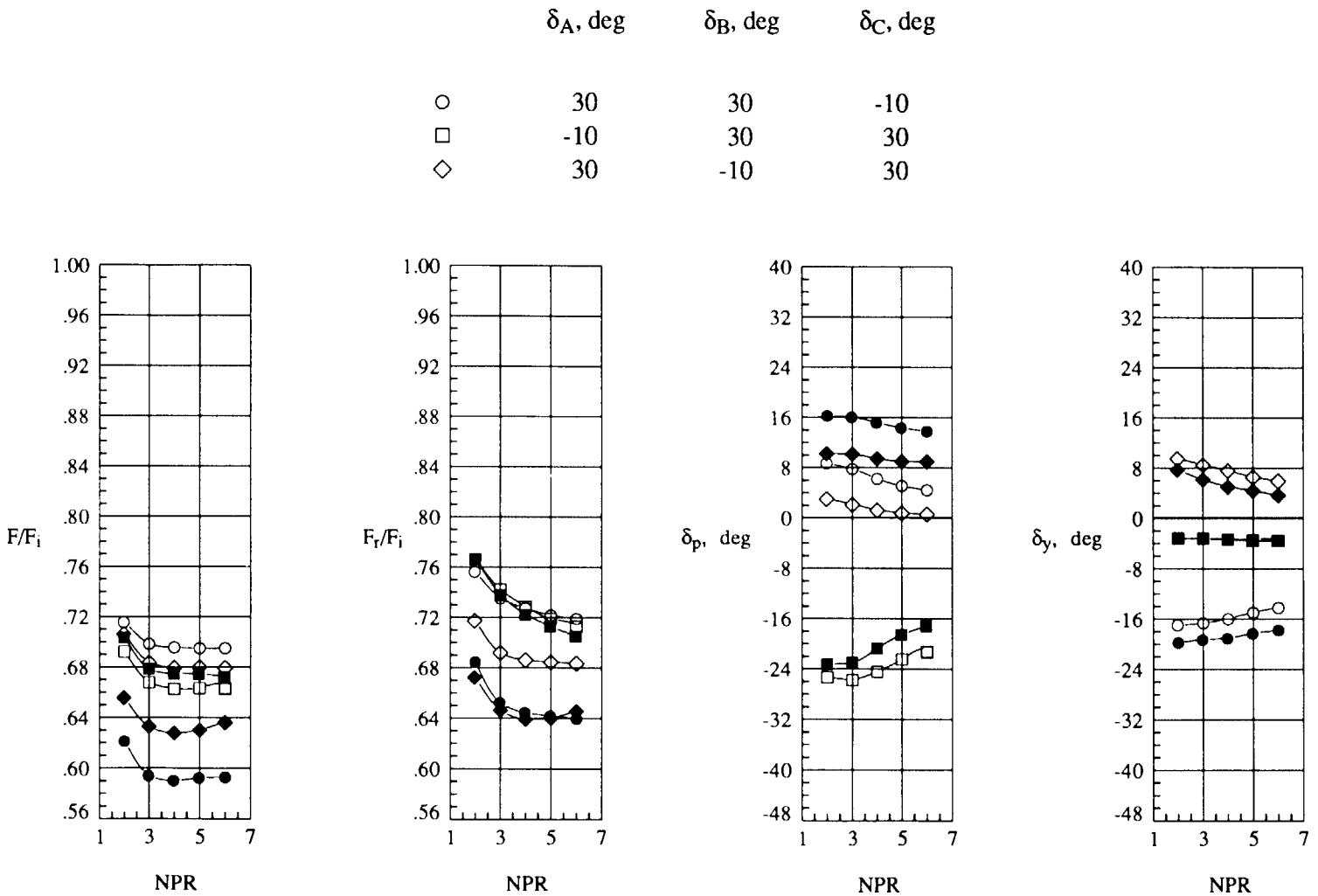

Figure 11. Effect of top vane size on performance of maximum A/B-power nozzle with rotating-vane actuation system. Open symbols denote standard top vane geometry; solid symbols denote large top vane geometry.

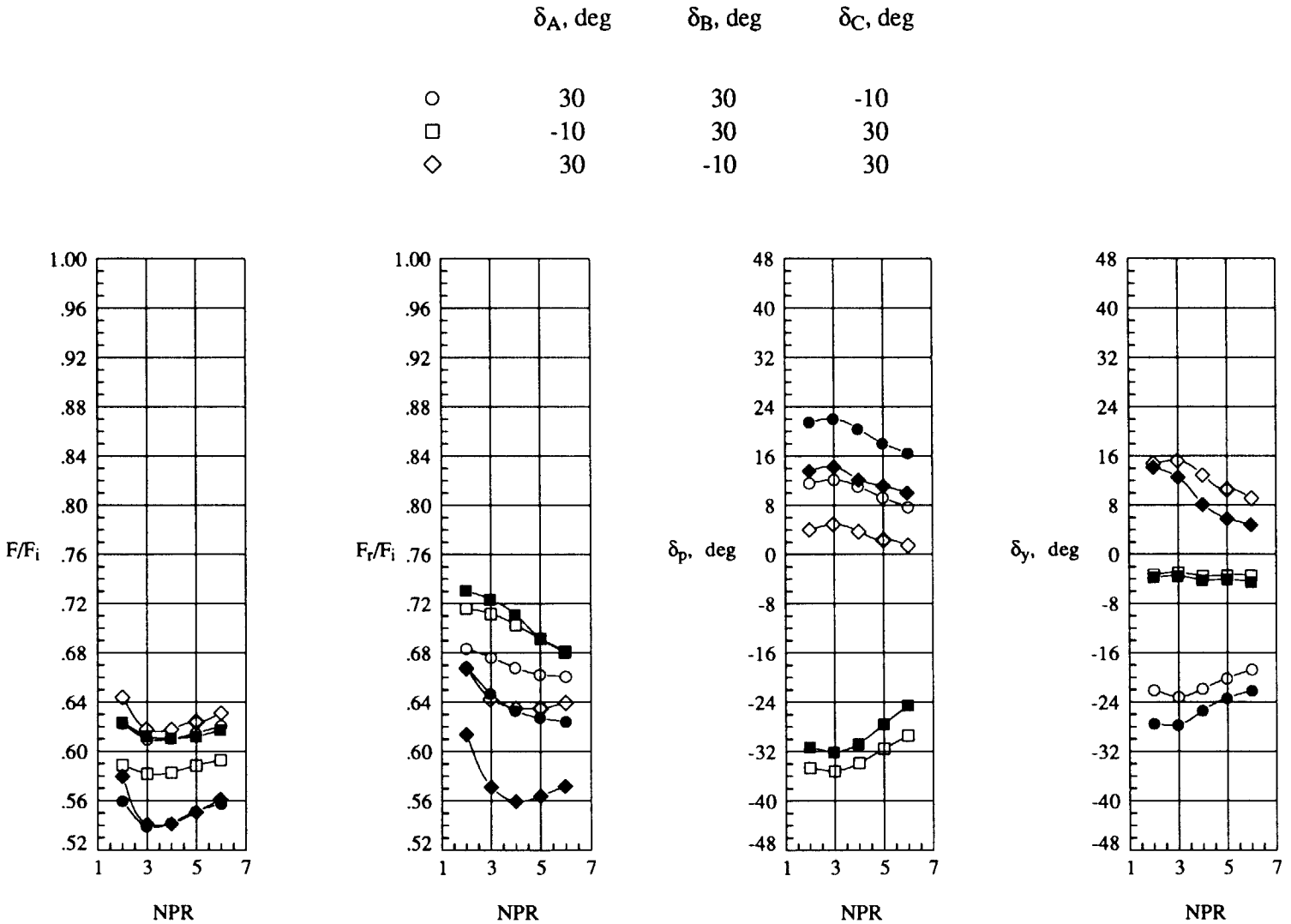

Figure 12. Effect of top vane size on performance of military-power nozzle with rotating-vane actuation system. Open symbols denote standard top vane geometry; solid symbols denote large top vane geometry.

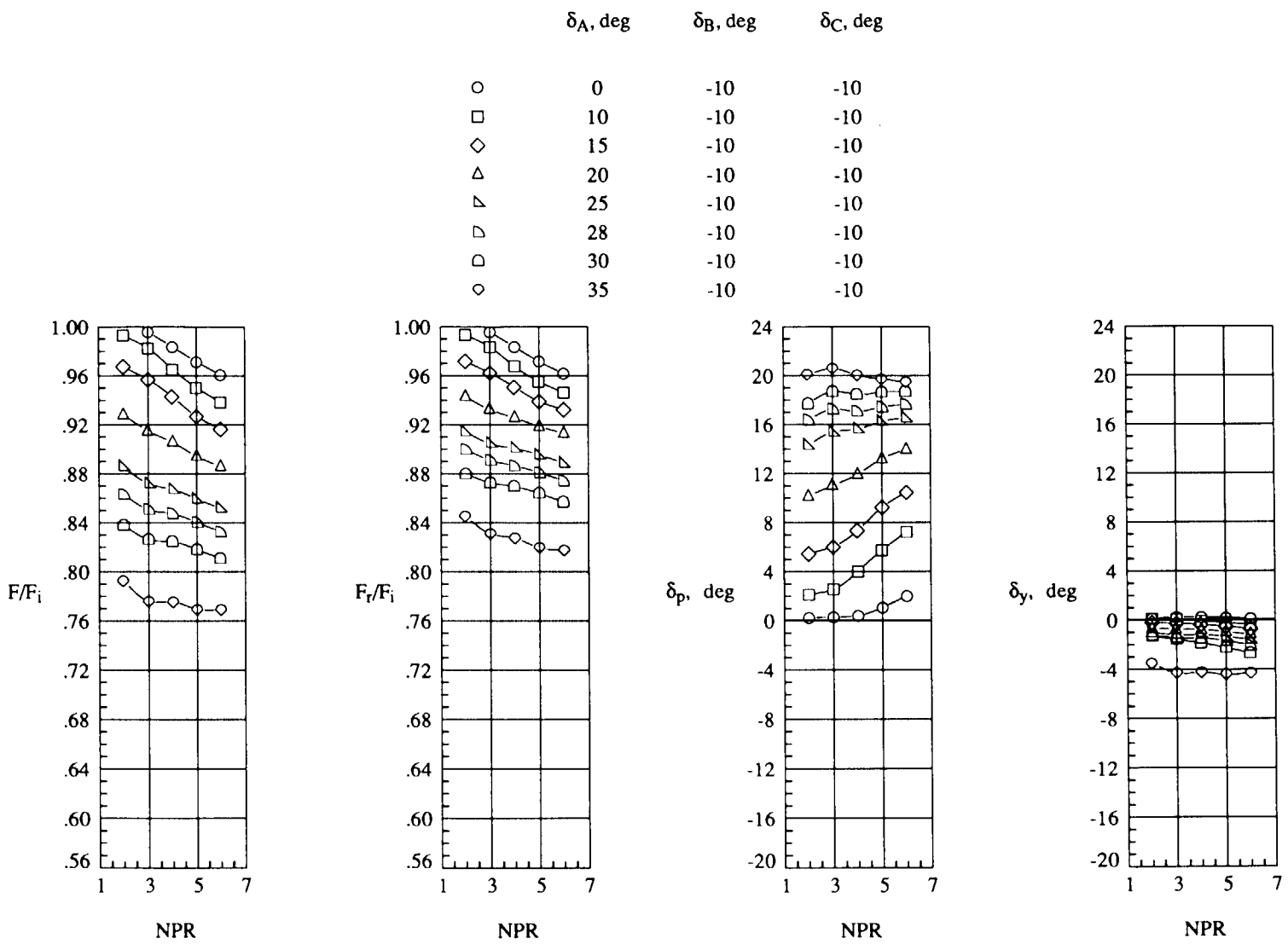

(a) Vane A deployed.

Figure 13. Thrust and turning performance for maximum A/B-power nozzle with large top vane.

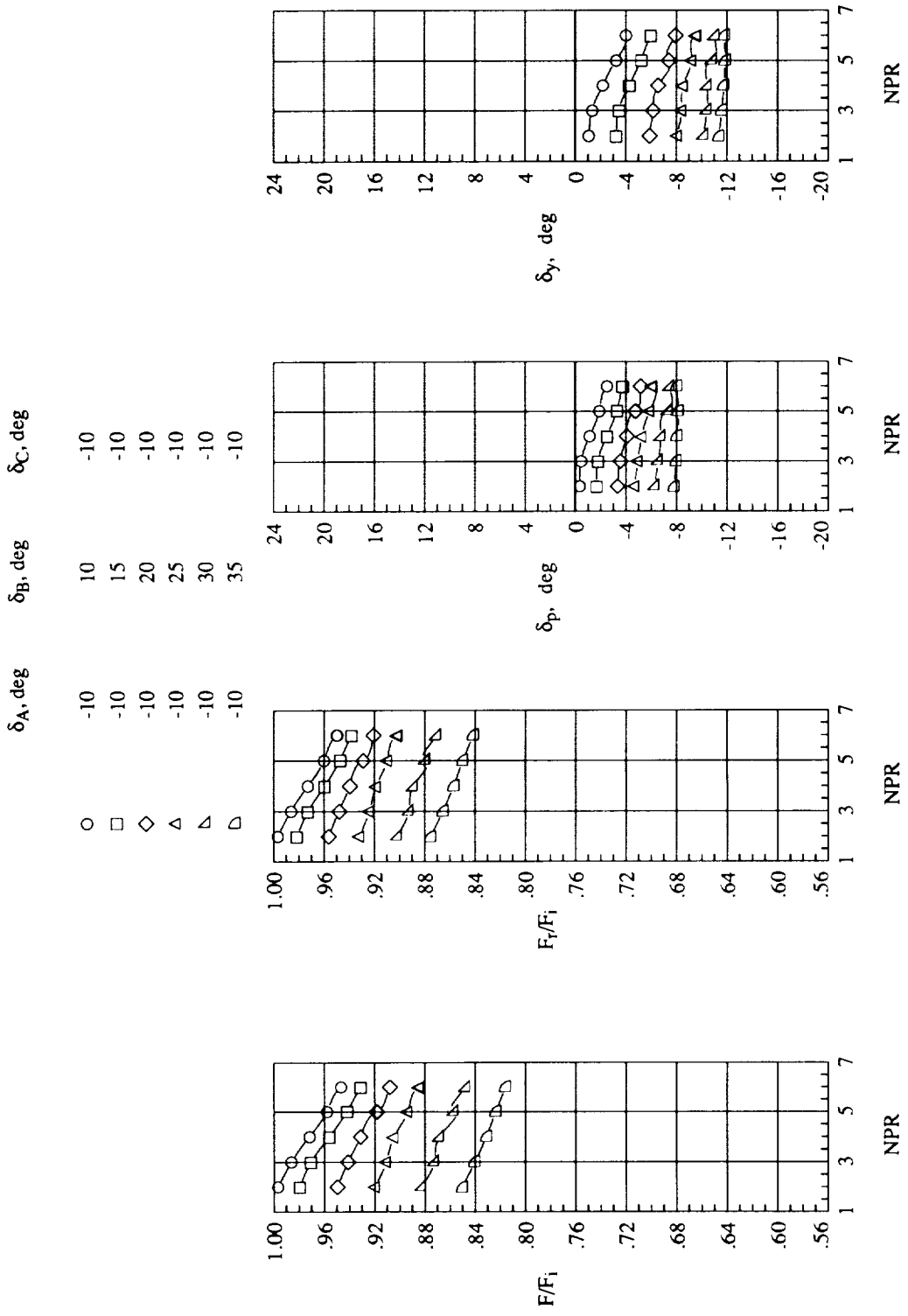

(b) Vane B deployed.

Figure 13. Continued.

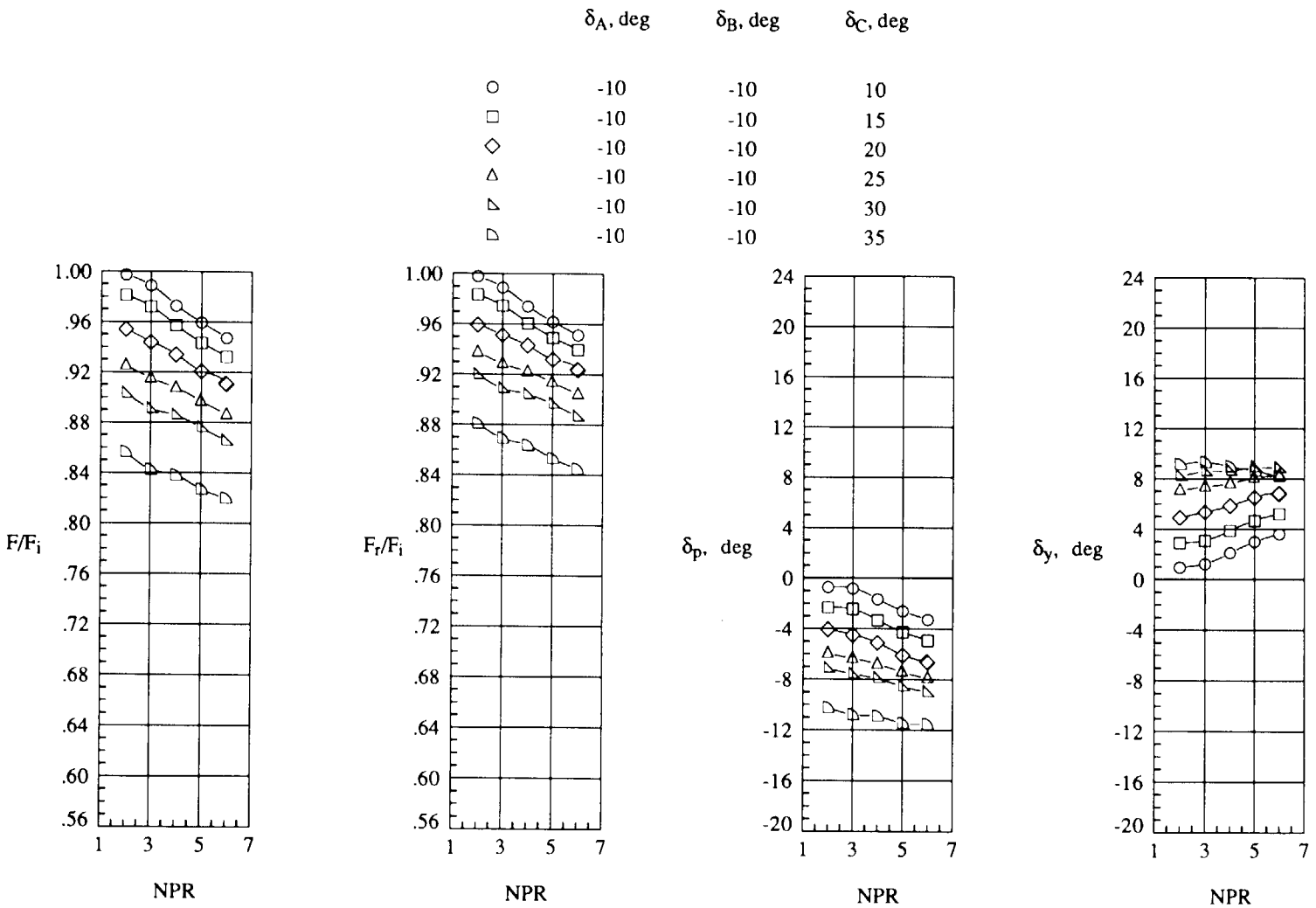

(c) Vane C deployed.

Figure 13. Concluded.

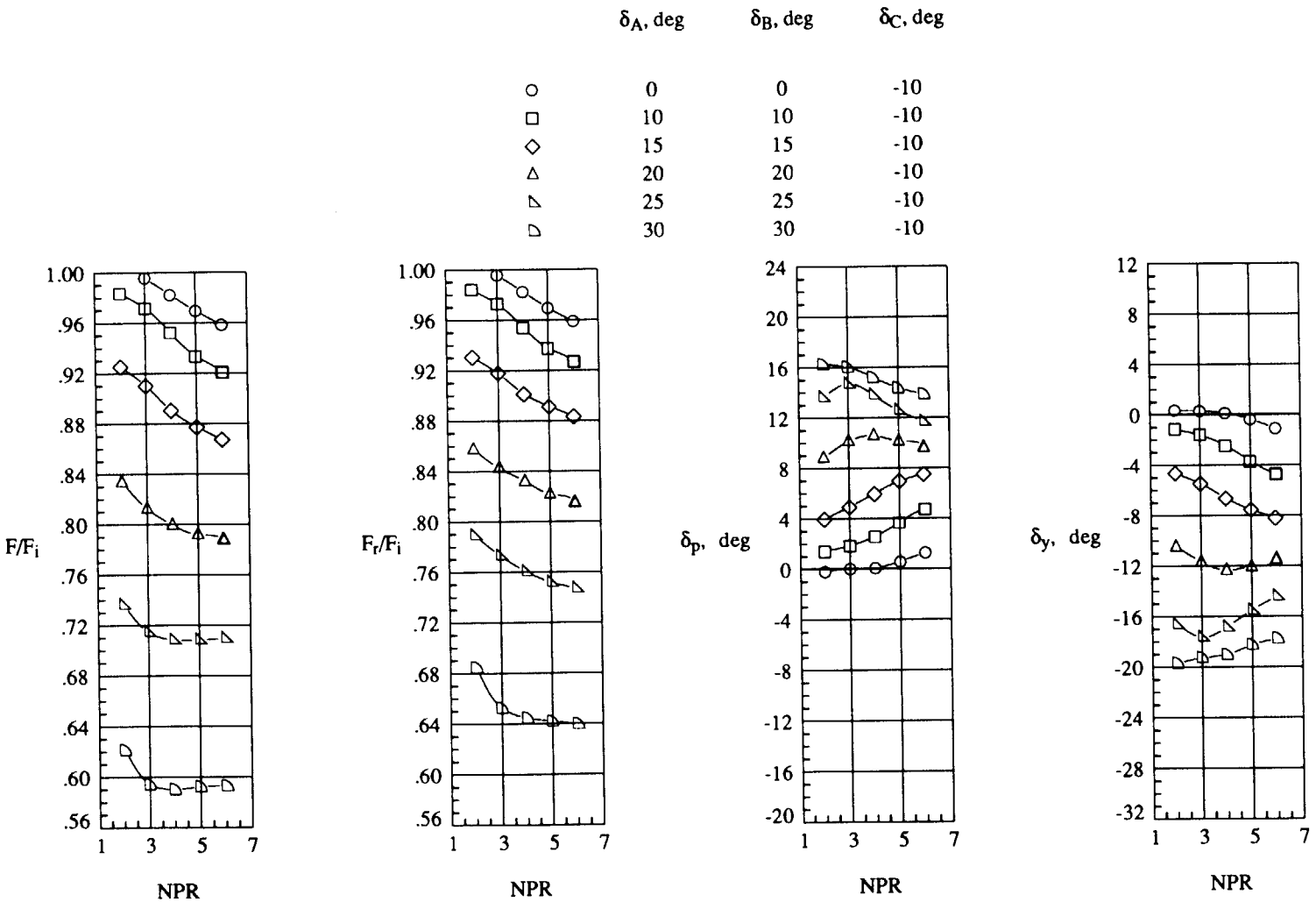

(a) Vanes A and B equally deployed.

Figure 14. Thrust and turning performance for maximum A/B-power nozzle.

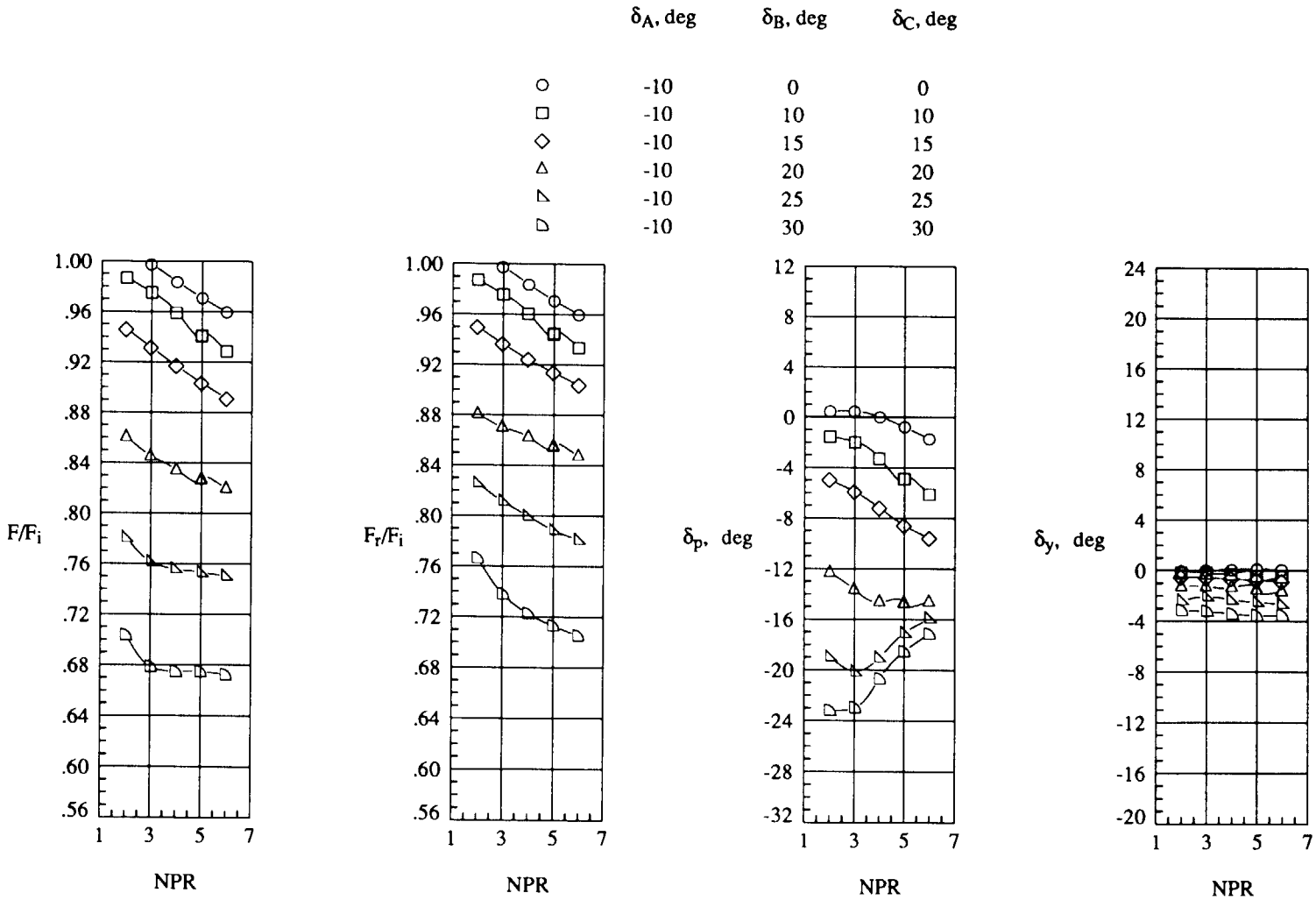

(b) Vanes B and C equally deployed.

Figure 14. Continued.

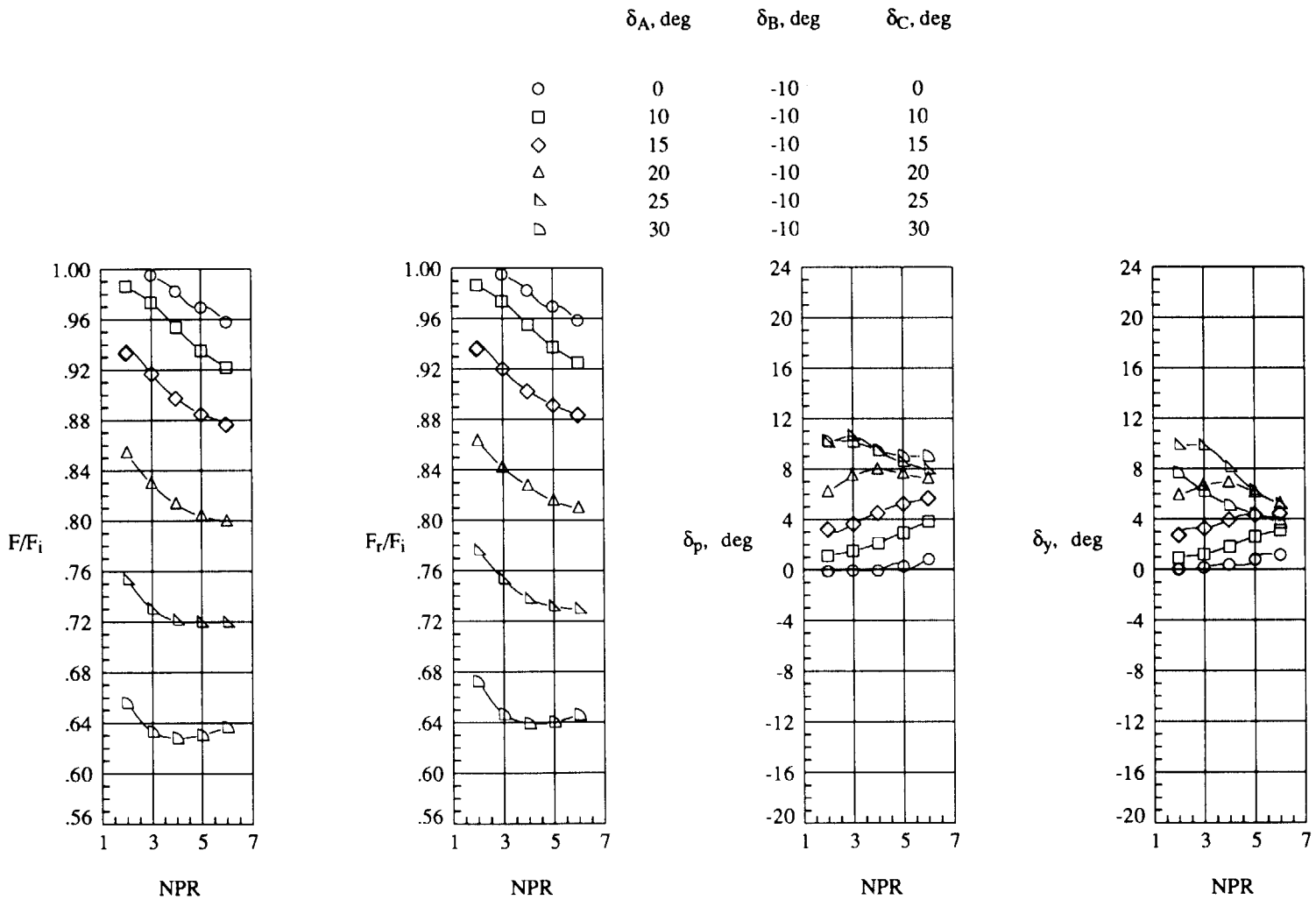

(c) Vanes A and C equally deployed.

Figure 14. Concluded.

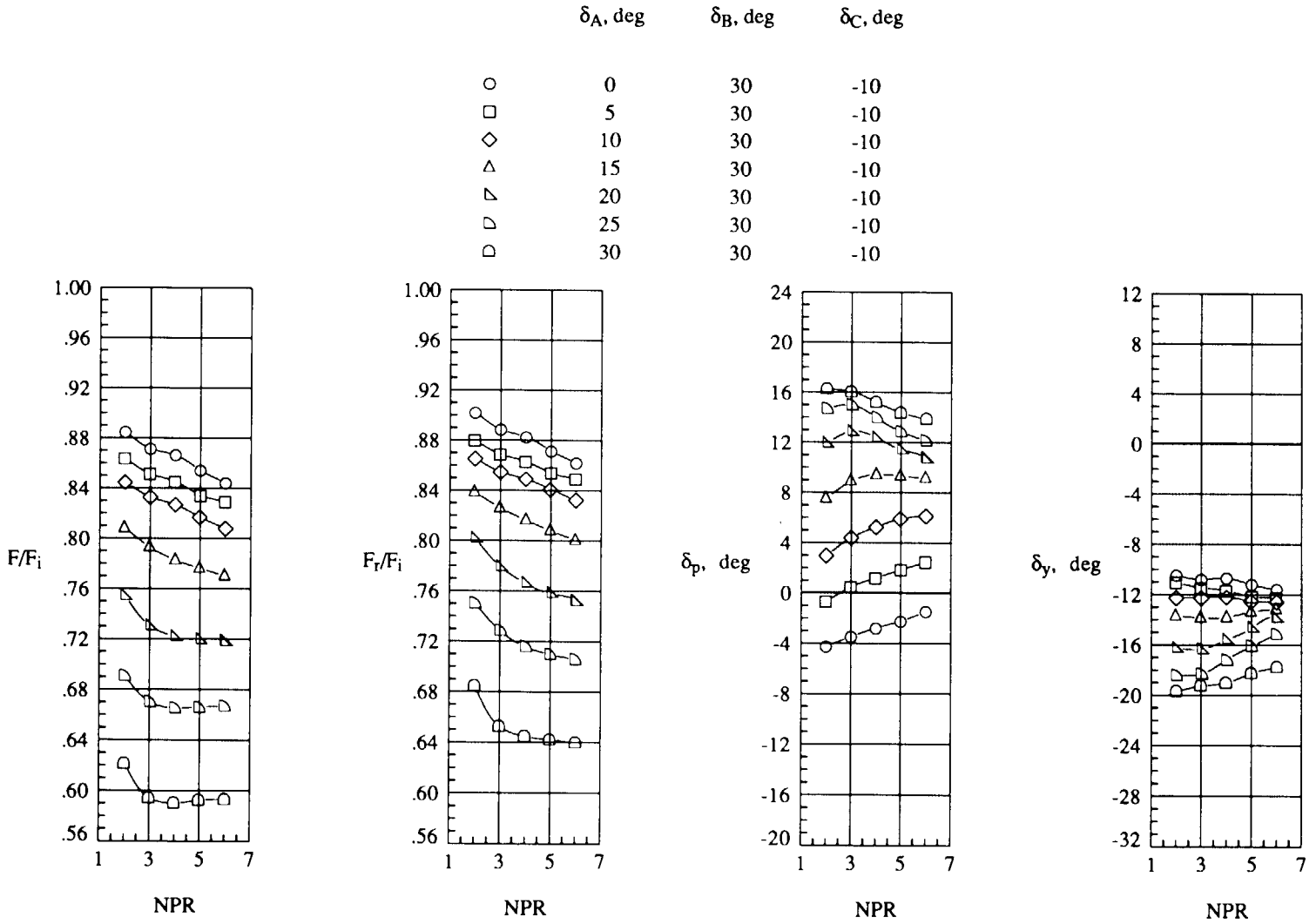

(a) Vanes A and B deployed with $\delta_B = 30°$.

Figure 15. Thrust and turning performance for maximum A/B-power nozzle with two vanes deployed and one vane retracted.

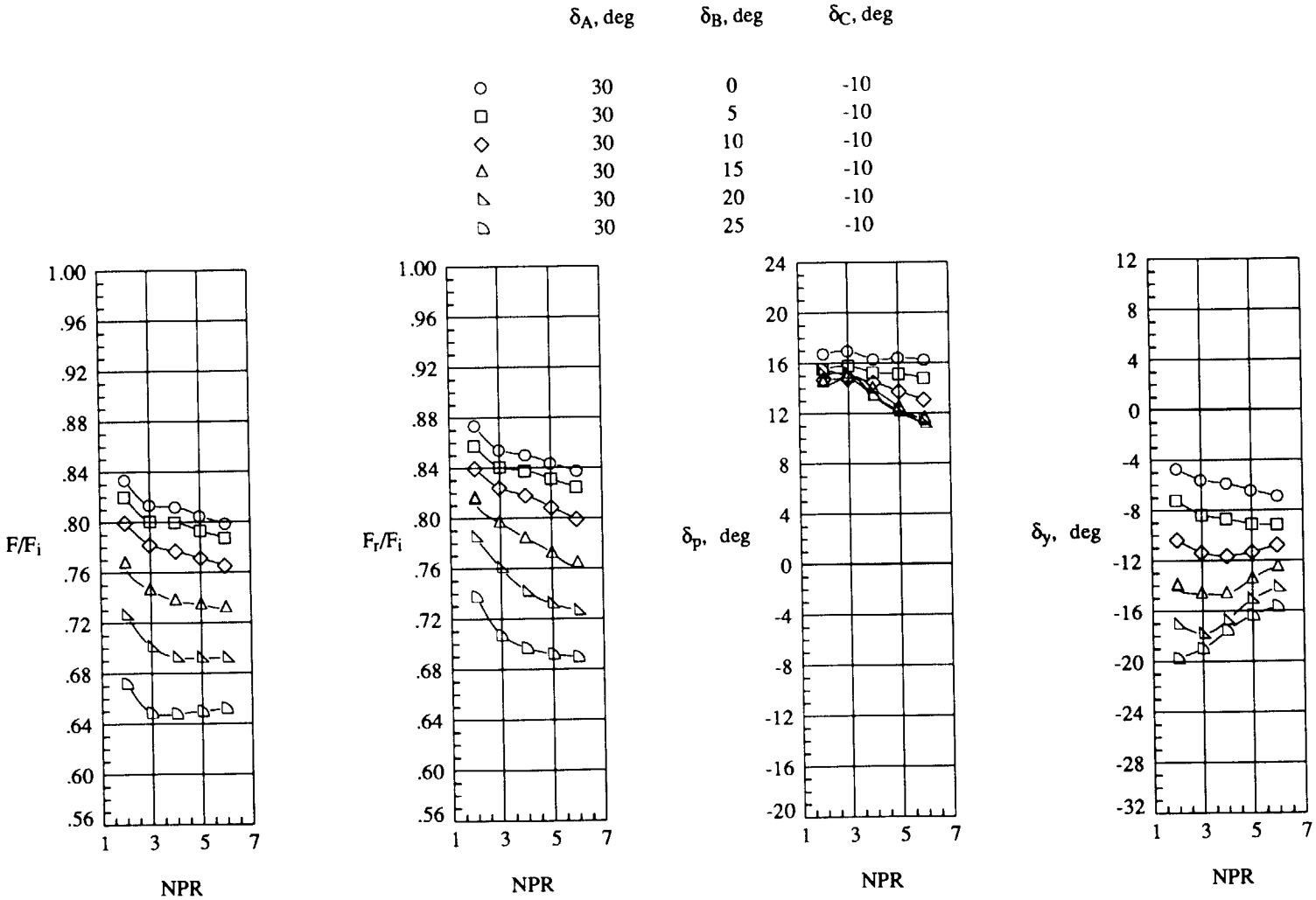

(b) Vanes A and B deployed with $\delta_A = 30°$.

Figure 15. Continued.

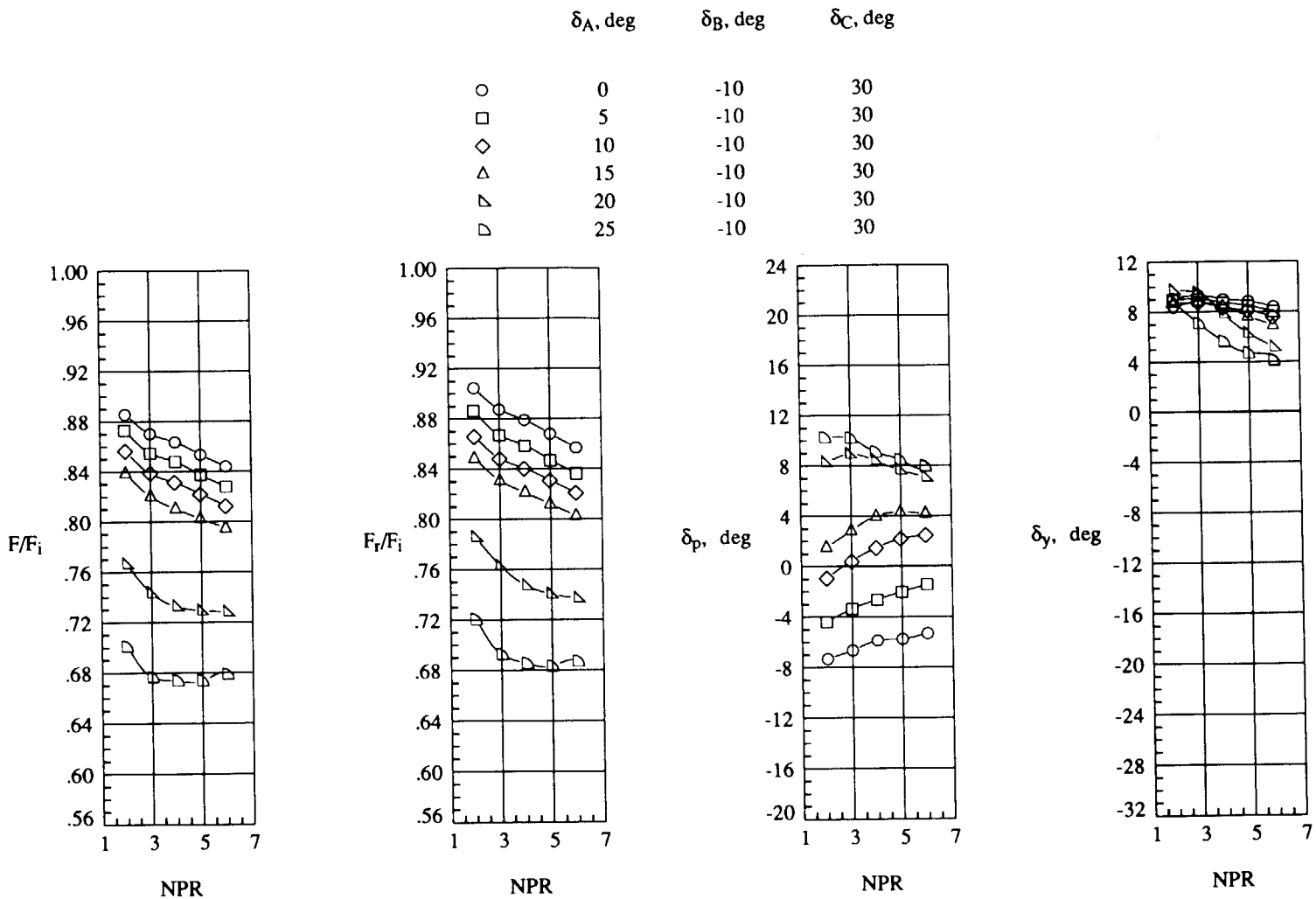

(c) Vanes A and C deployed with $\delta_C = 30°$.

Figure 15. Continued.

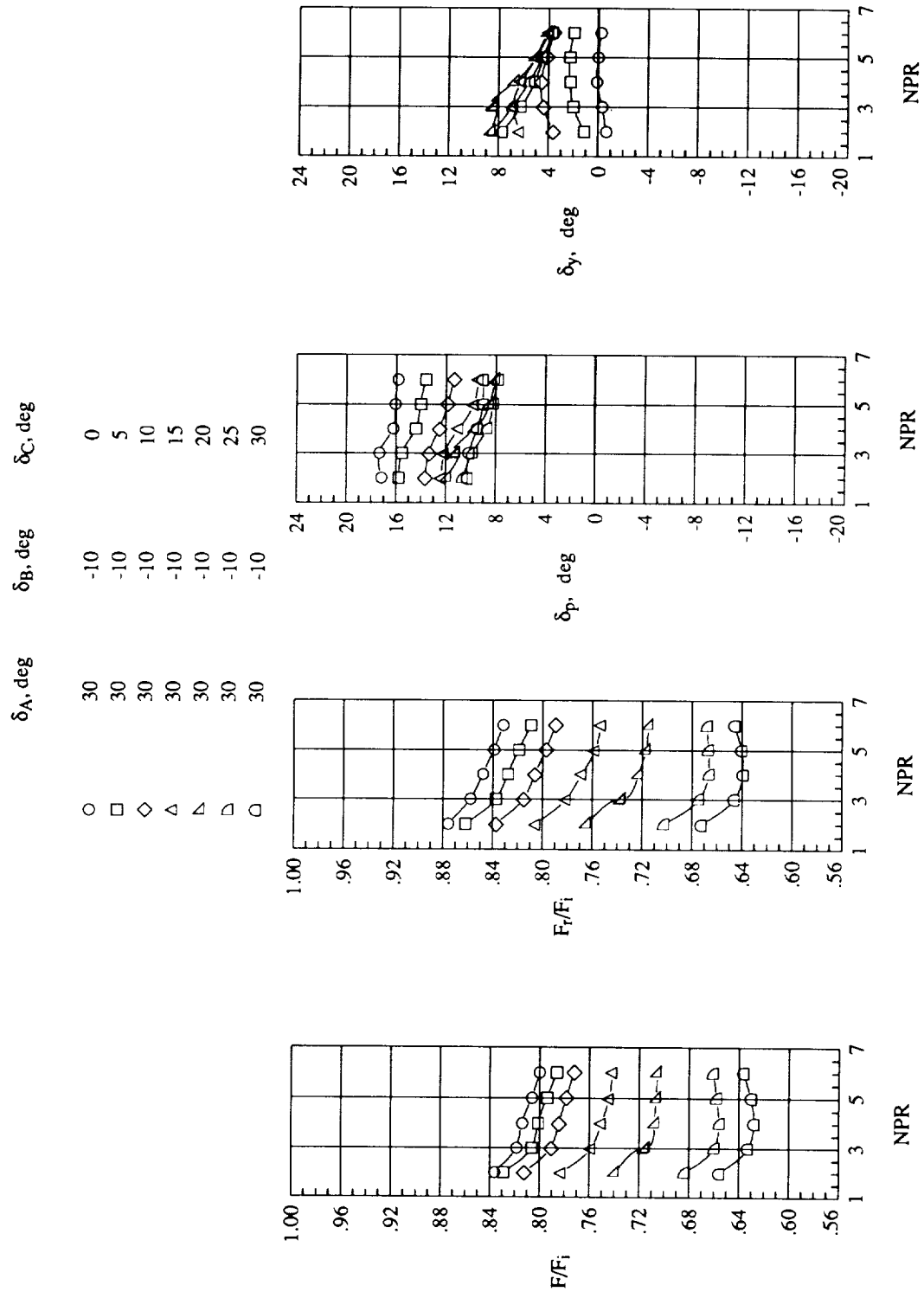

(d) Vanes A and C deployed with $\delta_A = 30°$.

Figure 15. Continued.

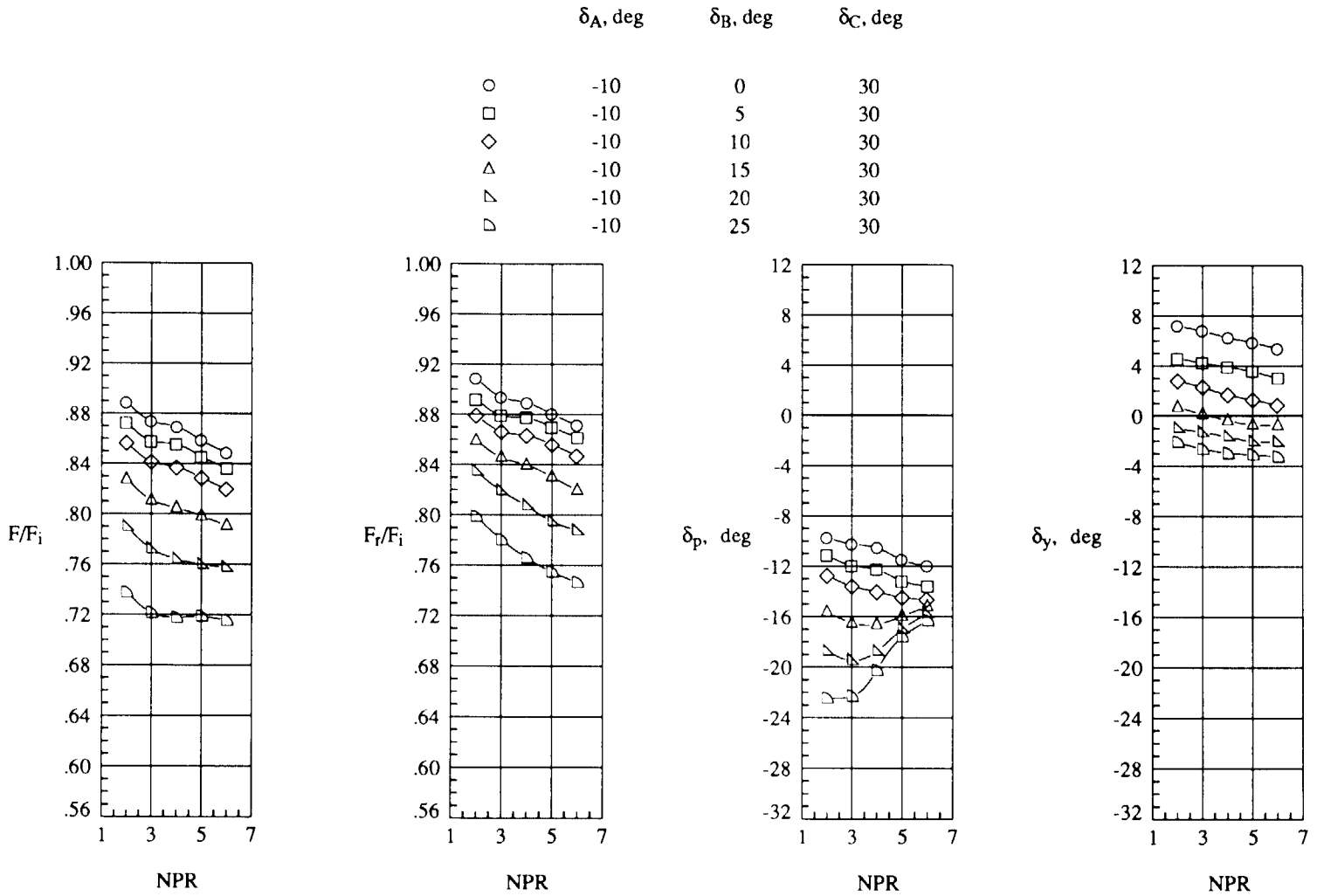

(e) Vanes B and C deployed with $\delta_C = 30°$.

Figure 15. Continued.

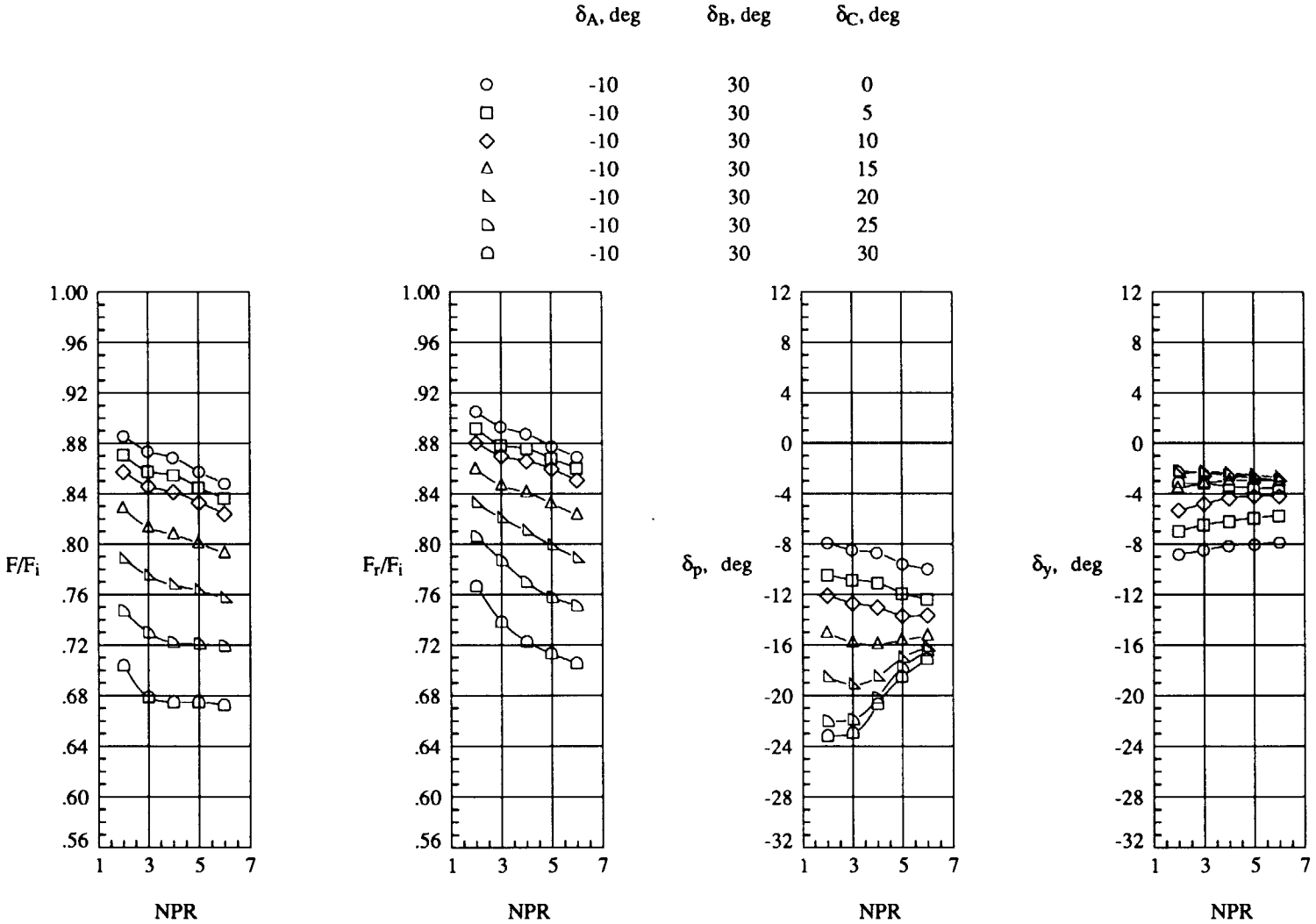

(f) Vanes B and C deployed with $\delta_B = 30°$.

Figure 15. Concluded.

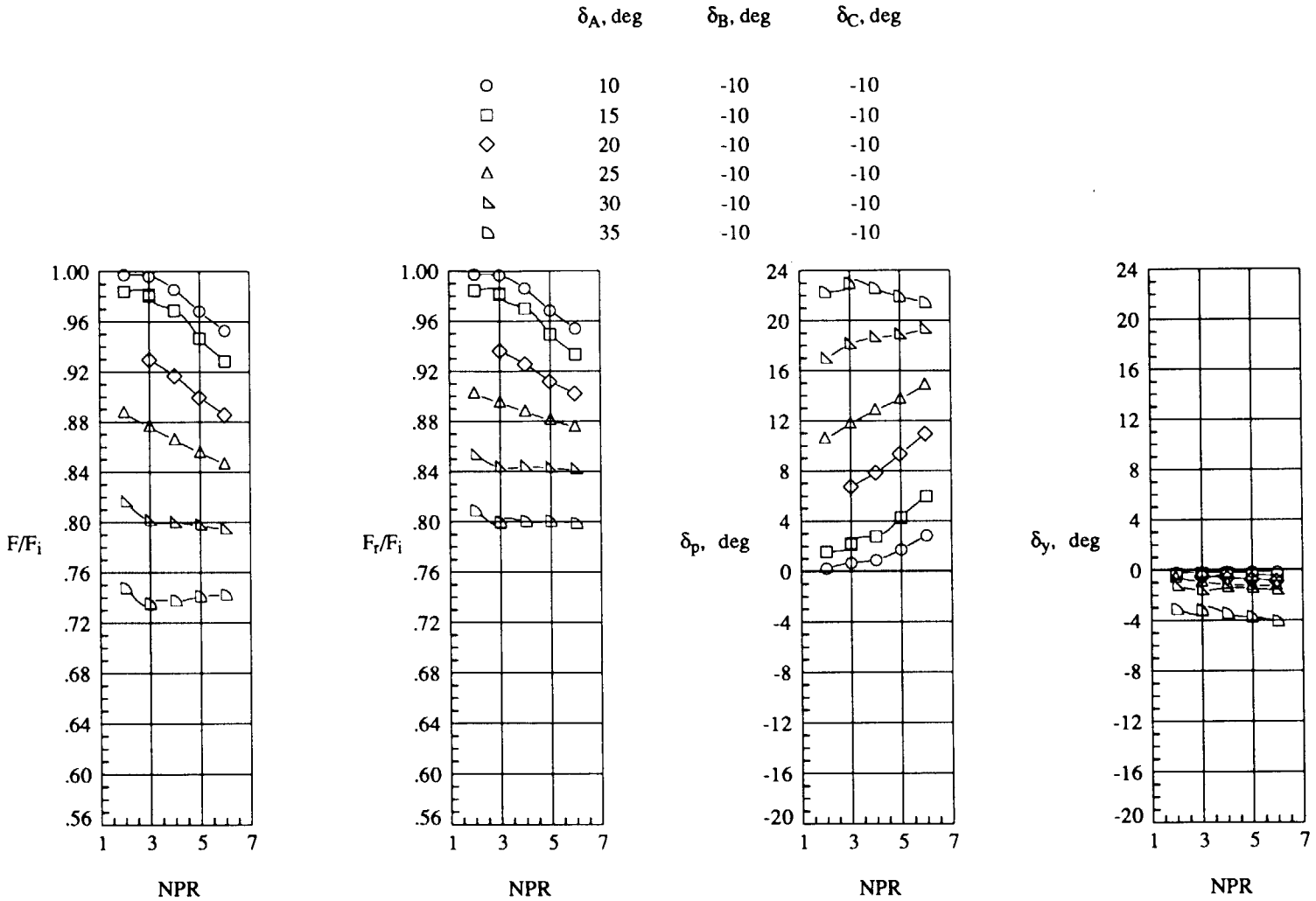

(a) Vane A deployed.

Figure 16. Thrust and turning performance for military-power nozzle with single vane deployed and two vanes retracted.

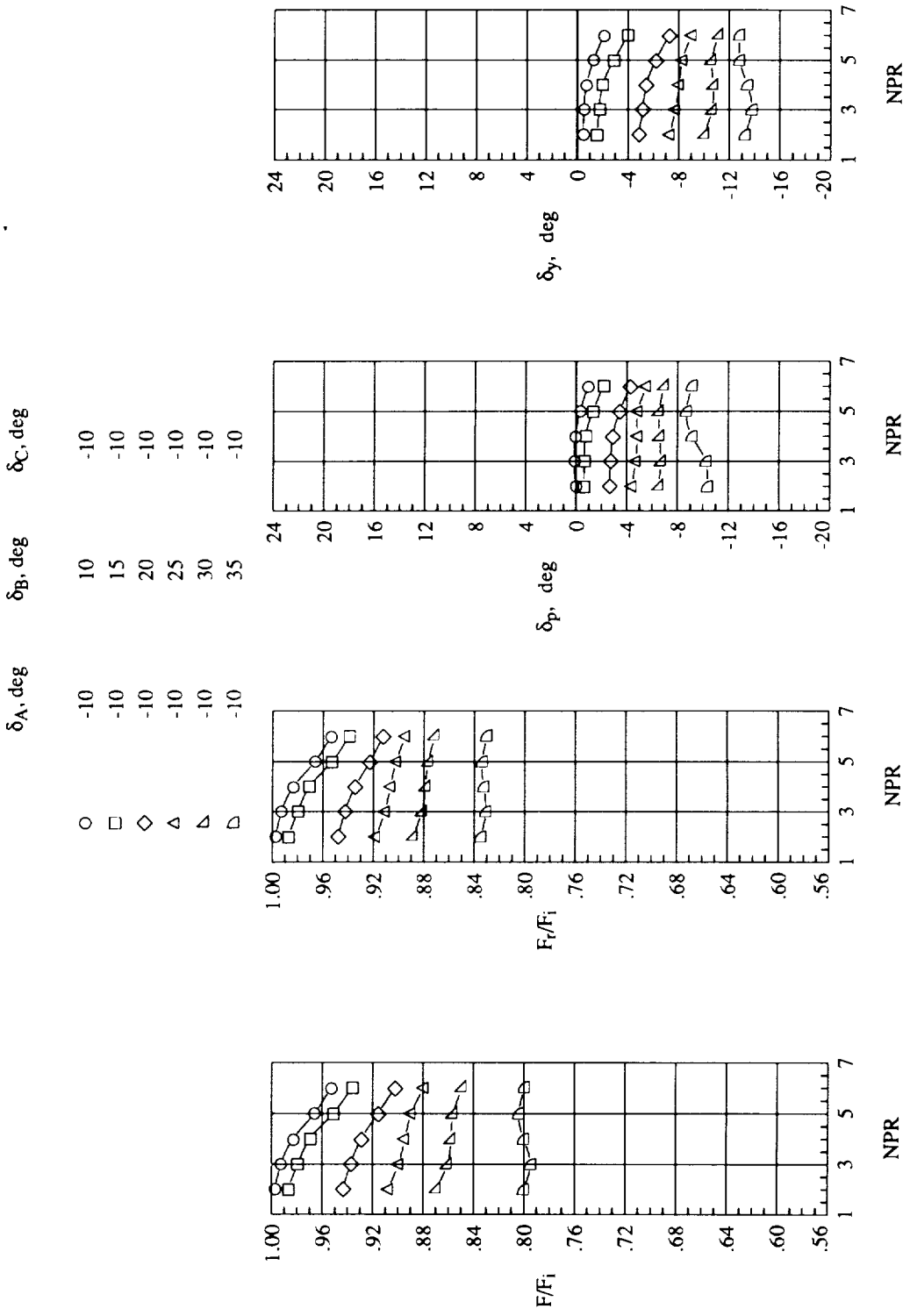

(b) Vane B deployed.

Figure 16. Continued.

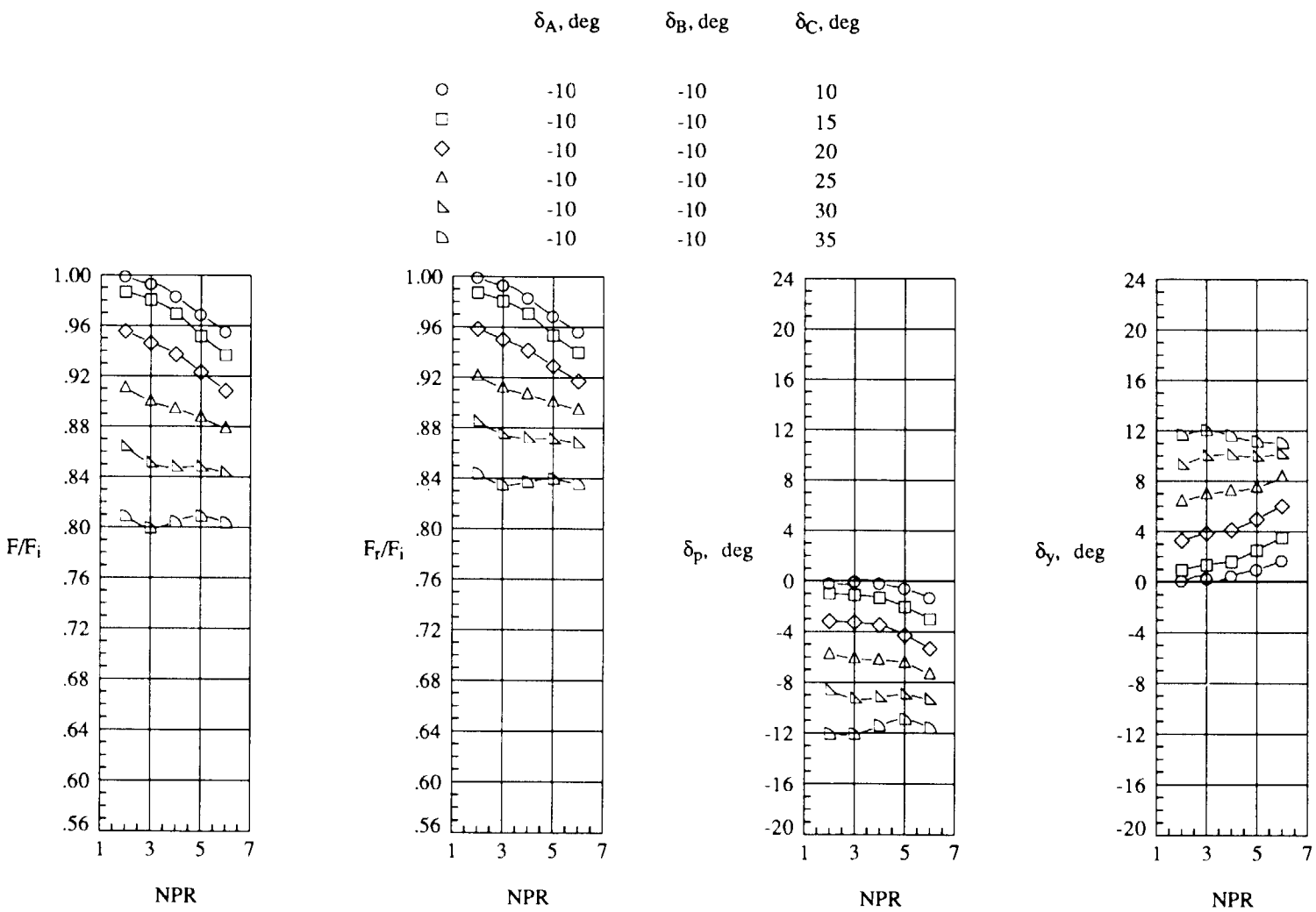

(c) Vane C deployed.

Figure 16. Concluded.

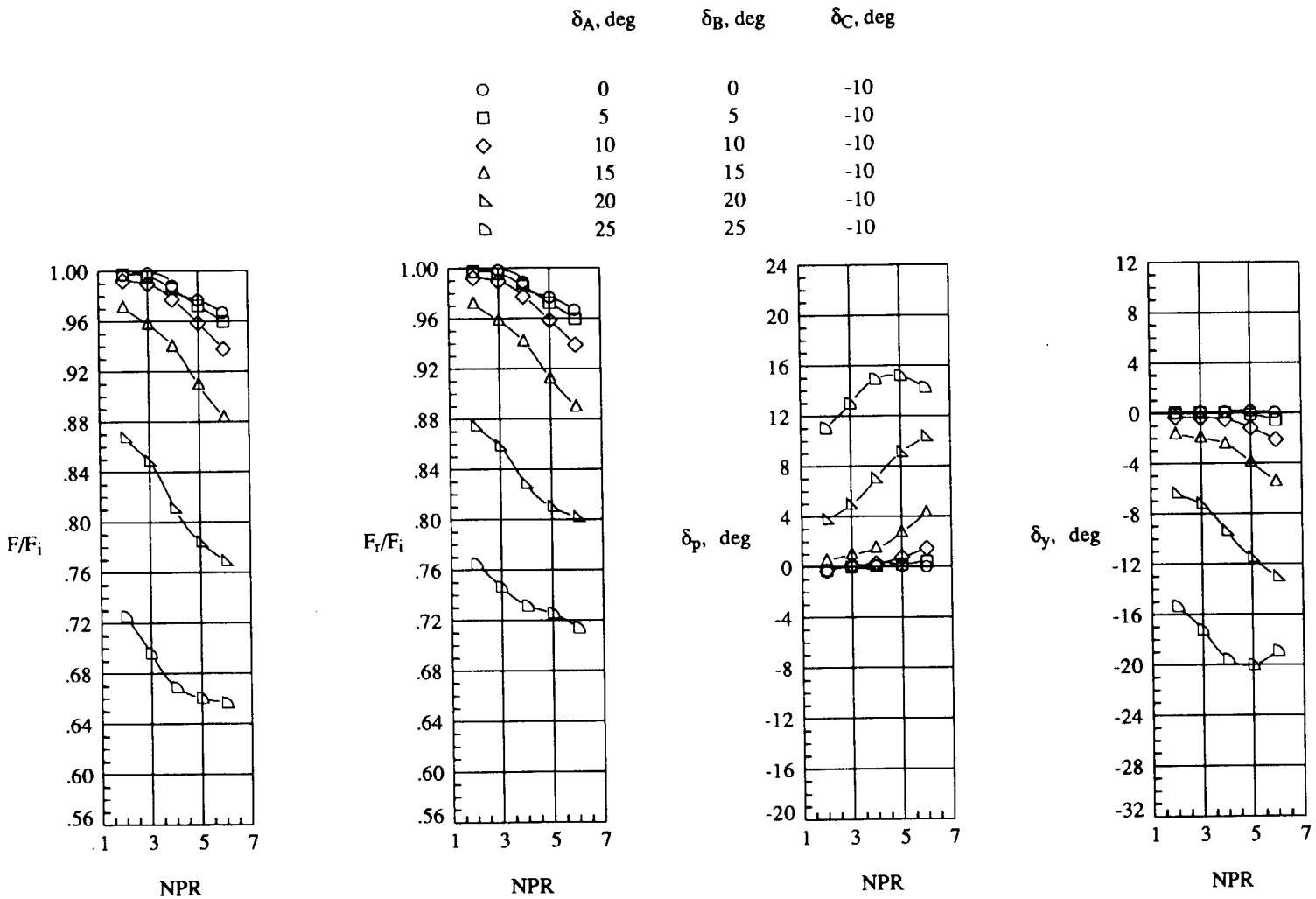

(a) Vanes A and B equally deployed.

Figure 17. Thrust and turning performance for military-power nozzle with two equally deployed vanes with one vane retracted.

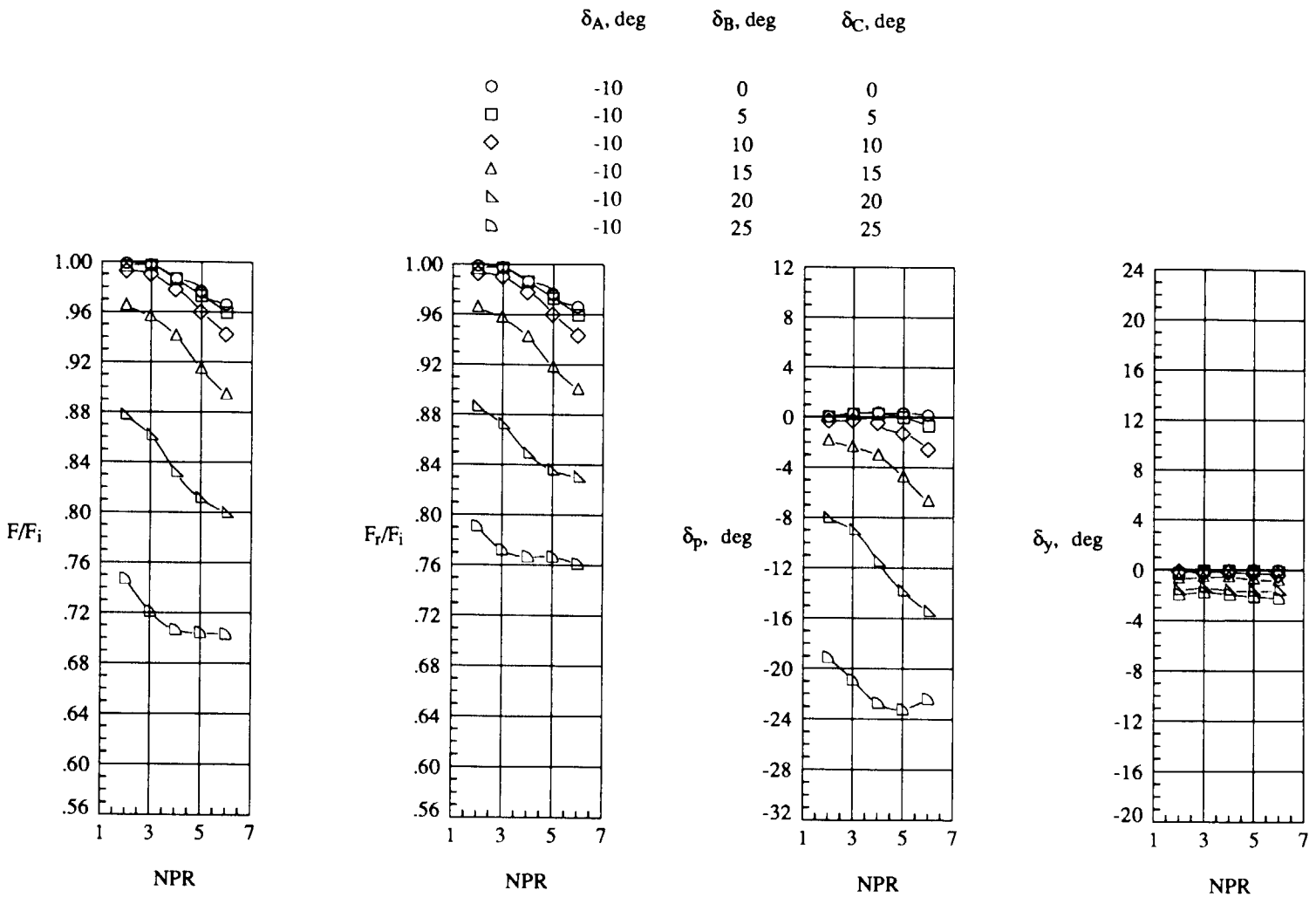

(b) Vanes B and C equally deployed.

Figure 17. Continued.

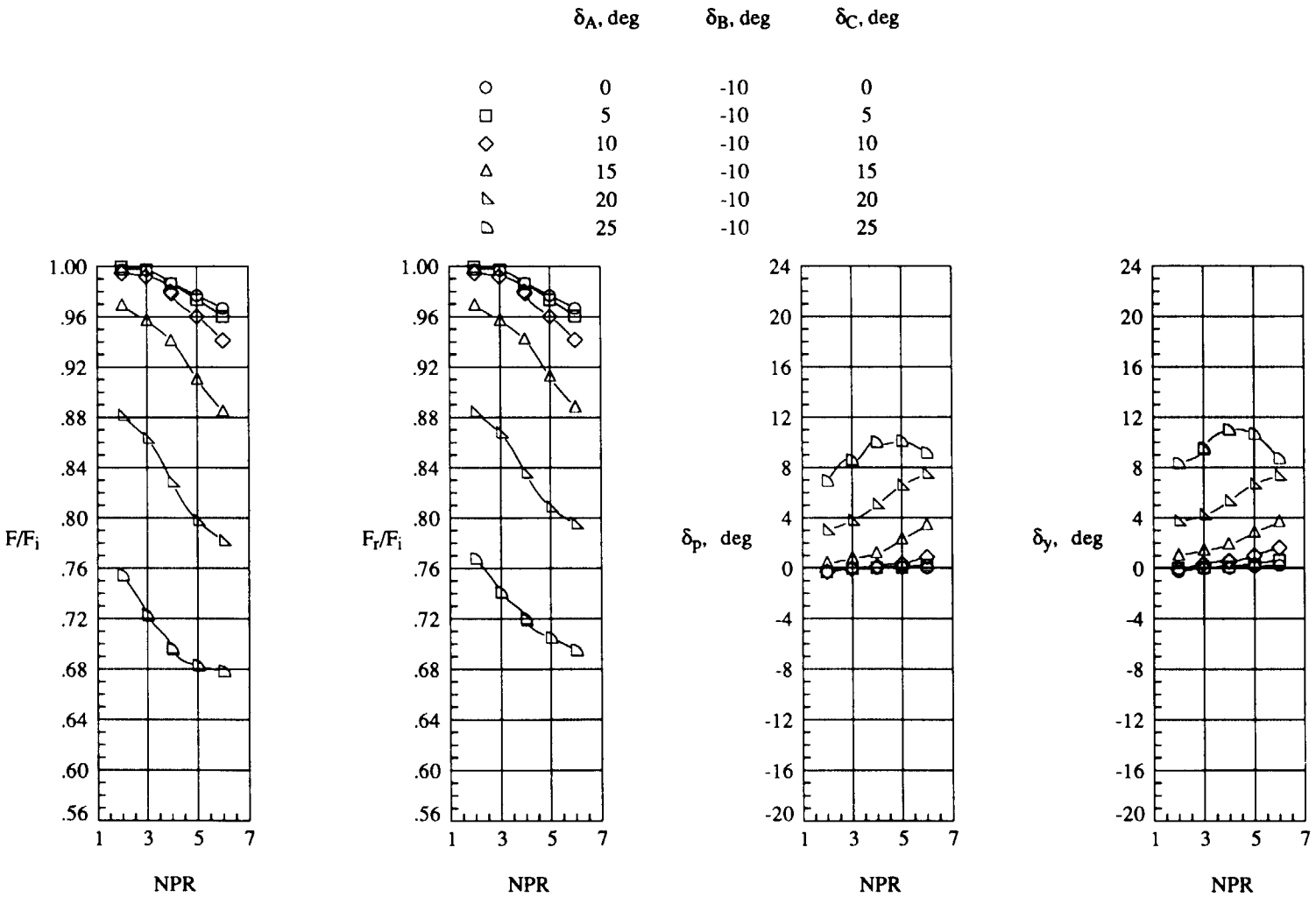

(c) Vanes A and C equally deployed.

Figure 17. Concluded.

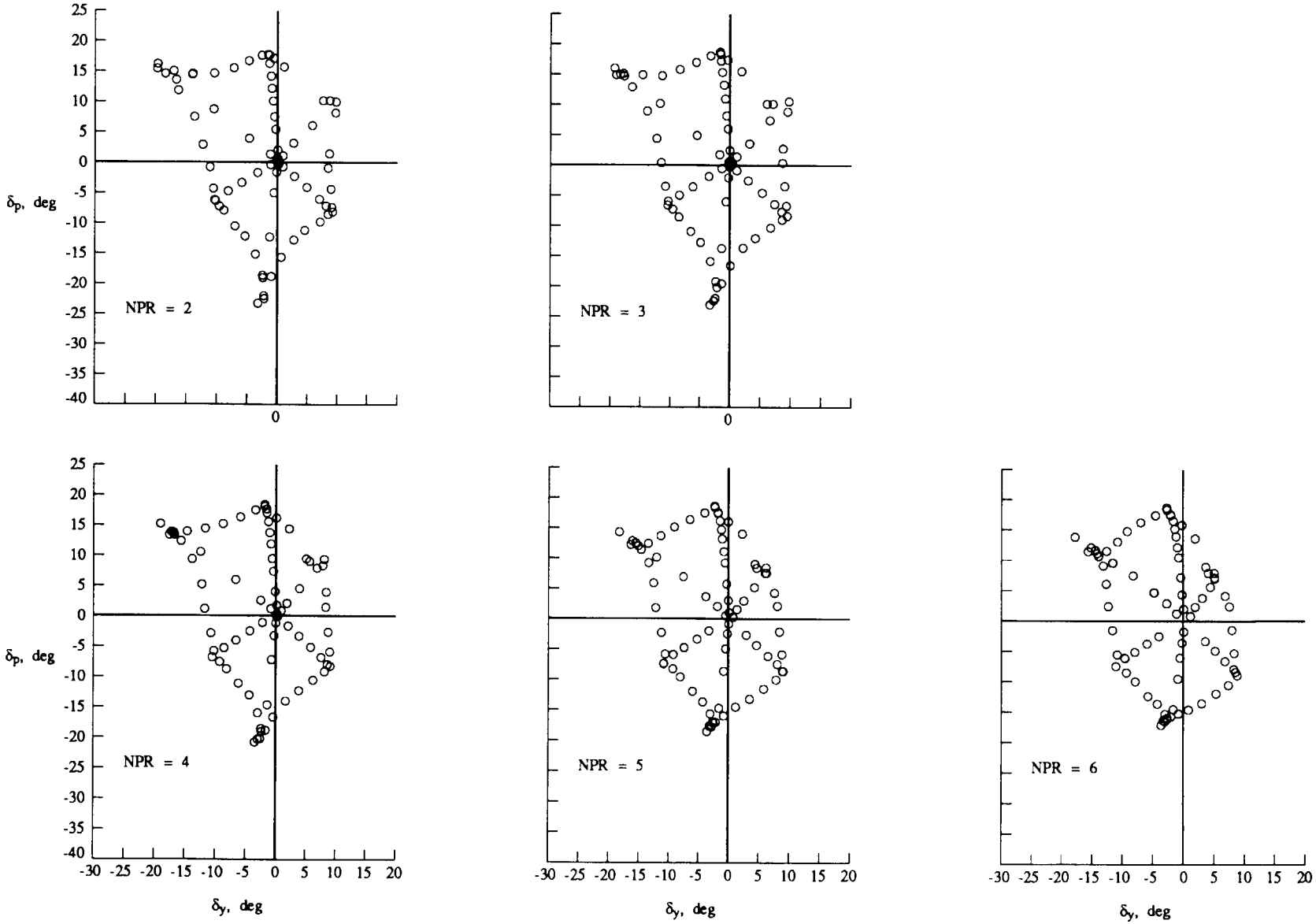

Figure 18. Resultant thrust vectoring envelope for maximum A/B-power nozzle for maximum deflection angle of 30° with one vane always fully retracted. Operating NPR for F/A-18 HARV is approximately 4.

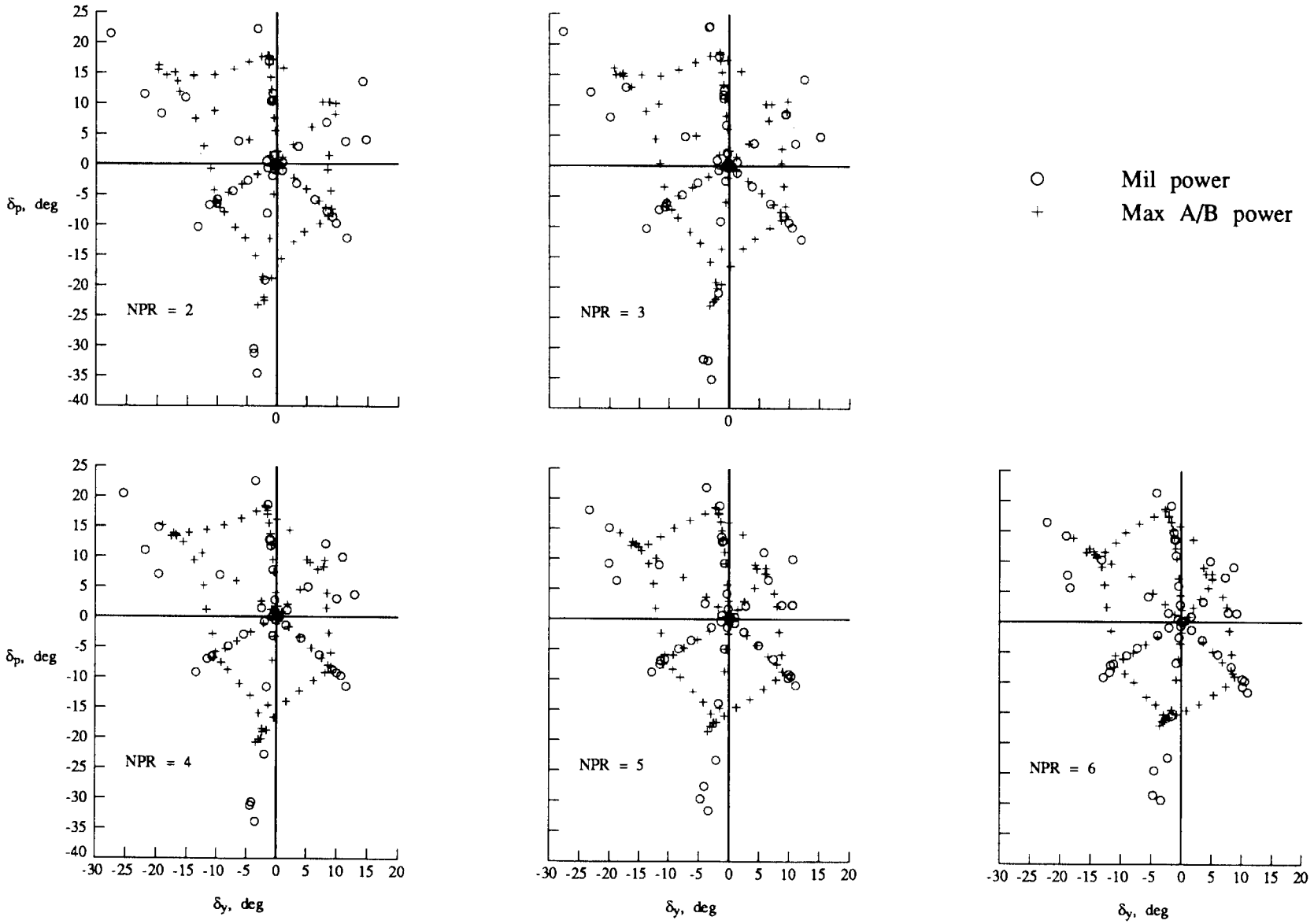

Figure 19. Resultant thrust vectoring envelope for military-power nozzle for maximum deflection angle of 30° with one vane always fully retracted. Operating NPR for F/A-18 HARV is approximately 4.

REPORT DOCUMENTATION PAGE

Form Approved
OMB No. 0704-0188

1. AGENCY USE ONLY *(Leave blank)*	2. REPORT DATE	3. REPORT TYPE AND DATES COVERED
	June 1992	Technical Memorandum

4. TITLE AND SUBTITLE
A Static Investigation of the Thrust Vectoring System of the F/A-18 High-Alpha Research Vehicle

5. FUNDING NUMBERS
WU 505-68-30-07

6. AUTHOR(S)
Mary L. Mason, Francis J. Capone, and Scott C. Asbury

7. PERFORMING ORGANIZATION NAME(S) AND ADDRESS(ES)
NASA Langley Research Center
Hampton, VA 23665-5225

8. PERFORMING ORGANIZATION REPORT NUMBER
L-17002

9. SPONSORING/MONITORING AGENCY NAME(S) AND ADDRESS(ES)
National Aeronautics and Space Administration
Washington, DC 20546-0001

10. SPONSORING/MONITORING AGENCY REPORT NUMBER
NASA TM-4359

11. SUPPLEMENTARY NOTES

12a. DISTRIBUTION/AVAILABILITY STATEMENT
Unclassified Unlimited

Subject Category 02

12b. DISTRIBUTION CODE

13. ABSTRACT *(Maximum 200 words)*

A static (wind-off) test was conducted in the static test facility of the Langley 16-Foot Transonic Tunnel to evaluate the vectoring capability and isolated nozzle performance of the proposed thrust vectoring system of the F/A-18 high-alpha research vehicle (HARV). The thrust vectoring system consisted of three asymmetrically spaced vanes installed externally on a single test nozzle. Two nozzle configurations were tested: a maximum afterburner-power nozzle and a military-power nozzle. Vane size and vane actuation geometry were investigated, and an extensive matrix of vane deflection angles was tested. The nozzle pressure ratio ranged from 2 to 6. The results indicate that the three-vane system can successfully generate multiaxis (pitch and yaw) thrust vectoring. However, large resultant vector angles incurred large thrust losses. Resultant vector angles were always lower than the vane deflection angles. The maximum thrust vectoring angles achieved for the military-power nozzle were larger than the angles achieved for the maximum afterburner-power nozzle.

14. SUBJECT TERMS	15. NUMBER OF PAGES
Nozzle internal performance; Multiaxis thrust vectoring; Axisymmetric nozzle; Thrust vectoring vanes	163
	16. PRICE CODE A08

17. SECURITY CLASSIFICATION OF REPORT	18. SECURITY CLASSIFICATION OF THIS PAGE	19. SECURITY CLASSIFICATION OF ABSTRACT	20. LIMITATION OF ABSTRACT
Unclassified	Unclassified		

NSN 7540-01-280-5500

Standard Form 298(Rev. 2-89)
Prescribed by ANSI Std. Z39-18
298-102

NASA-Langley, 1992